Molecular Rheology of Supramolecular Networks Formed by Temporary and Topological Crosslinks

A Doctoral Thesis

by

Yu Kashiwagi

Submitted to

the Graduate School of Science, Osaka University

February 2021

Acknowledgements

This thesis is based on my research carried out from 2015 to 2021 at Inoue Laboratory in Department of Macromolecular Science, Graduate School of Science, Osaka University. The author would like to express his sincere gratitude to Professor Tadashi Inoue for his guidance throughout this study. Grateful acknowledgement is made to Associate Professor Osamu Urakawa, and Assistant Professor Takuya Katashima (at The University of Tokyo) for their helpful discussions and advices. The author also thanks all members of Inoue laboratory for their cooperation and friendship.

The author would like to acknowledge Professor Yoshinori Takashima and Akira Harada for their kind helps and suggestions. The author also thanks to Professor Alexei P. Sokolov and all members of Sokolov laboratories in University of Tennessee, Knoxville and Oak Ridge National Laboratory for their helpful cooperation and many discussion.

The author appreciate the financial support from The Sumitomo Chemical Scholarship Program for Global Leadership Development 2019.

Finally, the author expresses sincere appreciation to his father, Koichi Kashiwagi and his mother Shigemi Kashiwagi for their warm encouragement.

February 2021

Yu Kashiwagi

Contents

Chapter 1

General Introduction

1-1. Polymer networks

Polymer networks such as gels and rubbers show rubbery elasticity. Compared with other materials such as metals and ceramics, they can be deformed much largely with a small applied force. The polymer networks normally have a three-dimensional network in which chemical or physical crosslinks connect polymer chains. The polymer networks usually have various structural defects, and thus, stress concentration is likely to occur, leading to low mechanical toughness. For applications in which the polymer networks are subjected to high load conditions for a long time, it is necessary to enhance the durability and crack resistance. For example, rubbers are filled with carbon black in practical uses. In general, mechanical brittleness is one of the most important problems to overcome because the enhancement of the toughness can reduce excessive waste and energy consumption and contribute to the realization of "low carbon society".

Last few decades, a new class of polymeric materials has been developed to enhance the toughness. One of the primary directions to accomplish the mechanical toughness is to incorporate some energy dissipation mechanism into the polymer network. For example, when hydrogen bonding[1-3], metal coordination[4-5], ionic interaction[6-7], or host-guest interaction[8-10] is introduced as a non-covalent mechanism, these bonding work as a "sacrificial bond" which repeated association and dissociation process under thermal equilibrium[5]. The other is the thermoplastic elastomers[11-12], which consists of hard associating segments and soft rubbery segments. When it is highly deformed, the hard segments are destroyed, and soft segments can be largely stretched. These polymer networks can dissipate the applied energy through the dissociation of associative parts, which results in superior mechanical toughness.

1-2. Types of crosslinks by cyclodextrin

Cyclodextrin is a ring-shaped molecule consisting of some glucose units and has a hydrophilic surface and hydrophobic cavity. Figure 1-1 shows the chemical structure and schematic illustration of α-cyclodextrin. Cyclodextrin can form inclusion complexes with various types of guest molecules[13]. Besides, since cyclodextrins have different cavity sizes depending on the number of connected glucose units, the types of guest molecules also differ. These properties can limit the types of the guest molecule, and thus the intermolecular interaction between cyclodextrins and guest molecules is called "host-guest interaction" [14]. Many studies on the supramolecular networks in which cyclodextrin works as physical and/or chemical crosslinks have been reported. In the following section, two types of supramolecular networks based on cyclodextrin crosslinks will be explained.

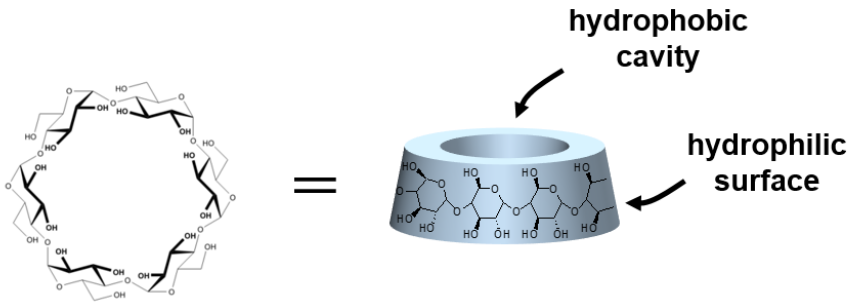

Figure 1-1. Chemical structure and schematic illustration of α-cyclodextrin.

1-3. Supramolecular networks formed by host-guest interaction

Harada *et al.* have developed a new class of tough polymer gels that utilizes the host-guest inclusion complexes between cyclodextrin and guest molecules as a physical crosslink[8, 14-17]. Such a supramolecular network is called "host-guest gel". The schematic illustration of the host-guest is shown in Figure 1-2. By incorporating cyclodextrin and guest molecules into polymer side chains, these molecules can form an inclusion complex and connected polymer chains physically. This inclusion complex repeats the dissociation and association process, resulting

in the temporary crosslinks. This host-guest gel is usually prepared by radical polymerization of cyclodextrin vinyl monomer and guest vinyl monomer in addition to conventional vinyl monomers as main components.

The host-guest interaction can work the energy dissipation mechanism and contribute to the tough mechanical property. Furthermore, thanks to the transient property of the host-guest interaction, the host-guest gel has a self-healing property. Even when the host-guest gel is ruptured, broken surfaces have self-adhesiveness by reassuring the host-guest inclusion complexes[18]. This self-healing property is one of the hoped material design toward the low-carbon society. Furthermore, depending on the guest molecules, it is possible to add the photo-responsibility[17, 19]. The host-guest gel is expected not only the tough material but also the biomaterial such as and an artificial muscle[17, 20].

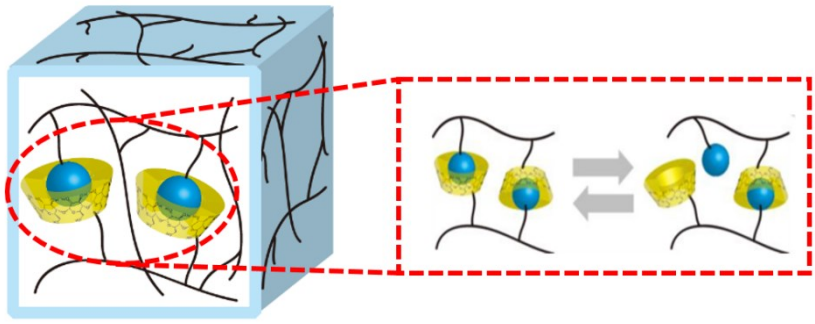

Figure 1-2. Schematic illustration of the dissociation/association process of host-guest interaction.

1-4. Supramolecular networks formed by topological crosslink

Cyclodextrins can also interact with a polymer chain and form a supramolecular complex. One of the most famous supramolecular complexes is the polyrotaxane developed by Harada *et al.*[21] Poly(ethylene oxide) chains are threaded through the cavity of α-cyclodextrin. In the polyrotaxane, α-cyclodextrin is not stabilized at a certain point of a polymer chain thus can slide along a polymer chain. Ito *et al.* developed the "slide-ring gel" utilizing this topologically

unique structure of polyrotaxane[22]. In the slide-ring gel, two cyclodextrins in polyrotaxanes are chemically connected and works as an eight-shaped topological crosslink. This crosslink can slide along the network strand, and accompanied entropy change is considered to contribute to the energy dissipation.

Recently, Takashima *et al.* reported the supramolecular elastomer formed by the "movable crosslink" utilizing a cyclodextrin. Figure 1-3 schematically shows the structure of the movable crosslinking network[23-24]. Their synthetic method is simple and one-step bulk polymerization: mixing hydrophobically modified cyclodextrin vinyl monomer and main chain vinyl monomer and polymerizing them result in the formation of an inclusion complex between them. In this system, a part of the polymerized backbone chain is threaded through the cavity of cyclodextrins attached to other chains. This method can easily introduce the movable crosslinks into the polymer structure. These movable crosslinking networks are revealed to show tougher mechanical properties than conventional bulk elastomers without movable crosslinks.

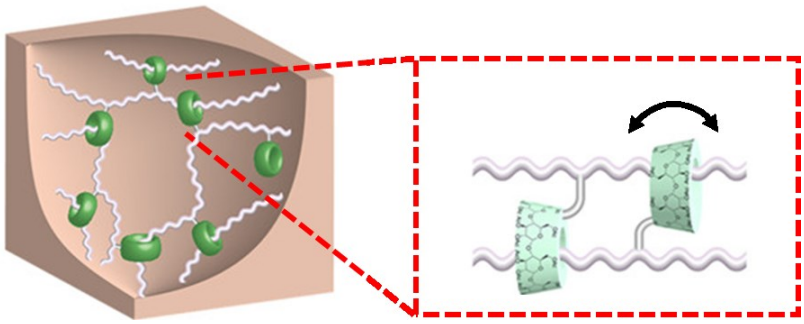

Figure 1-3. Schematic illustration of topological crosslinks and proposed sliding motion.

1-5. Scope of this thesis

The key objective of this thesis is to understand the molecular dynamics of the supramolecular networks formed by cyclodextrins and its derivatives shown in Figure 1-2 and 1-3. Based on

the rheological approach, the effect of the crosslinks formed by topologically specific ring-shaped molecules was investigated. Furthermore, the relationship between these topologically special structures and the toughing mechanism was studied. This thesis consists of five Chapters, including this Chapter.

In Chapter 2, the effect of the host-guest interaction on the dynamics of the networks is discussed. The host-guest gel is synthesized, which is formed by the host-guest interaction between β-cyclodextrin and adamantane introduced into the polymer side chain. This network should have only temporary crosslinks of host-guest interaction in the molecular design. However, this gel attains the equilibrium swollen state and does not dissolve even in a good solvent for main chains. In this Chapter, the dynamics of the temporary crosslinks via the host-guest interaction are investigated based on the linear viscoelastic measurements and observation of the swelling behavior. In particular, the role of the temporary crosslink in the network is investigated from the change in the dynamics when the host-guest interaction is inhibited by the addition of the competitor. Furthermore, the existence of the permanent crosslinks and possible network structures are discussed based on the NMR measurements.

In Chapter 3, the dynamics of the supramolecular network formed by the movable crosslinks are investigated. As discussed in Chapter 2, the topological structure in which a polymer chain is threaded through the cavity of the cyclodextrin exists in the host-guest gel. However, the effect of the topological structure on the dynamics of the whole network has not been investigated. In general, the linear viscoelastic measurements can connect the mechanical properties of the material and the dynamics of each relaxation mode, but it is difficult to evaluate and separate each mode quantitatively. In this Chapter, the dielectric measurement is focused on because the movable crosslink consists of the cyclodextrin that has a large dipole moment toward the axial direction. By the combination of the linear viscoelastic and dielectric measurements, the role of the movable crosslinks is discussed.

In Chapter 4, the nonlinear viscoelastic behavior of the movable crosslink is discussed by the large uniaxial deformation. The movable crosslinking network is stretched in the uniaxial direction with a constant crosshead speed, and the true stress-strain curves are obtained. The true stress shows large hysteresis, which might be due to the energy dissipation of the sliding motion induced by large deformation. The experimental results are reproduced by the constitutive equation consisting of the phenomenological BKZ model. Based on the temperature and deformation rate of the obtained fitting parameters, the behavior of the movable crosslinks is discussed.

In Chapter 5, the principal results and conclusion from Chapter 2 to Chapter 5 are summarized.

1-6. References

1. Ahmadi, M.; Hawke, L. G. D.; Goldansaz, H.; van Ruymbeke, E., Dynamics of Entangled Linear Supramolecular Chains with Sticky Side Groups: Influence of Hindered Fluctuations. *Macromolecules* **2015,** *48* (19), 7300-7310.
2. Callies, X.; Fonteneau, C.; Véchambre, C.; Pensec, S.; Chenal, J. M.; Chazeau, L.; Bouteiller, L.; Ducouret, G.; Creton, C., Linear rheology of bis-urea functionalized supramolecular poly(butylacrylate)s: Part I – weak stickers. *Polymer* **2015,** *69*, 233-240.
3. Lewis, C. L.; Stewart, K.; Anthamatten, M., The Influence of Hydrogen Bonding Side-Groups on Viscoelastic Behavior of Linear and Network Polymers. *Macromolecules* **2014,** *47* (2), 729-740.
4. Kumpfer, J. R.; Wie, J. J.; Swanson, J. P.; Beyer, F. L.; Mackay, M. E.; Rowan, S. J., Influence of Metal Ion and Polymer Core on the Melt Rheology of Metallosupramolecular Films. *Macromolecules* **2012,** *45* (1), 473-480.
5. Seiffert, S.; Sprakel, J., Physical chemistry of supramolecular polymer networks. *Chemical Society Reviews* **2012,** *41* (2), 909-930.
6. Sun, T. L.; Kurokawa, T.; Kuroda, S.; Ihsan, A. B.; Akasaki, T.; Sato, K.; Haque, M. A.; Nakajima, T.; Gong, J. P., Physical hydrogels composed of polyampholytes demonstrate high toughness and viscoelasticity. *Nat Mater* **2013,** *12* (10), 932-937.
7. Ihsan, A. B.; Sun, T. L.; Kuroda, S.; Haque, M. A.; Kurokawa, T.; Nakajima, T.; Gong, J. P., A phase diagram of neutral polyampholyte - from solution to tough hydrogel. *Journal of Materials Chemistry B* **2013,** *1* (36), 4555-4562.
8. Nakahata, M.; Takashima, Y.; Yamaguchi, H.; Harada, A., Redox-responsive self-healing materials formed from host–guest polymers. *Nature Communications* **2011,** *2* (1), 511.
9. Appel, E. A.; del Barrio, J.; Loh, X. J.; Scherman, O. A., Supramolecular polymeric hydrogels. *Chemical Society Reviews* **2012,** *41* (18), 6195-6214.
10. Yan, X.; Cook, T. R.; Pollock, J. B.; Wei, P.; Zhang, Y.; Yu, Y.; Huang, F.; Stang, P. J., Responsive Supramolecular Polymer Metallogel Constructed by Orthogonal Coordination-Driven Self-Assembly and Host/Guest Interactions. *Journal of the American Chemical Society* **2014,** *136* (12), 4460-4463.
11. Holden, G., Thermoplastic Elastomers. In *Rubber Technology*, Morton, M., Ed. Springer US: Boston, MA, 1987; pp 465-481.
12. Spontak, R. J.; Patel, N. P., Thermoplastic elastomers: fundamentals and applications. *Current Opinion in Colloid & Interface Science* **2000,** *5* (5), 333-340.
13. Rekharsky, M. V.; Inoue, Y., Complexation thermodynamics of cyclodextrins. *Chem Rev* **1998,** *98* (5), 1875-1917.
14. Harada, A.; Takashima, Y.; Nakahata, M., Supramolecular Polymeric Materials via Cyclodextrin–Guest Interactions. *Accounts of Chemical Research* **2014,** *47* (7), 2128-2140.
15. Kakuta, T.; Takashima, Y.; Nakahata, M.; Otsubo, M.; Yamaguchi, H.; Harada, A.,

Preorganized Hydrogel: Self-Healing Properties of Supramolecular Hydrogels Formed by Polymerization of Host–Guest-Monomers that Contain Cyclodextrins and Hydrophobic Guest Groups. *Advanced Materials* **2013,** *25* (20), 2849-2853.

16. Nakahata, M.; Takashima, Y.; Harada, A., Highly Flexible, Tough, and Self-Healing Supramolecular Polymeric Materials Using Host-Guest Interaction. *Macromol Rapid Commun* **2016,** *37*, 86–92.

17. Takashima, Y.; Hatanaka, S.; Otsubo, M.; Nakahata, M.; Kakuta, T.; Hashidzume, A.; Yamaguchi, H.; Harada, A., Expansion–contraction of photoresponsive artificial muscle regulated by host–guest interactions. *Nature Communications* **2012,** *3* (1), 1270.

18. Herbst, F.; Döhler, D.; Michael, P.; Binder, W. H., Self-Healing Polymers via Supramolecular Forces. *Macromol Rapid Comm* **2013,** *34* (3), 203-220.

19. Nakahata, M.; Takashima, Y.; Hashidzume, A.; Harada, A., Redox-Generated Mechanical Motion of a Supramolecular Polymeric Actuator Based on Host–Guest Interactions. *Angewandte Chemie International Edition* **2013,** *52* (22), 5731-5735.

20. Iwaso, K.; Takashima, Y.; Harada, A., Fast response dry-type artificial molecular muscles with [c2]daisy chains. *Nature Chemistry* **2016,** *8* (6), 625-632.

21. Harada, A.; Kamachi, M., Complex formation between poly(ethylene glycol) and α-cyclodextrin. *Macromolecules* **1990,** *23* (10), 2821-2823.

22. Okumura, Y.; Ito, K., The Polyrotaxane Gel: A Topological Gel by Figure-of-Eight Cross-links. *Advanced Materials* **2001,** *13* (7), 485-487.

23. Ikura, R.; Park, J.; Osaki, M.; Yamaguchi, H.; Harada, A.; Takashima, Y., Supramolecular Elastomers with Movable Cross-Linkers Showing High Fracture Energy Based on Stress Dispersion. *Macromolecules* **2019,** *52* (18), 6953-6962.

24. Ikura, R.; Ikemoto, Y.; Osaki, M.; Yamaguchi, H.; Harada, A.; Takashima, Y., Preparation of hydrophilic polymeric materials with movable cross-linkers and their mechanical property. *Polymer* **2020,** *196*, 122465.

Chapter 2

Effect of Host-Guest Interaction on the Dynamics of Polymer Networks

2-1. Introduction

Polymer gels are a three-dimensional crosslinked polymer network and contain a large number of solvent molecules. Especially for hydrogels, the solvent is water, and about 90 wt% of hydrogels' constituents are water. They have the potential to be used as biomaterials due to their excellent biocompatibility. One of the problems in the application of hydrogels is their mechanical brittleness. One reason for this mechanical brittleness is the inhomogeneity of the network structure, which induces stress concentration in the material. Polymer networks usually have a spatial heterogeneity of the crosslinking points due to the nature of chemical crosslinks. Moreover, a large amount of solvent in polymer gels makes the mechanical brittleness more prominent. For the last few decades, there have been many studies to improve the mechanical toughness of polymer gels.

Recently, Harada and Takashima *et al.* have developed the host-guest gel, which is known to be tough hydrogels[1]. In the previous study, it was shown that one of the host-guest gel exhibited more than 1000% rupture strain under uniaxial stretching and the resistance to large compression (~90%)[2], which is practically more useful than conventional chemically crosslinked gels. This host-guest gel is prepared by the radical polymerization of *β*-cyclodextrin-acrylamide (*β*CD-AAm) and adamantane-acrylamide (Ad-AAm) in addition to standard acrylamide monomers as main components. Therefore, the host-guest gel is designed to be a linear polymer chain having a few host and guest monomers randomly in one chain. In an aqueous solution, *β*-cyclodextrin and adamantine can form the stable inclusion complex

through hydrophobic interaction. The inclusion complexes with βCD-AAm and Ad-AAm are expected to work as temporary crosslinks.

Furthermore, the host-guest gel has a specific swelling property. From the molecular design viewpoint, the host-guest gels do not have any permanent crosslinks, and hence they are expected to be soluble in good solvents. However, the host-guest gel was insoluble to water, suggesting that both temporary crosslinks and some permanent crosslinks are involved. For conventional transiently crosslinked networks such as polyvinyl alcohol-borax and hydrophobically modified ethoxylated urethanes, the networks finally dissolve and cannot keep their original shape when they are immersed in the solvent. Theoretically, the swollen state in equilibrium is determined by the balance between the osmotic and elastic free energies[3-5]. The osmotic free energy of polymer gels is often described in the same manner as semi-dilute polymer solution[6-12]. On the other hand, the elastic free energy of the equilibrium swelling gel is determined by the plateau modulus, which is proportional to the number density of effective permanent crosslinks. Since temporary crosslinks dissociate in a finite time-scale, they do not contribute to the elastic free energy at equilibrium swelling state. In general, they dissolve in the equilibrium state and have terminal relaxation in a long time region. In this context, the swelling behavior of the host-guest gel is a surprising phenomenon, and further studies are desired.

As explained above, high mechanical toughness and unique swelling properties make the host-guest gel a particular entity. However, the molecular origin of these excellent properties remains unclear. In this Chapter, they are examined based on the host-guest gel's linear viscoelastic and swelling behaviors.

2-2. Experimental

2-2-1. Sample preparation of the host-guest gel

The preparation method of 6-acrylamido-*β*-cyclodextrin (*β*CD-AAm) and adamantane acrylamide (Ad-AAm) is discussed elsewhere[1]. An equivalent amount of βCD-AAm as a host monomer and Ad-AAm as a guest monomer were added in distilled water. This solution was mixed at 90°C for 3 hours to form and solubilize the inclusion complex between βCD-AAm and Ad-AAm. After the solution was cooled to room temperature, the solution was filtrated by a cellulose acetate filter with 0.8 μm pores to remove the insoluble Ad-AAm. Acrylamide (AAm) monomer, ammonium persulfate (APS), and *N, N, N′, N′*-tetramethylethylenediamine (TEMED) were added to this solution of inclusion complexes as the main chain monomer and an initiator. Then, the free radical copolymerization was performed at 25°C. AAm, APS, and TEMED concentrations were fixed at 2.0 mol L^{-1}, 0.020 mol L^{-1}, and 0.020 mol L^{-1}, respectively. The concentration of inclusion complexes at preparation, C_c, was 0.040 mol L^{-1}. Details of the preparation method were reported in the previous paper[2]. The transparent pre-gel solution was poured into a mold with 1 mm thickness or a capillary with 1 mm diameter and allowed to stand at 25°C for at least 12 hours in order to complete the reaction.

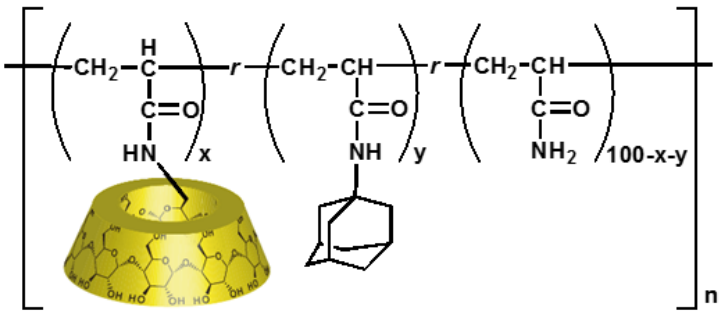

Figure 2-1. Chemical struvture of the host-guest gel used in this study.

2-2-2. Sample preparation and characterization of the linear polyacrylamide polymer

As a counterpart of the host-guest crosslinks, linear polyacrylamide (PAAm) polymers without host-guest interaction were synthesized. AAm monomer, APS and TEMED were dissolved in the distilled water and polymerized with the free radical polymerization at 25°C. The concentrations of AAm were tuned from 2.0 to 6.0 mol L^{-1}. All the samples were prepared under the condition that the ratio of the initiator concentration to that of the monomer was fixed to be 0.01, which is the same ratio used to prepare the host-guest gels.

Obtained samples were characterized using the size exclusion chromatography (SEC) measurements with a DAWN HELLEOS II multiangle light scattering (MALS) photometer (Wyatt Technology Co.) and an Optilab DSP interferometric refractometer (Wyatt Technology Co.). The elution solvent was 0.1 mol L^{-1} NaCl aqueous solution, and monodisperse linear poly(ethyleneoxide) purchased from TOSOH were utilized as the RI standards as well as the elution volume standards. Two SB-806M HQ (Shodex) columns were connected in series, and SEC OHpak SB-G 6B (Shodex) was used as a guard column. The flow rate was set to be 1.0 mL min^{-1}. Table 1 summarizes the weight-average molecular weight, M_w, and the polydispersity index, M_w/M_n, of the PAAm samples utilized in this study.

Table 2-1 Characteristics of the PAAm samples.

Monomer Concentration /mol L^{-1}	M_w / 10^5	M_w / M_n
2.0	5.86	2.55
4.0	5.74	2.34
5.0	7.24	3.38
6.0	5.83	2.47

2-2-3. Sample preparation of the host-guest gels with partially capped Ad groups

To understand the contribution of the βCD-Ad inclusion complex, the host-guest gels with

partially capped adamantane groups were prepared by introducing free *β*CD-AAm as an inhibitor. At first, the host-guest gels were swollen in distilled water until reaching equilibrium to remove the unreacted monomers. Then, they were immersed in *β*CD-AAm solution in which the concentration of *β*CD-AAm (C_{host}) was tuned from 0 to 4.0×10^{-3} mol L^{-1}. After swelling in the *β*CD-AAm solution for at least 1 day and reaching equilibrium swollen state, the host-guest gel samples were partly dried until the polymer volume fraction returned back to that at as prepared state. The partly dried samples were kept in the microtubes at room temperature for some days to achieve the equilibrium state. These samples have the same polymer volume fractions and different amounts of associative parts.

2-2-4. Sample preparation of the PAAm polymers including only *β*CD groups

To understand the contribution of the free *β*CD interaction to the dynamics of the host-guest gel, the PAAm polymers with only *β*CD side groups were prepared. AAm and *β*CD-AAm monomer were dissolved in the distilled water, and polymerized with the free radical polymerization at 25°C. APS and TEMED were used as the initiator. The concentrations of AAm, APS and TEMED were 2.0 mol L^{-1}, 0.020mol L^{-1}, and 0.020mol L^{-1}, respectively. The concentration of *β*CD-AAm ($C_{\beta CD}$) was tuned from 0 to 5.0×10^{-2} mol L^{-1}.

2-2-5. 1D and 2D nuclear magnetic resonance (NMR) measurements

The 1D ^{1}H NMR measurements were performed to evaluate the concentrations of host and guest monomers in the monomer solution after filtration. All the measurements were performed at 400 MHz with JEOL JNM-ECS 400 NMR spectrometer. 4,4-dimethyl-4-silapetane-1-sulfonic acid (DSS, 10 mM) was added as an internal standard in D_2O. Chemical shifts of all the NMR measurements were referenced to methyl protons of DSS ($\delta = 0$ ppm). Integral values of peaks in ^{1}H NMR spectra with δ_{ppm} = 5.15 (s, C_1H) for βCD-AAm, 2.05 (s, CH_2) and 2.15

(s, C*H*) for Ad-AAm were used for quantitative estimation.

To confirm the complex formation in PAAm polymers only including *β*CD groups, 2D NMR (NOESY) spectra were recorded at 600MHz with a VNMR system spectrometer (Agilent).

2-2-6. Linear viscoelastic measurements

The dynamic oscillatory and creep measurements were performed with the stress-controlled rheometer MCR302 (Anton Paar). All the measurements were performed using parallel-plate fixtures with 25 mm and 12 mm in diameters. For the dynamic oscillatory measurements, the angular frequency sweep tests were carried out from 0.1 to 100 s^{-1}. Measurements for the host-guest gels and those with partially capped Ad groups were carried out at 25°C. Measurements for the PAAm and those including only CD groups were carried out from 0 to 25°C. The oscillatory shear strain amplitudes for all the tests were within the range of linear regime. For creep measurements, the applied stress was ranged from 30 Pa to 50 Pa, which were preliminarily checked to be within the range of linear regime.

2-2-7. Observation of swelling behavior

Cylindrical host-guest gels are swelled in distilled water at 25°C and their diameter change to the equilibrium swollen state were monitored using an optical microscope (ECLIPSE400, NIKON). The swelling ratio, Q, were determined form the diameter ratio between as prepared state, d_0, and equilibrium swollen state, d_∞. Then, the polymer volume fraction at equilibrium swollen state, φ_e, were determined from Q and the polymer volume fraction at as prepared state, φ_0.

The swelling test of the host-guest gel in host monomer aqueous solutions (*β*CD-AAm aqueous solutions) were conducted similarly. For this measurement, cylindrical samples were

washed thoroughly to remove unreacted monomers before the measurements. After that, the samples were immersed in βCD-AAm aqueous solution with the concentration of 0.010 to 0.040 mol L^{-1}. The diameter change of cylindrical samples was measured and calculated the swelling degrees in βCD-AAm aqueous solutions.

2-3. Results

2-3-1. Characterization using ^{1}H NMR

Before discussing the linear viscoelasticity and swelling properties of the host-guest gel, the effective concentration of host and guest molecules before gelation were estimated using 1D NMR. From the ratio of integral values of corresponding peak to that of DSS standard, the concentration of βCD-AAm and Ad-AAm were calculated. Figure 2-2 shows the dependence on the feed concentration of the βCD-Ad complex (C_c) for the estimated concentrations of βCD-AAm and Ad-AAm (C_{CD} and C_{Ad}, respectively) in the pre-gel solution after filtration. Both C_{CD} and C_{Ad}, increased linearly with increasing C_c, and the slopes of C_{CD} and C_{Ad} were 1.0 and 0.56, respectively. These results suggests the βCD-AAm completely dissolve in distilled water, but the Ad-AAm are almost 60% of the feed concentrations. Since Ad-AAm is hydrophobic and bulky guest monomer and neat Ad-AAm cannot dissolve in water, only when βCD-AAm and Ad-AAm form the inclusion complex, it can dissolve in water. As a result, only 60% of Ad-AAm were incorporated into the host-guest gel when polymerized.

Based on these results, the number of host-guest inclusion complexes, the βCD groups which do not form the inclusion complex, and entanglements per chain are summarized in Table 2-2. These values are estimated from the plateau modulus of G' at ω = 0.1 s^{-1} at 25°C for each crosslinker concentration based on the affine network model and molecular weight of a polymer chain in Table 2-1. The βCD groups which do not form the inclusion complex with Ad is denoted as free βCD.

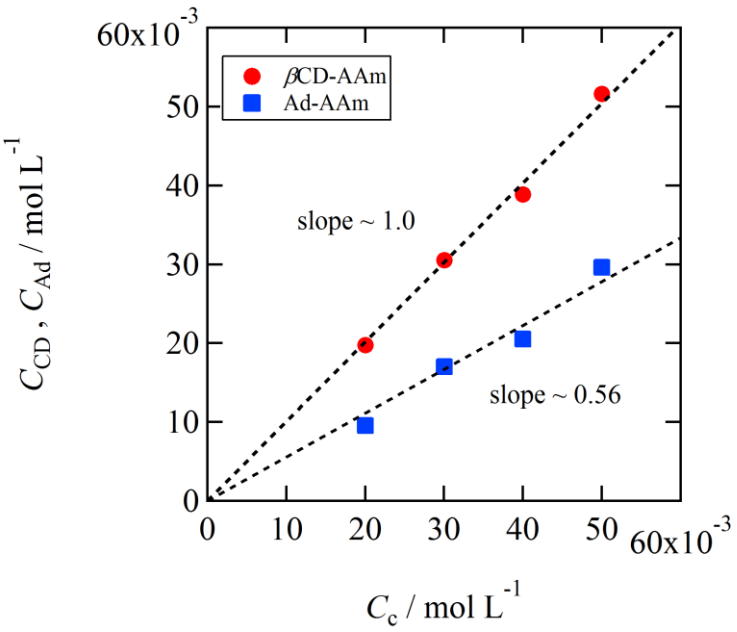

Figure 2-2. Concentrations of host monomer and guest monomer in the monomer solution against the feed concentration, C_c.

Table 2-2. Characterization of host-guest gels.

C_c / mol L^{-1}	Entanglements per chain	Free βCD per chain	βCD-Ad complexes per chain
0.020	6.76	29.3	37.3
0.030	8.69	40.8	52.0
0.040	9.65	47.8	60.8
0.050	13.6	53.5	68.1

2-3-2. Linear viscoelastic measurements for the host-guest gel

Figure 2-3 shows the frequency dependence of the storage and loss moduli for the host-guest gel with C_c = 0.040 mol L^{-1} and the composite curve of PAAm solutions. The composite curve of polyacrylamide solution was constructed from the data at monomer concentration equal to 2.0, 4.0, 5.0, and 6.0 mol L^{-1}. G' and G'' of each concentration were vertically and horizontally shifted to overlap with each other based on the scaling theory of entangled polymer solutions. The reference concentration is 2.0 mol L^{-1}.

For the host-guest gel, G' was always higher than G'' in the whole frequency range examined in this study. Both G' and G'' monotonically decreased with decreasing angular frequency, ω, but the plateau region was not observed definitely. Furthermore, in ω = 100 – 10 s^{-1}, G'' show the frequency dependence, $G'' \sim \omega^{0.5}$, which is attributed to the Rouse relaxation mode of polyacrylamide chains[13]. On the other hand, for the polyacrylamide solutions, typical spectra for entangled polymer solutions is observed. G' and G'' shows the crossover at $\omega \sim 100$ s^{-1}, which suggests that the relaxation process from rubbery plateau to terminal relaxation in this frequency range. Compared with the polyacrylamide solutions, the Rouse mode of the host-guest gel is significantly delayed. This means that the friction coefficient of the network chains is higher for the host-guest gel than that for the solutions. The higher friction is attributed to the association and dissociation process of the host-guest inclusion complexes. In addition, the both rubbery plateau moduli for the host-guest gel and polyacrylamide solution are same order (G_{ent}: dotted line), which indicates the host-guest is basically the entangled network.

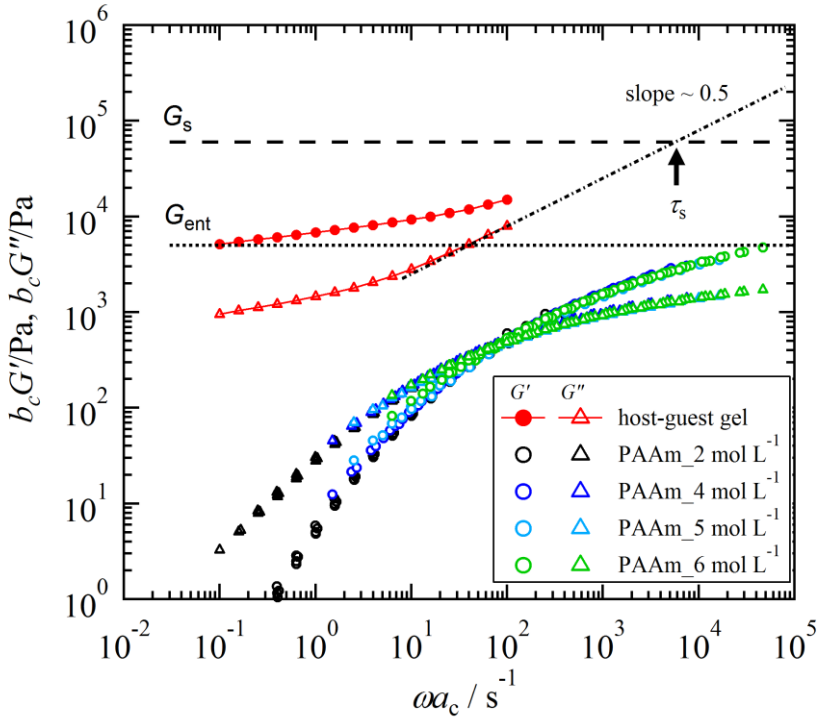

Figure 2-3. Frequency dependence of G' (circle) and G'' (triangle) measured at 25°C for the host-guest gel with $C_c = 0.040$ mol L^{-1} and the composite curve constructed by the superposition of the G' and G'' data for PAAm solutions with different monomer concentrations, 2.0, 4.0, 5.0, and 6.0 mol L^{-1}, where 2.0 mol L^{-1} was chosen as standard. The measurements were performed at 0 - 25°C and the results were referred to 25°C.

To describe the above characteristics of G' and G'', the sticky reptation model is adopted[14]. The sticky reptation model has been proposed by Leibler, Rubinstein, and Colby, to consider the effects of temporary crosslinks (stickers) on reptation dynamics of the entangled networks composed of linear chains (reptation model). In this model, each chain has sticky points, and consequently the segmental and reptation dynamics are influenced by the life time of the stickers, τ_s. The frequency dependence of the storage modulus for the sticky reptation model is depicted in Figure 2-4. Compared with the ordinary entangled system represented by the broken line, on the frequency scale of $(\tau_e^0)^{-1}$ (the equilibration time of an entangled strand) $> \omega > \tau_s^{-1}$, an additional rubbery plateau region with $G_s \propto \nu_s k_B T$ appears, originating from the

network formed by temporary crosslinks. Here, ν_s is the number density of stickers. At the time when the temporal crosslinks break (= τ_s), the modulus reduces to the plateau originating from pure entanglements through the Rouse mode. The terminal relaxation motion (reptation) is remarkably delayed compared with that of ordinary entangled polymers, because the chains need to reptate in the tube accompanied by breaking the stickers. Based on this model, the life time of the stickers is roughly estimated to be ~ 2×10^{-4} s from the cross point of the Rouse mode and the plateau originating from the stickers shown in Figure 2-3. This evaluated value is smaller than the dissociation time previously reported (~ 10^{-2} s) for αCD and guest molecules[15].

It should be noted that the sticky reptation model gives only finite relaxation time estimated by the delay of the Rouse mode. Then, the longest relaxation time in the Rouse modes of the host-guest gel and polyacrylamide solutions, τ_e and τ_e^0, are calculated, respectively. The τ_e is estimated from G' in the power low range where $G' \sim a\omega^{0.5}$. According to Osaki *et al.*, the longest Rouse relaxation time τ_R can be evaluated from the coefficient a with $\tau_R = (aM/1.111cRT)^{0.5}$, where c is the polymer concentration, M is the molar mass, R is the gas constant, T is the absolute temperature[16]. From this relationship, τ_e is estimated to be 1.93 s. On the other hand, since the Rouse relaxation is not observed for polyacrylamide solutions, τ_e^0 is estimated from the viscosity. The relationship between τ_R and η for a well-entangled system ($M \geq 1.5M_e$) in a good solvent is described as follows:

$$\tau_R = \frac{6M\eta}{\pi^2 cRT}\left(\frac{1.5M_e}{M}\right)^{2.4}$$

From this relationship, τ_e^0 is estimated to be 4.43×10^{-4} s.

In Figure 2-5, the PAAm composite curve is horizontally shifted so that τ_e become equal to τ_e^0. The terminal relaxation time is estimated to be located in $\omega \sim 10^{-3}$ s^{-1}. However,

the dynamic viscoelastic measurement cannot cover such a wide range of frequencies. Thus, in the following section, the terminal relaxation behavior of the host-guest gel will be discussed based on the creep measurement.

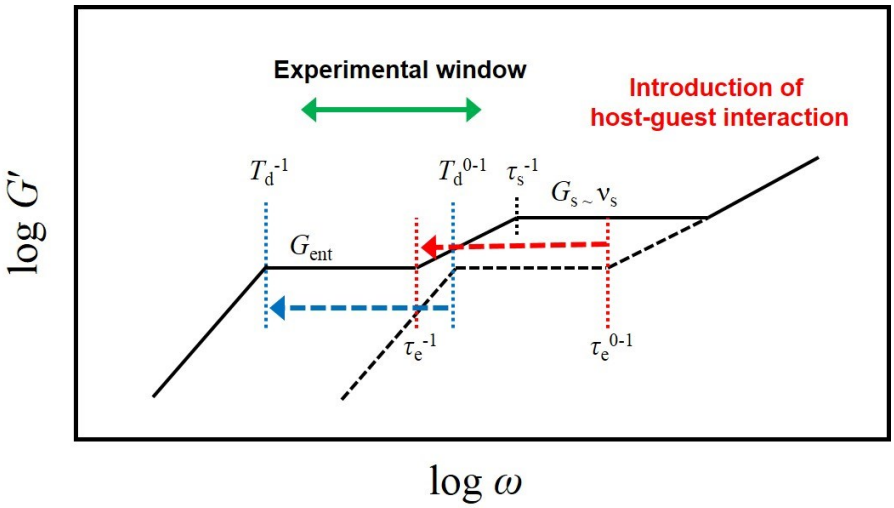

Figure 2-4. Illustration of storage modulus for the ordinary entangled system (broken lines) and sticky reptation model (continuous lines).

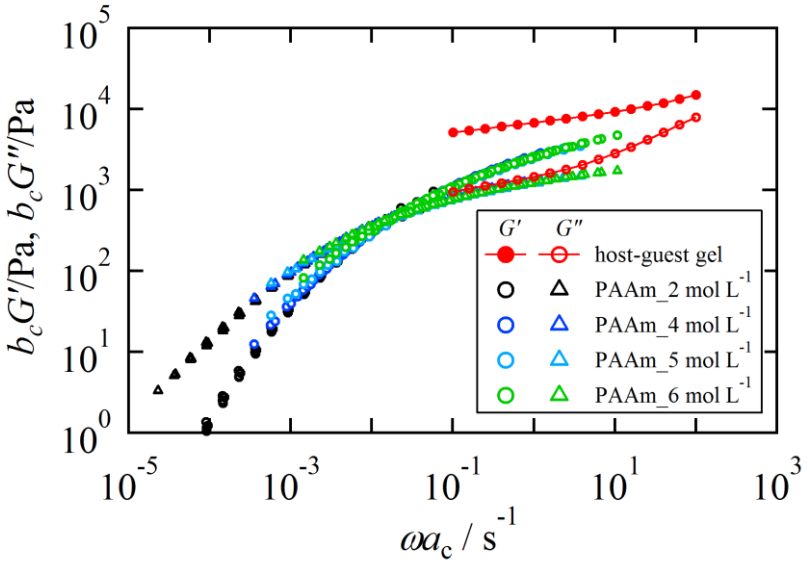

Figure 2-5. Frequency dependences of G' and G'' for PAAm and the host-guest gel of C_c = 0.040 mol L^{-1}. PAAm composite curves are horizontally shifted to correspond τ_e^0, with τ_e.

2-3-3. Creep measurements for the host-guest gel

To evaluate the relaxation behavior in the longer time region, creep measurements were performed. Figure 2-6 shows the time dependence of creep compliances, $J(t)$, of the host-guest gel with C_c = 0.040 mol L^{-1} at as prepared state and equilibrium swollen state in water. $J(t)$ calculated from the results of linear viscoelastic measurements are also included as black dotted lines. In this calculation, G' and G'' were firstly described using the discrete relaxation spectrum as follows;

$$G'(\omega) = \sum_p h_p \frac{\omega^2 \tau_p^2}{1+\omega^2 \tau_p^2} \tag{2-1}$$

$$G"(\omega) = \sum_p h_p \frac{\omega \tau_p}{1+\omega^2 \tau_p^2} \tag{2-2}$$

Here, h_p and τ_p are the relaxation strength and time of the p-th component. The relaxation modulus can be written as follows.

$$G(t) = \sum_p h_p \exp\left(-\frac{t}{\tau_p}\right) \tag{2-3}$$

According to the linear viscoelastic theory, the relationship between $G(t)$ and $J(t)$ is expressed in the following equation

$$\int_0^\infty J(t-t')G(t)\mathrm{d}t' = t \tag{2-4}$$

The relaxation strength and times of each mode were extracted by eqs. 2-1 and 2-2, and $J(t)$ was numerically estimated from eq. 2-4 with $G(t)$ described by eq. 2-3. $J(t)$ obtained from the creep experiment and that obtained by eq. 2-4 overlapped with each other. This result indicates

that creep measurements were successfully performed within the linear viscoelastic regime. $J(t)$ gradually increases with increasing the time, and in the long time region ($t \sim 10^4$ s), $J(t)$ looks like to reach a constant value which corresponds to the equilibrium compliance, J_N. This could also be supported by the monotonic decrease of shear rate during the creep test shown in Figure 2-7. Even the swollen sample also exhibited similar behavior with the as prepared sample. These results suggest that the host-guest gel behaves as a viscoelastic solid and have some kinds of long-lived crosslinks within the experimental time scale examined in this study. To further investigate the origin of the long-lived crosslinks in the host-guest gels, the swelling behavior of the host-guest gels is observed in the next section.

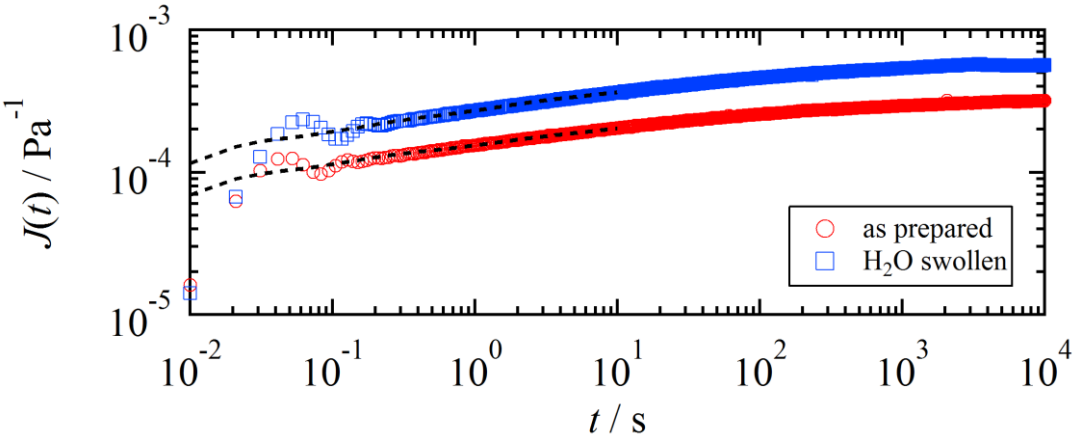

Figure 2-6. Creep compliances as a function of time. Black circle and gray square symbols represent $J(t)$ of as prepared state and equilibrium swollen state, respectively. Dashed lines represent $J(t)$ estimated from the linear viscoelastic measurements. Both measurements were performed at 25°C.

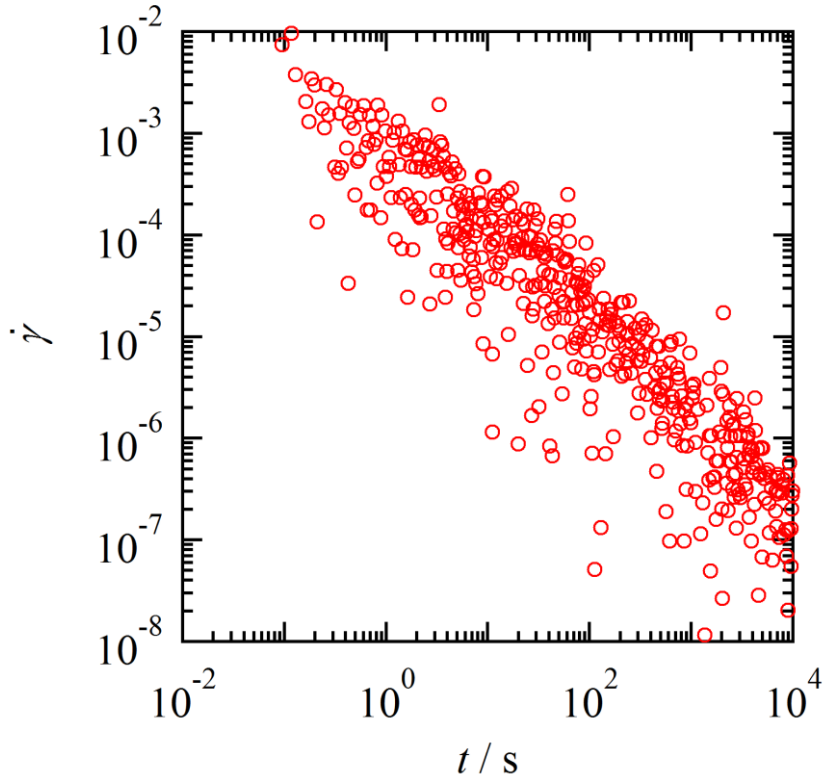

Figure 2-7. Time dependence of the shear rate under the creep test for the as prepared sample at 25°C.

2-3-4. Swelling behavior of the host-guest gel

As discussed in the above sections, the host-guest gel behaves as if it is the viscoelastic solid, even though it does not include any permanent crosslinks in this molecular design. To consider whether the host-guest gel is really a viscoelastic solid or eventually behaves like a liquid over a very long period of time, the swelling behavior was examined. Figure 2-8(A) shows the time dependence of the gel diameter in the swelling process of the host-guest gel with C_c = 0.040 mol kg^{-1}. Here, $d(t)$ and d_0 are the diameter of cylindrical gel at time t and t = 0, respectively. The gel diameter increased with increasing time and reached the constant value, which indicated the host-guest gel reached an equilibrium swollen state. This is similar swelling behavior with chemically crosslinked gels. According to Tanaka *et al.*, the swelling behavior of a polymer gel is dominated by the cooperative diffusion of network strands and solvent molecules[17-18]. They

observed the swelling behavior of spherical gels consisting of polyacrylamide in a good solvent, and determined the swelling function d_n defined by eq 2-5. The time dependence of d_n is known to be approximated by a single exponential decay function at a long time region.

$$d_n = \frac{d_\infty - d(t)}{d_\infty - d_0} \approx \frac{6}{\pi^2} \exp\left(-\frac{t}{\tau}\right) \tag{2-5}$$

where d_0 is the gel diameter in the initial state, $d(t)$ is the gel diameter at time t, and d_∞ is the gel diameter at the equilibrium swollen state. Figure 2-8(B) shows a semi-logarithmic plot of the time dependence of d_n for the host-guest gels with different C_c. The results of fitting by eq. 2-5 in the long time region are also shown with black dotted lines. Only single relaxation process over a long time region was observed for each of a host-guest gel, and the experimental values and fitting results show good agreement in the long time region. The apparent relaxation time τ of the cylindrical gels can be determined from this fitting.

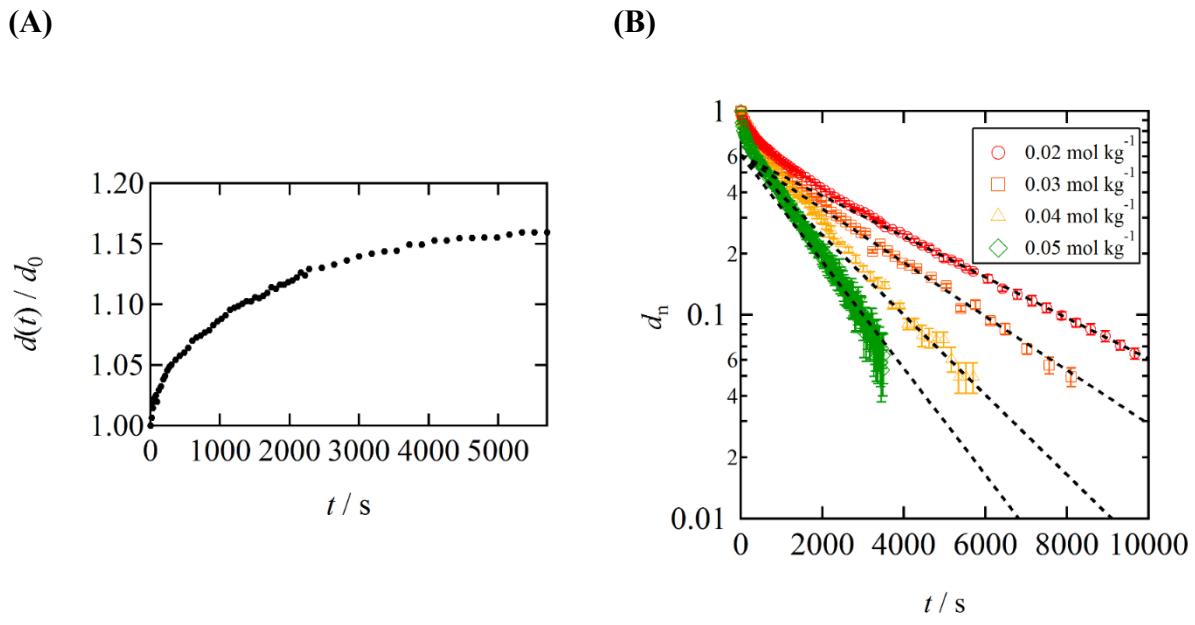

Figure 2-8. (A) Time dependence of the normalized diameter $d(t)/d_0$ in the swelling process. (B) The time dependence of normalized diameter change, d_n, of host-guest gels. Black dotted lines represent the fitting curves derived from eq. 2-5.

For chemically crosslinked gels, the relaxation time in a swelling process depends on the diameter d_∞ and swelling ratio in the case of a cylindrical gel, and it also depends on the cooperative diffusion coefficient D of the network strand. Therefore, the comparison should be made with D instead of τ to ignore the difference of d_∞. The coefficient D in the cylindrical gel is estimated by the following equation from τ in the swelling process[18-20]:

$$D = \frac{3d_\infty^2}{8\pi^2\tau} \tag{2-6}$$

This relationship is adopted to the swelling process of the host-guest gels. Figure 2-9 shows the C_c dependence of D calculated from the relaxation time τ and the gel diameter d_∞ obtained from fittings by eq. 2-5. D was slightly larger at C_c = 0.050 mol kg^{-1}, but became almost constant (~ 2.2×10^{-7} cm^2 s^{-1}) independent of C_c. This average value is consistent with the order of diffusion coefficient (10^{-6} ~ 10^{-7} cm^2 s^{-1}) in the swelling/shrinking process of general polymer gels[19], and also with the coefficient (~ 3×10^7 cm^2 s^{-1}) for the chemically crosslinked acrylamide gel reported by Tanaka *et al*[17].

These results suggest that cooperative diffusion of the network strands of the host-guest gel in the swelling process is hardly affected by the host-guest interaction, although the linear rheological dynamics is significantly delayed by the host-guest interaction. According to Li and Tanaka, D in the swelling process of polymer gels can be related to the moduli as $D = (K + 4G/3)/\zeta$, where K is the bulk modulus associated with the osmotic pressure, G is the network shear modulus, and ζ is the friction coefficient of the network strand[18]. In the case of the host-guest gel, D is generally rewritten as $D \approx K/\zeta$ because K is much larger than G. In the temperature range of this measurement (~ 25°C), the rate of dissociation and reassociation of the host-guest crosslinking is sufficiently fast (~ 2×10^{-4} s)[15, 21]. Therefore, in the time scale of the swelling process, the sticker itself has almost no effect on the bulk modulus since the whole

network structure composed mainly of trapped entanglements is essentially unvaried at C_c > 0.02 mol kg^{-1}. Furthermore, viscoelastic measurements revealed that the Rouse mode of network strands was significantly delayed by the sticker, but relaxation similar to the usual entanglement system was observed after the sticker relaxation. When the dissociation and reassociation time scale of the sticker is sufficiently fast, the host-guest crosslink does not apparently act as a sticker in that time scale, and has no role in changing the friction coefficient of the network strand ζ, significantly in the swelling process. Therefore, D does not depend on the concentration of the host-guest crosslinks.

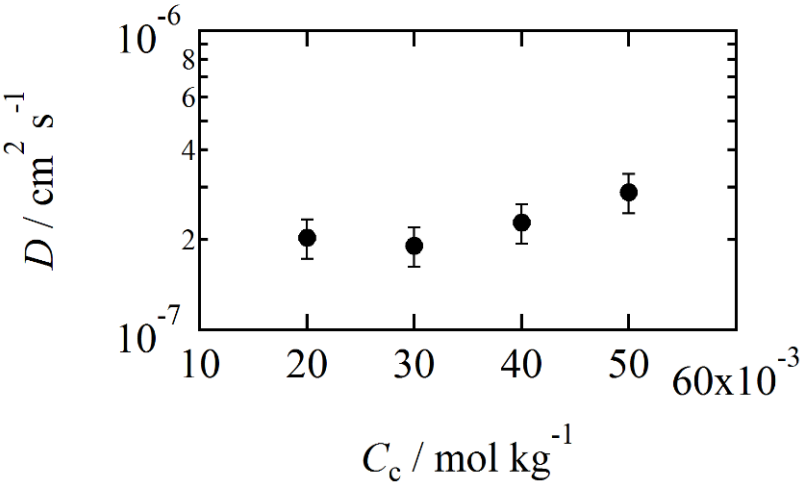

Figure 2-9. The feed crosslinking concentration C_c dependence on the diffusion coefficient D calculated by eq. 2-6.

2-3-5. Swelling behavior in the existence of host-competitors

To ensure the host-guest gel is viscoelastic solid or not, it is investigated how the host-guest gel swells in the host-competitor solution. If the host-guest gel has only temporary crosslinks formed between βCD and Ad molecules as designed, the host-guest gel is expected to dissolve in sufficiently high competitor (βCD-AAm) concentration and not show any equilibrium swollen state. Figure 2-10 shows the host competitor (βCD-AAm) concentration C_{Host}

dependence of the polymer volume fractions at the equilibrium swollen state φ_{e2} under coexistence of host competitor for the host-guest gel with different C_c. The result of φ_{e2} with $C_{Host} = 0$ corresponds to the result with no competitor. φ_{e2} decreases with increasing C_{Host}, but shows the constant value independent of C_{Host} over a certain C_{Host}.

In general, the equilibrium swollen state of the polymer gel is determined by Flory-Rhener's equation[4]. In this equation, the equilibrium swollen state is determined by the balance between the mixing energy and the elastic energy of the network. The relationship is described using the following equation;

$$\nu V_c \left[\frac{\varphi}{2\varphi_0} - \left(\frac{\varphi}{\varphi_0}\right)^{1/3}\right] = \ln(1-\varphi) + \varphi + \chi\varphi^2 \qquad (2\text{-}7)$$

Where φ_0 and φ represent the polymer volume fractions in the reference state and the equilibrium swollen state, ν is the effective network chain density, V_c is the unit volume of the solvent, χ is the interaction parameter of the network chain. When the guest molecules started to be capped with the introduction of the competitive agent, the affinity between the solvent and the network strand could be increased by suppressing the hydrophobicity of guest molecules. In short, the degree of swelling is increased with the reduction of the apparent χ.

In addition, C_{Ad} determined by 1H NMR measurements are also shown by black arrows. The threshold values are with good agreements with C_{Ad}. These results suggest that the host-guest gel is viscoelastic solid and the host-guest interaction behaves like a temporary crosslink with a finite life time. Next, I discuss more details of the host-guest interaction in the swelling state. Since φ_{e2} decreased exponentially with respect to C_{Host}, fitting was performed using the following equation;

$$\varphi_{e2} = \varphi_{pla} + A\exp\left(-\left(\frac{C_{Host}}{C}\right)^{B}\right) \quad (2\text{-}8)$$

where φ_{pla}, A, B, and C are fitting parameters. φ_{pla} corresponds to the polymer volume fraction of the host-guest gels when it does not depend on C_{Host}. The fitting result by eq. 2-8 is also shown in Figure 2-10(A) with black dotted lines. The C_{Host} dependence of φ_{e2} could be described well by eq. 2-8 and C_c dependence of φ_{pla} was obtained. The result is shown in Figure 2-10(B). Though the experimental error at C_c = 0.020 mol kg^{-1} is a little bigger, φ_{pla} increased linearly with increasing C_c. In the state where φ_{e2} is equal to φ_{pla}, it is considered that all temporary crosslinks are dissociated, and all guest molecules are capped because the threshold values of C_{Host} are equal to C_{Ad}. These results suggest that some kinds of the permanent crosslinks except host-guest crosslinks exist in the host-guest gel.

(A)

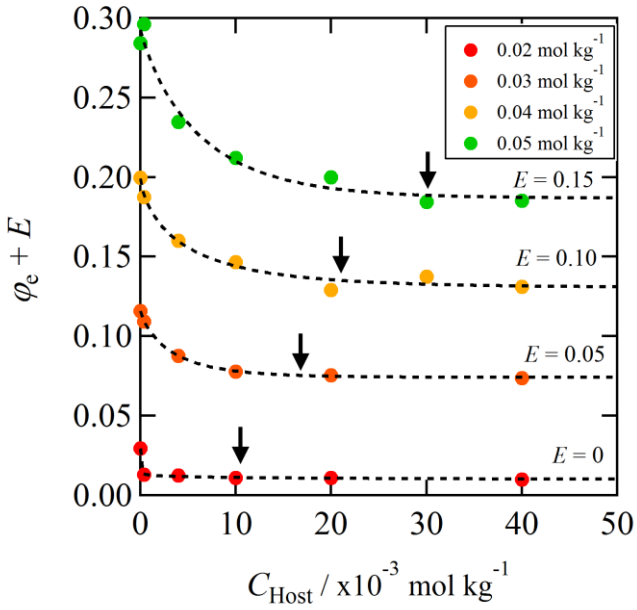

(B)

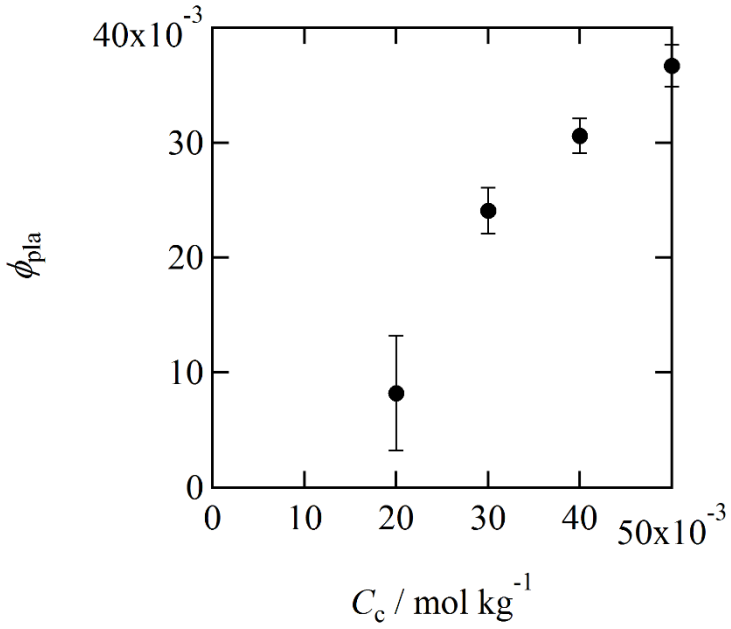

Figure 2-10. (A) Polymer volume fractions φ_{e2} for the host-guest gels in various host solution as a function of host competitor concentration C_{Host}. E is the vertical shift factors to show the results clearly. Black dotted line represents the experimental result, and the fitting line derived by eq. 2-8. (B) The C_c dependence of φ_{pla}.

2-3-6. Dynamic oscillatory measurements for the host-guest gel with partially capped Ad groups

To promote the dissociation of the host-guest interaction, it is investigated the viscoelastic properties of the host-guest gels in which the amount of the temporary chains is precisely tuned by swelling in βCD competitor aqueous solutions with different C_{Host}. The results of frequency sweep measurements of G' and G'' for these samples are shown in Figure 2-12. The values of G' and G'' decrease with increasing C_{Host}, and the frequency dependence becomes slightly weaker. As for lower C_{Host} samples, G' and G'' are proportional to $\omega^{0.5}$ in the high-frequency region, which is the typical behavior of the Rouse mode ($G' \sim G'' \sim \omega^{0.5}$) [13]. Generally, it can be observed in a higher frequency region for polymer solutions or gels. Figure 2-13 shows the composite curves constructed only horizontally shifting G' and $G''$for the host-guest gels with different C_{Host}. Here, the data with C_{Host} = 0 M (as prepared state) was employed as a reference state, and the data with high C_{Host} were shifted to a lower frequency region with increasing C_{Host}. Furthermore, this composite curve well overlapped the complex modulus evaluated from the creep compliance for the reference sample. This correspondence is the same analogy with the time-temperature superposition. The conventional time-temperature superposition means that all the molecular modes from local to global motions are governed by the single temperature-dependent friction coefficient. This correspondence means that the host-guest interaction retards the Rouse molecular motion of the network strands and works only as a sticker defined in the sticky reptation model. These results suggest that not only host-guest interaction but also a new class of permanent crosslink must exist in the host-guest gel. Considering the composition of the host-guest gel, the free βCDs could affect the permanent crosslink. For this purpose, the PAAm only including the βCD groups are synthesized and dynamic viscoelastic properties are investigated in the next section.

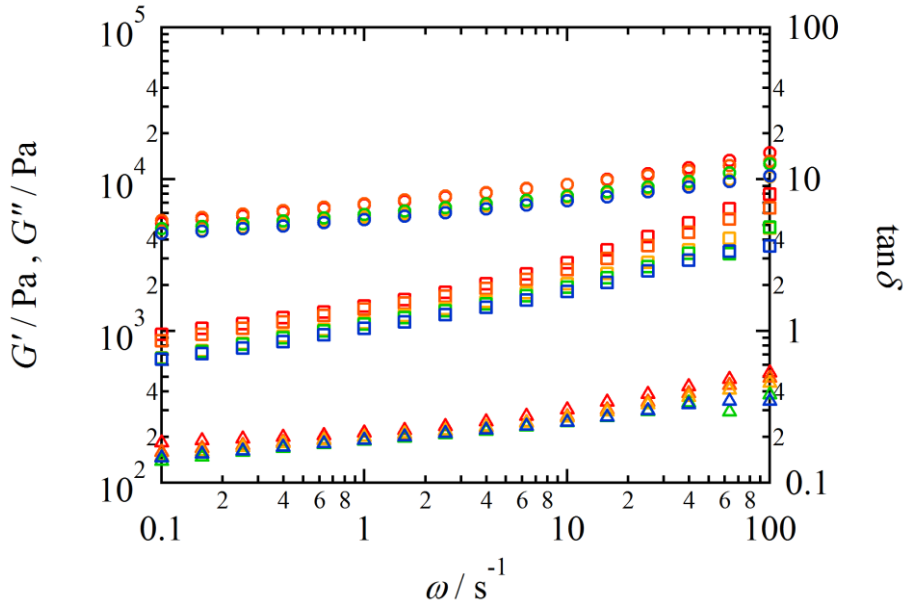

Figure 2-12. Frequency dependences of G' (circle), G'' (square) and tanδ (triangle) for the host-guest gels swollen in solutions of various host monomer concentrations (Red: C_{Host} = 0 mol L^{-1}, Orange: C_{Host} = 0.010 mol L^{-1}, Yellow: C_{Host} = 0.020 mol L^{-1}, Green: C_{Host} = 0.030 mol L^{-1}, Blue: C_{Host} = 0.040 mol L^{-1}). All measurements were performed at 25°C.

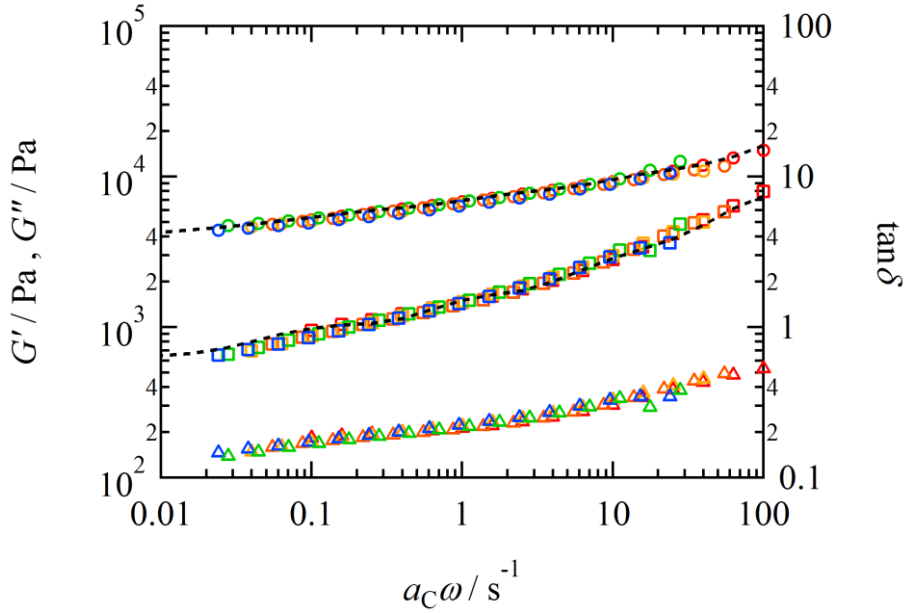

Figure 2-13. Composite curve of the frequency dependence of storage and loss moduli for the host-guest gels with various C_{Host} at 25°C.

2-3-7. Dynamic oscillatory measurements for the PAAm polymer including only βCD.

To evaluate the effect of free *β*CD groups, the viscoelastic properties of the PAAm polymers introduced only *β*CD groups (*β*CD polymer) are investigated. Frequency sweep results of G' and G'' for these samples are shown in Figure 2-14. The results of the host-guest gel with C_c = 0.020 mol kg^{-1} and PAAm composite curve are also shown. For the samples with lower $C_{\beta CD}$, the power-law relaxation close to $G' \sim \omega^2$ and $G'' \sim \omega^1$ was observed, which indicates the similar behavior with PAAm composite curves. On the other hand, for the samples with higher $C_{\beta CD}$, the slopes of G' and G'' becomes closer, which is similar to the critical gel behavior, *i.e.*, $G' \sim G'' \sim \omega^{n}$[22-25]. Further increasing $C_{\beta CD}$, G' always become higher than G'', and the second plateau region of G' is observed in the low ω region as well as the host-guest gel. Comparing these data with PAAm composite curve, the longer relaxation component becomes pronounced accompanied by increasing $C_{\beta CD}$, while the plateau modulus originating from entanglements does not seem to be changed.

As discussed in the previous section, the *β*CD-Ad complex simply retards the Rouse mode, which is qualitatively different from this system. These characteristics in the terminal relaxation region are similar to the relaxation of the entangled branched polymers. Studies on entangled branched polymers including the star-shaped polymers[26-29] revealed that G' and G'' in the terminal flow region showed the broader relaxation mode distribution compared with that of the linear polymer while the rubbery plateau modulus is not affected by branching. These features have been explained by the reptation model considering the retraction of branches in a tube. The data shown in Figure 2-14 strongly suggests that *β*CD causes some crosslinks or junction points with a long life time, $T_L > T_d^0$, and the effect of branching is demonstrated in Figure 2-14. The small number of branches does not affect the height of the rubbery plateau modulus but increases only the terminal relaxation time. This effect would disappear on a longer time scale than T_L. With increasing branching points, the broadening of the terminal flow region

becomes significant. Above a certain threshold of branches, the system can be percolated or gelated, resulting in the appearance of another plateau region. It should be noted that the plateau modulus at low-frequency region for βCD polymer was approximately 300 Pa at the highest concentration: $C_{\beta CD}$ = 0.050 mol kg^{-1}. Based on the affine network model, the number density of the crosslinks is calculated to be 0.12 mol m^{-3}. This value corresponds to only 0.24% of the total βCD molecules compared with the feed concentration. Thus, the number of junctions is much less than that of entanglements, and the lifetime of the junction is longer than T_D^0.

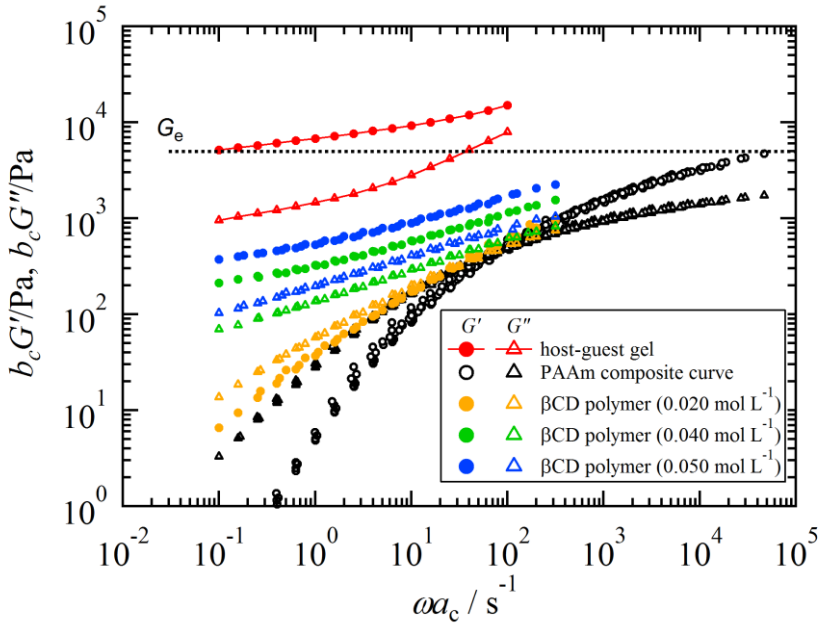

Figure 2-14. Frequency dependences of G' (circle) and G'' (triangle) for the βCD polymers (Yellow: $C_{\beta CD}$ = 0.020 mol L^{-1}, Green: $C_{\beta CD}$ = 0.030 mol L^{-1}, Blue: $C_{\beta CD}$ = 0.050 mol L^{-1}). Black symbols represent the composite curve for the PAAm, and red lines represent the data for the host-guest gel.

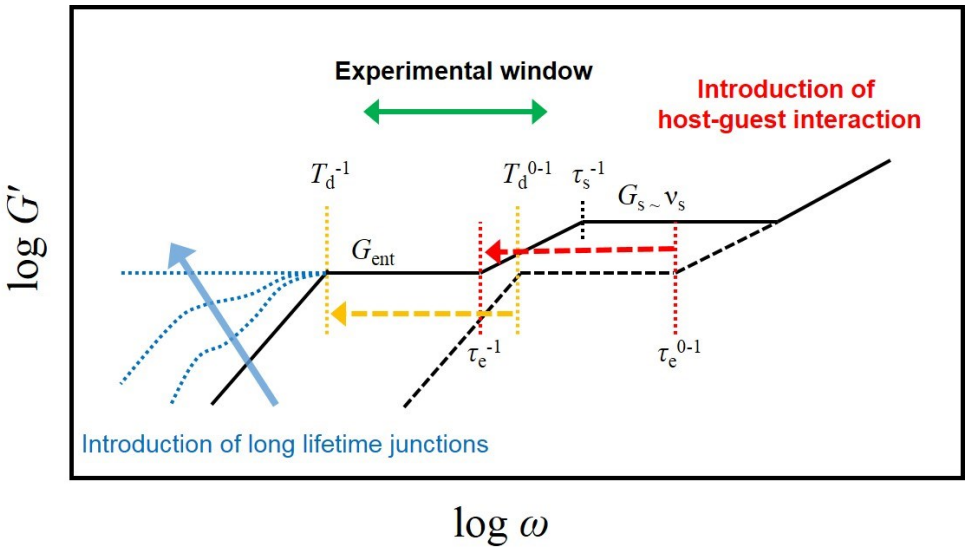

Figure 2-15. Illustration of storage modulus for the reptation model having a few long lifetime junction points (blue lines). Some chains behave as branched chains.

2-3-8. 2D NMR Measurements of *β*CD Polymer

One of the possible reasons for the appearance of the second plateau region is the formation of topological junction structures such as rotaxane architectures between *β*CD and the main chain. In previous work, Harada *et al.* reported that polyethylene glycol forms the inclusion complex with *α*CD in an aqueous solution, and forms the physically crosslinked gel[30]. To confirm such an inclusion formation, they examined (1) X-ray scattering of the crystalline sample, (2) chemical shift of the 1D HNMR, and (3) 2D nuclear Overhauser enhancement (NOESY) NMR. X-ray scattering is the most reliable way to confirm the complex formation. The pioneering study elucidated that, when the polyrotaxane structure was formed, polymer chains took the extended column structure in the crystalline state, which could be detected by the X-ray diffraction[31]. Unfortunately, in my case, samples are in the gel state, and it is difficult to prepare the crystalline samples. In the second method, the NMR peaks from the guest molecules in the inclusion complex would shift or split up, depending on the condition whether the exchange rate is faster or slower than the NMR time scale, respectively. However, the pronounced peak

shift was not observed because the peaks from the main chains are broadened, and only less than 1% of the *β*CD is expected to form the inclusion complex as discussed in the previous section. The third one, which was employed here, is widely used for spatial relationships among protons. The NOE is observed by the cross-relaxation of nuclei that are spatially close. When the inclusion complex is formed, the signals of the *β*CD proton directing toward the inside of the cavity are higher than those directed toward the outside of the cavity as shown in Figure 2-16(A). The 2D NOESY NMR spectrum of the *β*CD polymer ($C_{\beta CD}$ = 0.020 mol L^{-1}) in the D_2O solution is shown in Figure 2-16(B). The spectrum showed that the signals of H-3, 5, 6 protons of *β*CD, which are directed toward the inside of the cavity, correlate with the resonance of the CH_2 of the PAAm main chains. Furthermore, the strength of the correlation between H-3, 5, 6 protons and main chains are higher than from H-2,4 protons, which are directed toward the outside of the cavity. These results suggest that the main chain threads through the cavity of βCDs, which supports the molecular speculation. It should be noted that the 2D NOESY for the mixture of PAAm polymers and the *β*CD molecules are also measured. In this measurement, the signals of the *β*CD proton directing toward the inside of the cavity were higher than those directed toward the outside, which also indicates the penetration between the main chains and *β*CDs. According to all the obtained data, the *β*CD molecules in the host-guest gel take three states. Half of the *β*CDs forms the complex with Ad, less than 1% of the *β*CDs forms the complex with PAAm (penetrating the main chains), and the remaining *β*CD does not form any complex.

Finally, we make a brief comment on the outstanding toughness of the host-guest gel. The toughness of the host-guest gel can be attributed to two origins. Firstly, the basic network structure of the host-guest gel is the entangled network. Entanglements work as crosslinks but they can prevent the stress concentration of network strands by working like a pulley. The life time of the host-guest inclusion complex is rather short, and the complex works as the sticky

points to retard the segmental and reputation motions significantly. Secondly, a very small amount of rotaxane structures between βCDs and main chains exist and work as permanent crosslinks. These permanent crosslinks prevent the entire reptation mode of the chain and make the terminal relaxation time infinite, resulting in the gel-like behavior. It should be noted that both the structures are effective in dissipating the elastic energy under the larger deformation through the dissociation of the inclusion complexes and the sliding motion of the rotaxanes like slide-ring gel[32]. As a result, these structural characteristics provide the host-guest gel with excellent toughness.

(A)

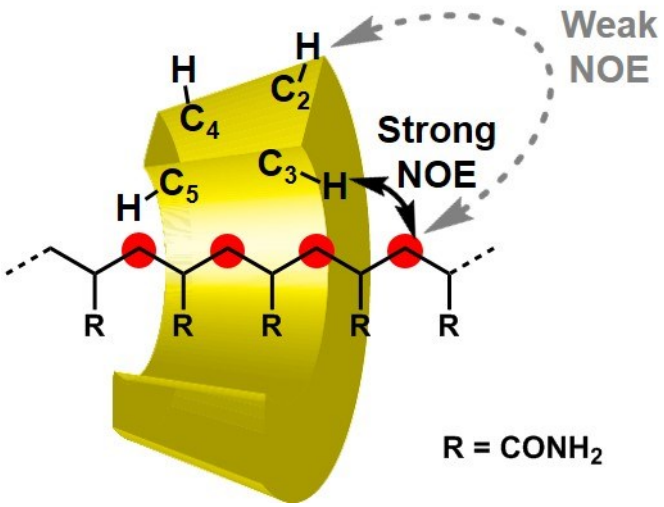

(B)

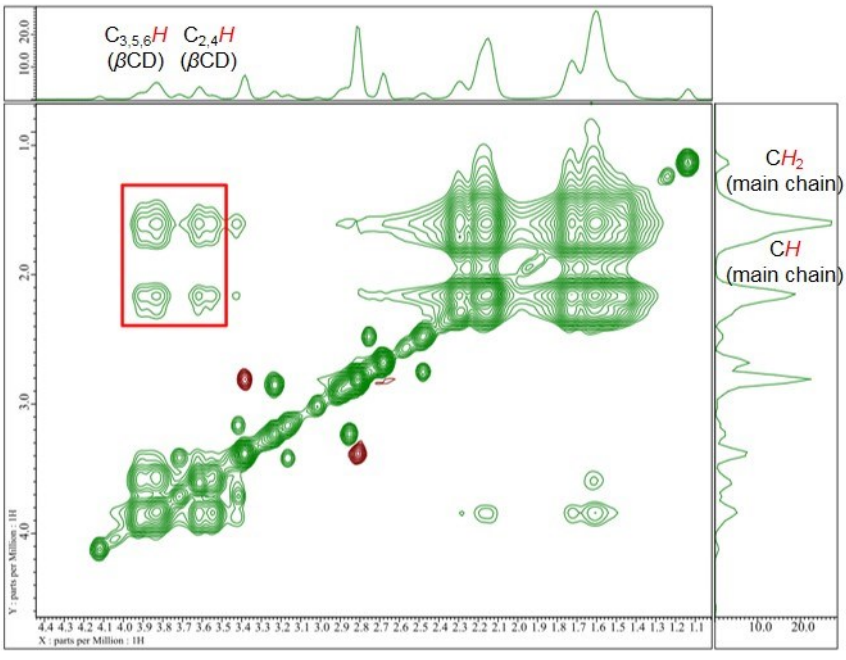

Figure 2-16. (A) Schematic illustration of the rotaxane structure between *β*CD and the PAAm main chain. **(B)** 2D NOESY NMR spectrum of *β*CD polymer with $C_{\beta CD}$ = 0.020 mol kg^{-1} in D_2O. Red rectangle shows correlation peaks between CH_2 and CH of main.

2-4. Conclusion

This chapter has described the results of the viscoelastic properties of the host-guest gel in addition to swelling properties. The results are summarized as follows: (1) the linear viscoelastic measurements of host-guest gels showed the retarded Rouse model and very long relaxation modes; (2) the host-guest interaction did not affect the swelling properties of the host-guest gel, which indicated the existence of permanent crosslinks unexpected from the molecular design; (3) the free host monomers as a competitor made the Rouse mode accelerate, and the composite curve was obtained only with horizontal shifts from the frequency sweep measurements of partially capped host-guest gel polymers, indicating that the host-guest interaction works only as a sticker defined in the sticky reputation model; (4) the PAAm polymer with only βCDs showed the star-shaped or gel-like spectrum, suggesting that the βCD forms physical junction points such as rotaxane structures. It suggests that this unique structure including sticky points and long-life junction points provide a special entity of the host-guest gel.

2-5. References

1. Kakuta, T.; Takashima, Y.; Nakahata, M.; Otsubo, M.; Yamaguchi, H.; Harada, A., Preorganized Hydrogel: Self-Healing Properties of Supramolecular Hydrogels Formed by Polymerization of Host–Guest-Monomers that Contain Cyclodextrins and Hydrophobic Guest Groups. *Advanced Materials* **2013,** *25* (20), 2849-2853.
2. Nakahata, M.; Takashima, Y.; Harada, A., Highly Flexible, Tough, and Self-Healing Supramolecular Polymeric Materials Using Host-Guest Interaction. *Macromol Rapid Commun* **2016,** *37*, 86–92.
3. Flory, P. J.; Rehner, J., Statistical mechanics of cross-linked polymer networks I Rubberlike elasticity. *Journal of Chemical Physics* **1943,** *11* (11), 512-520.
4. Flory, P. J.; Rehner, J., Statistical mechanics of cross-linked polymer networks II Swelling. *Journal of Chemical Physics* **1943,** *11* (11), 521-526.
5. Flory, P. J., *Principles of polymer chemistry*. Cornell University Press: Ithaca, 1953.
6. Bastide, J.; Duplessix, R.; Picot, C.; Candau, S., Small angle neutron scattering and light spectroscopy investigation of polystyrene gels under osmotic deswelling. *Macromolecules* **1984,** *17* (1), 83-93.
7. Candau, S.; Bastide, J.; Delsanti, M., Structural, elastic, and dynamic properties of swollen polymer networks. In *Polymer Networks*, Dušek, K., Ed. Springer Berlin Heidelberg: 1982; Vol. 44, pp 27-71.
8. Candau, S.; Peters, A.; Herz, J., EXPERIMENTAL-EVIDENCE FOR TRAPPED CHAIN ENTANGLEMENTS - THEIR INFLUENCE ON MACROSCOPIC BEHAVIOR OF NETWORKS. *Polymer* **1981,** *22* (11), 1504-1510.
9. Horkay, F.; Hecht, A.-M.; Stanley, H. B.; Geissler, E., Scattering in polymer solutions: Determination of osmotic properties in the concentrated regime. *European Polymer Journal* **1994,** *30* (2), 215-219.
10. Katashima, T.; Chung, U.-i.; Sakai, T., Effect of Swelling and Deswelling on Mechanical Properties of Polymer Gels. *Macromolecular Symposia* **2015,** *358* (1), 128-139.
11. Sakai, T.; Kurakazu, M.; Akagi, Y.; Shibayama, M.; Chung, U.-i., Effect of swelling and deswelling on the elasticity of polymer networks in the dilute to semi-dilute region. *Soft Matter* **2012,** *8* (9), 2730-2736.
12. Shibayama, M., Spatial inhomogeneity and dynamic fluctuations of polymer gels. *Macromol Chem Physic* **1998,** *199* (1), 1-30.
13. Rouse, P. E., A Theory of the Linear Viscoelastic Properties of Dilute Solutions of Coiling Polymers. *The Journal of Chemical Physics* **1953,** *21* (7), 1272-1280.
14. Leibler, L.; Rubinstein, M.; Colby, R. H., Dynamics of reversible networks. *Macromolecules* **1991,** *24* (16), 4701-4707.
15. Park, J. W., Kinetics and Mechanism of Cyclodextrin Inclusion Complexation Incorporating Bidirectional Inclusion and Formation of Orientational Isomers. *The Journal of Physical Chemistry B* **2006,** *110* (49), 24915-24922.

16. Osaki, K.; Inoue, T.; Uematsu, T.; Yamashita, Y., Evaluation methods of the longest Rouse relaxation time of an entangled polymer in a semidilute solution. *Journal of Polymer Science Part B: Polymer Physics* **2001,** *39* (14), 1704-1712.
17. Tanaka, T.; Fillmore, D. J., Kinetics of swelling of gels. *Journal of Chemical Physics* **1979,** *70* (3), 1214-1218.
18. Li, Y.; Tanaka, T., Kinetics of swelling and shrinking of gels. *Journal of Chemical Physics* **1990,** *92* (2), 1365-1371.
19. Shibayama, M.; Nagai, K., Shrinking Kinetics of Poly(N-isopropylacrylamide) Gels T-Jumped across Their Volume Phase Transition Temperatures. *Macromolecules* **1999,** *32* (22), 7461-7468.
20. Kamata, H.; Chung, U.-i.; Sakai, T., Shrinking Kinetics of Polymer Gels with Alternating Hydrophilic/Thermoresponsive Prepolymer Units. *Macromolecules* **2013,** *46* (10), 4114-4119.
21. Kashiwagi, Y.; Katashima, T.; Nakahata, M.; Takashima, Y.; Harada, A.; Inoue, T., Linear viscoelastic studies on a transient network formed by host–guest interaction. *Journal of Polymer Science Part B: Polymer Physics* **2018,** *56* (15), 1109-1117.
22. Chambon, F.; Petrovic, Z. S.; MacKnight, W. J.; Winter, H. H., Rheology of model polyurethanes at the gel point. *Macromolecules* **1986,** *19* (8), 2146-2149.
23. Chambon, F.; Winter, H. H., Linear Viscoelasticity at the Gel Point of a Crosslinking PDMS with Imbalanced Stoichiometry. *Journal of Rheology* **1987,** *31* (8), 683-697.
24. Izuka, A.; Winter, H. H.; Hashimoto, T., Molecular weight dependence of viscoelasticity of polycaprolactone critical gels. *Macromolecules* **1992,** *25* (9), 2422-2428.
25. Winter, H.; Mours, M., Rheology of Polymers Near Liquid-Solid Transitions. In *Neutron Spin Echo Spectroscopy Viscoelasticity Rheology*, Springer Berlin Heidelberg: 1997; Vol. 134, pp 165-234.
26. Graessley, W. W.; Masuda, T.; Roovers, J. E. L.; Hadjichristidis, N., Rheological Properties of Linear and Branched Polyisoprene. *Macromolecules* **1976,** *9* (1), 127-141.
27. Graessley, W. W.; Roovers, J., Melt Rheology of Four-Arm and Six-Arm Star Polystyrenes. *Macromolecules* **1979,** *12* (5), 959-965.
28. Masuda, T.; Ohta, Y.; Onogi, S., Rheological Properties of Anionic Polystyrenes. III. Characterization and Rheological Properties of Four-Branch Polystyrenes. *Macromolecules* **1971,** *4* (6), 763-768.
29. Raju, V. R.; Menezes, E. V.; Marin, G.; Graessley, W. W.; Fetters, L. J., Concentration and molecular weight dependence of viscoelastic properties in linear and star polymers. *Macromolecules* **1981,** *14* (6), 1668-1676.
30. Li, J.; Harada, A.; Kamachi, M., Sol-Gel Transition during Inclusion Complex Formation between [alpha]-Cyclodextrin and High Molecular Weight Poly(ethylene glycol)s in Aqueous Solution. *Polym J* **1994,** *26* (9), 1019-1026.
31. Harada, A.; Kamachi, M., Complex formation between poly(ethylene glycol) and α-

cyclodextrin. *Macromolecules* **1990,** *23* (10), 2821-2823.
32. Okumura, Y.; Ito, K., The Polyrotaxane Gel: A Topological Gel by Figure-of-Eight Cross-links. *Advanced Materials* **2001,** *13* (7), 485-487.

Chapter 3

Rheological and Dielectric Characterization of Supramolecular Networks formed by Movable Crosslinks

3-1. Introduction

As shown in Chapter 2, the existence of permanent crosslinks is confirmed even in the host-guest gel designed to have temporary crosslinks and PAAm only with βCD groups in the side chain[1-2]. These results suggest that polymer chains can be threaded through the cavities of cyclodextrin in polymer materials containing cyclodextrins. In this topological structure, cyclodextrins are not stabilized at a certain point of a polymer chain and can work as movable crosslinks. It is considered that the movable crosslinks work as an energy dissipation mechanism, but the details of the toughening mechanism have not been well understood. Therefore, fundamental studies of their dynamics are required to unravel microscopic information of the toughing mechanism.

Recently, Takashima *et al*. have developed the movable crosslinking networks (MCN) which have topologically similar permanent crosslinks with the host-guest gel and PAAm with only βCD groups[3]. Furthermore, MCNs do not include any solvent molecules, and thus the dynamics of MCNs can be examined over a wide temperature and time scales. Therefore, MCNs can play a key role in govering the dynamics of such a topological structure. These movable crosslinks are topologically a unique structure. It remains unclear how the microscopic dynamics of the movable crosslinks affect the macroscopic physical properties of the network material. Another representative example of such special topological networks is a "slide-ring gel" developed by Ito *et al*[4]. In the slide-ring gel, the crosslinker has a figure-of-eight shape consisting of covalently connected two CD molecules. This crosslinker links two polymer chains via a rotaxane-type structure and can slide along the polymer backbones when

they are largely deformed. This sliding motion of the crosslinker is considered to dissipate external energy and also to reduce a stress concentration under a large deformation, resulting in the enhancement of the toughness[5-6]. MCN is also expected to have similar mechanism to the sliding gel in terms of having movable crosslink but there is a difference: a crosslinking point in MCN links two polymer chains via one covalent bond and one rotaxane structure while that in slide-ring gels consists of two rotaxane structures. In addition, there exist a large number of free threaded CDs in slide ring gels while MCNs have only a few crosslinks in one polymer chain. Therefore, there may be difference in the dynamical feature of the movable crosslinks between these two topologically crosslinked networks.

This chapter summarizes the results of the investigation for the dynamics of MCN especially focusing on the hierarchical dynamics of the CD moieties and polymer chains based on rheological measurements and broadband dielectric spectroscopy. Rheological measurements such as the dynamic viscoelastic measurement are powerful to examine the polymer chain dynamics, while it is difficult to separately observe the dynamics of CD moieties. In contrast, broadband dielectric spectroscopy (BDS) detects the rotational motion of electric dipoles, and thus the motion of CDs having relatively large dipole moment[7] (shown in Figure 3-1) can be visualized in addition to the segmental motion. The presented study is expected to facilitate the fundamental understanding of the dynamics of movable crosslinks and to elucidate the origin of the tough mechanical property of such materials.

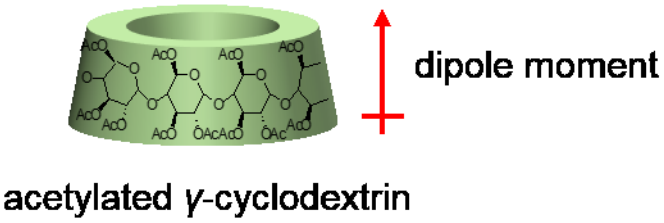

Figure 3-1. Schematic illustration of acetylated γ-cyclodextrin and its electric dipole moment.

3-2. Experimental

3-2-1. Sample preparation

The preparation method of peracetylated γ-cyclodextrin and β-cyclodextrin (PAcγCD and PAcβCD) was reported in the previous paper[3]. One of these CD monomers was mixed as a movable crosslinker with ethyl acrylate (99%, TCI) by ultrasonic stirrer for 1 hour to make a completely mixed monomer solution. 1-hydroxycyclohexyl phenyl ketone (99%, Sigma Aldrich) was mixed with this monomer solution by an ultrasonic stirrer for 5 minutes. The obtained solution was poured into the mold and UV light was irradiated through a 1 mm thick glass plate for 30 minutes at 25°C to initiate bulk radical copolymerization. After this polymerization, the supramolecular networks formed by movable crosslinks (PEA-AcγCD(x) and PEA-AcβCD(x)) were obtained (Figure 3-2). Here, x is the feed molar ratio of CD monomers to the total monomers. The CD content is varied to be x = 0, 0.5, 1.0, and 1.5 mol%. The initiator concentration ratio, x_{ini}, was 0.2, 0.5, or 1.0 mol% to the total monomer concentration. For a comparison, radical copolymerization was performed with the combination of butyl acrylate (99%, TCI) and AcβCD. All obtained samples were dried in a vacuum oven at 60°C for 1 day after the polymerization to remove the unreacted monomer components before the measurements. The detailed characterization was also discussed elsewhere[3].

3-2-2. Differential scanning calorimetry

Differential scanning calorimetry (DSC) measurements were performed to determine the glass transition temperatures with Discovery DSC 2500 (TA instruments). The heating and cooling rate was 10°C/min constant, and the temperature range was from −70°C to +70°C in all measurements. The heating and cooling process was repeated three times to remove the thermal history hysteresis in the samples. The glass transition temperatures, T_g, were determined as the midpoint in the heat flow step during the third heating process after confirming that the second and third-run results were almost the same and that the thermal history was eliminated.

3-2-3. Linear viscoelastic measurements

Linear dynamic viscoelastic measurements were performed with the strain-controlled rheometer ARESG2 (TA instruments). The stainless steel parallel plates with 4 mm diameter were used for the measurements. The temperature range was from −20°C to +130°C and the frequency range was from 100 rad s^{-1} to 0.1 rad s^{-1}. Only at the highest temperature 130°C, the frequency range was extended to 0.01 rad s^{-1} to investigate the terminal behavior. The applied strains were confirmed to be small enough to be within the linear regime for all the measurements.

3-2-4. Broadband dielectric spectroscopy

Broadband dielectric spectroscopy (BDS) measurements were performed with Alpha-A impedance analyzer with Quatro Cryosystem temperature controller (Novocontrol). Samples were vacuum dried at 100°C and sandwiched between two gold-plated electrodes with diameter a 25 mm. The measurements were performed using Active Sample Cell ZGS thermally equilibrated within ±0.2°C in a dry nitrogen flow. The temperature range was from −20°C to +100°C. The measured frequency range was from 10^{6} to 10^{-1} Hz.

For the determination of the dipole moment of peracetylated γ-cyclodextrin, high-frequency dielectric measurement (from 1MHz to 3GHz) was conducted by using RF impedance analyzer 4287A (Keysight Technology) on the benzene solutions of Acγ CD with concentrations of 1~10 wt% at 24°C.

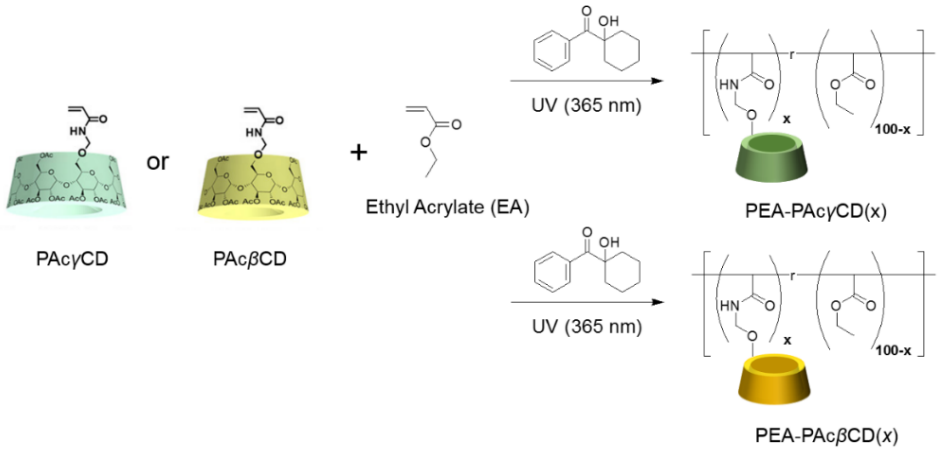

Figure 3-2. Synthesis process of PEA-AcγCD(x) and PEA-AcβCD(x).

3-3. Results

3-3-1. Differential scanning calorimetry

Figure 3-3(A) and (B) show the heat flows of PEA-AcγCD(x) and PEA-AcβCD(x) with x_{ini} = 1.0mol% in the third heating cycle of DSC measurements, respectively. Heat flow curves were vertically shifted not to overlap with each other. As for both PEA-AcγCD(x) and PEA-AcβCD(x), the glass transition points shift to the higher temperature and the glass transitions become broader with increasing x. The glass transition temperatures, T_g, for PEA-AcγCD(x) and PEA-AcβCD(x) were determined from the midpoint of the transition in the heat flow curves.

(A) **(B)**

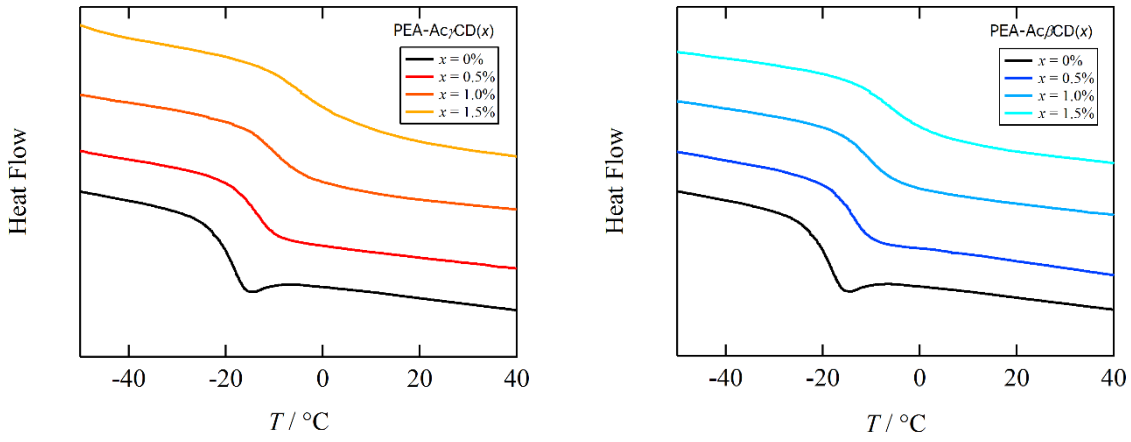

Figure 3-3. Heat flows of **(A)** PEA-AcγCD(x) and **(B)** PEA-AcβCD(x) with x_{ini} = 1.0 mol%.

Figure 3-4(A) shows the x dependence of T_g for PEA-AcγCD(x) and PEA-AcβCD(x) with x_{ini} = 1.0mol%. As is seen in Figure 3-3, T_g increases with x for both systems and the values for PEA-AcγCD(x) are slightly larger than those of PEA-AcβCD(x) compared at the same x. Generally, T_g of random copolymers is described in terms of the component weight fractions, w_1 and w_2 ($w_1 + w_2 = 1$) and neat component T_g values (T_{g1} and T_{g2}); for example Gordon-Taylor equation[8-9]: $T_g = (w_1T_{g1} + Kw_2T_{g2})/(w_1 + Kw_2)$ where K is a parameter, and Fox equation[10]: $1/T_g = w_1/T_{g1} + w_2/T_{g2}$. Since the molecular weights of acetylated CD monomers ($m_{\beta CD}$ = 2057.6 g mol^{-1}, $m_{\gamma CD}$ = 2345.7 g mol^{-1}) are more than 10 times larger than that of ethyl acrylate monomer (m_{EA} = 100.1 g mol^{-1}), the weight fractions of the CD component w_{CD} given by $w_{CD} = m_{CD}x/\{m_{CD}x + m_{EA}(1\text{-}x)\}$ is largely different from x. Therefore, plots of T_g versus w are also shown in Figure 3-4(B). The results indicate that T_g of both PEA-AcγCD(x) and PEA-AcβCD(x) are approximately described by a universal function of w_{CD} in these composition regions, suggesting that pure βCD and γCD homopolymers, which could not be prepared by the bulk polymerization in this study, might have similar T_g in their bulk state. The number of rotaxane type crosslinks schematically shown in Figure 3-1 is small (as will be explained in the discussion section), and thus the effect of rotaxane formation on T_g might be small. The increase of T_g with x and/or w is thought to be mainly due to the intrinsically high T_g of the CD monomer components.

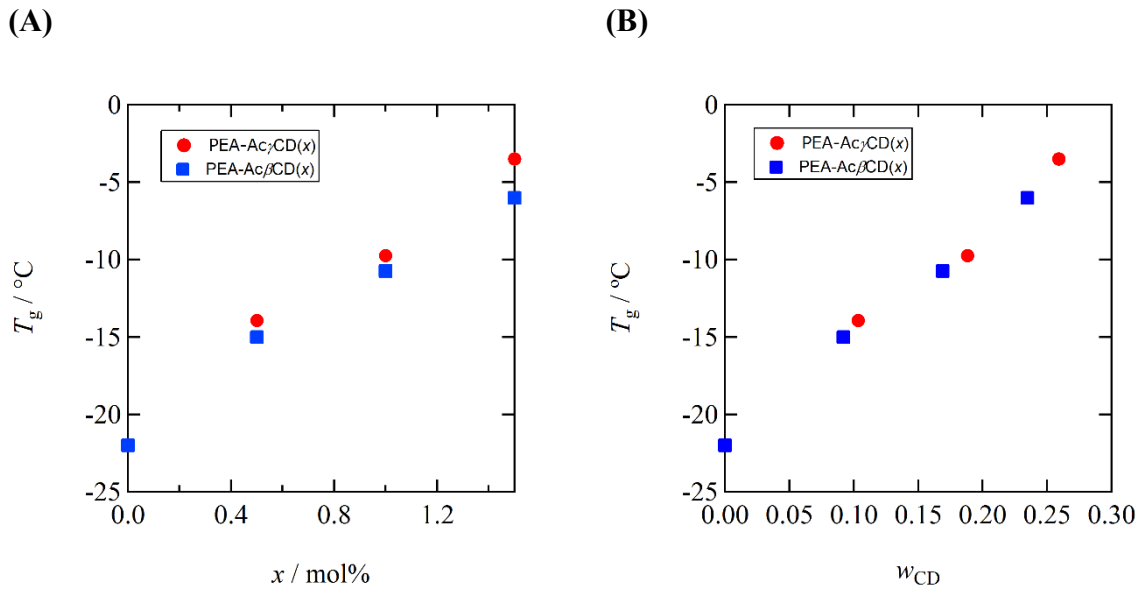

Figure 3-4 (A) Molar fraction and **(B)** weight fraction dependence of the glass transition temperatures for PEA-AcγCD(x) and PEA-AcβCD(x) determined by DSC measurements.

3-3-2. Linear viscoelastic measurements

Figure 3-5 show the angular frequency, ω, dependencies of storage modulus G', loss modulus G'', and loss tangent tanδ (= G''/G') for PEA-AcγCD(x) with x_{ini} = 1.0 mol%, respectively. These composite curves are constructed by the superposition of each data measured at different temperatures to the reference data at $T_r = T_g + 50$°C (reference temperature) through the horizontal shift. Time-temperature superposition principle apparently held for all the samples including other data that are not shown here. For PEA homopolymer (PEA-AcγCD(0)), well-known hierarchical relaxation processes, *i.e.*, glass region, glass transition (segmental relaxation) region, rubbery plateau region, and terminal relaxation region, are observed from high to low frequencies. On the other hand, by introducing movable crosslinks, composite curves largely changed on three different frequency region: (1) broadening of the segmental relaxation (corresponds to the G'' peak at around $a_T\omega = 10^{10} - 10^5$ s^{-1}); (2) appearance of the slow Rouse mode (appearing in the glass transition region around $a_T\omega = 10^5 - 10^1$ s^{-1}) indicated by masked area in Figure 3-5(A) and (B); (3) appearance of a long relaxation time component

or non-relaxing component (second plateau) in the lowest frequency terminal region at around $a_T\omega < 10^{-5}$ s^{-1}.

Regarding (1) the broadening of the glass transition and (2) appearance of the slow Rouse mode result in the shift of the tanδ peak to the lower frequency side. The mechanism of these phenomena will be discussed later, including the results of dielectric measurements. Regarding (3), PEA-AcγCD(0) shows typical terminal relaxation behavior as for amorphous polymers: $G' \sim \omega^2$ and $G'' \sim \omega$. On the other hand, as for PEA-AcγCD(0.5) and PEA-AcγCD(1.0), the frequency dependence of the G' and G'' become weaker: $G' \sim G'' \sim \omega^n$, which is similar behavior of critical networks[11]. In addition, PEA-AcγCD(1.5) does not show definite terminal relaxation and has a second plateau region of G'. These features indicate that the movable crosslinks form the permanent or long-lived network structure since they are topologically trapped. The detailed mechanism will also be discussed later.

(A)

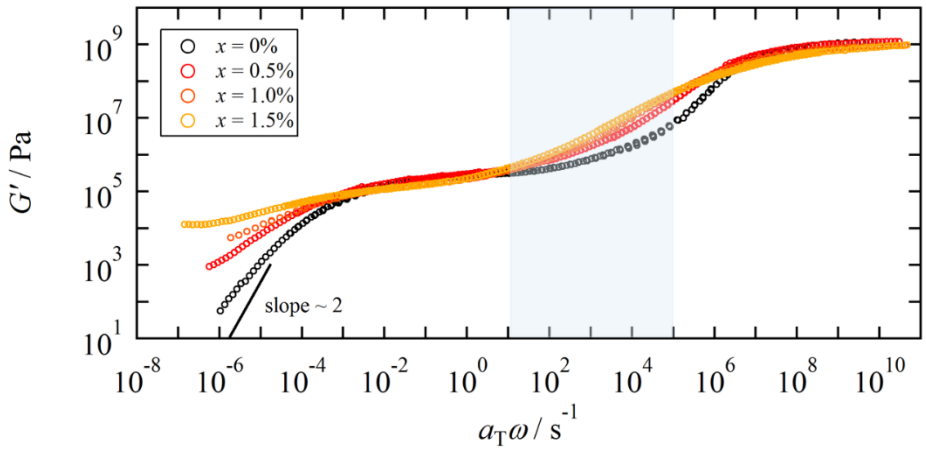

(B)

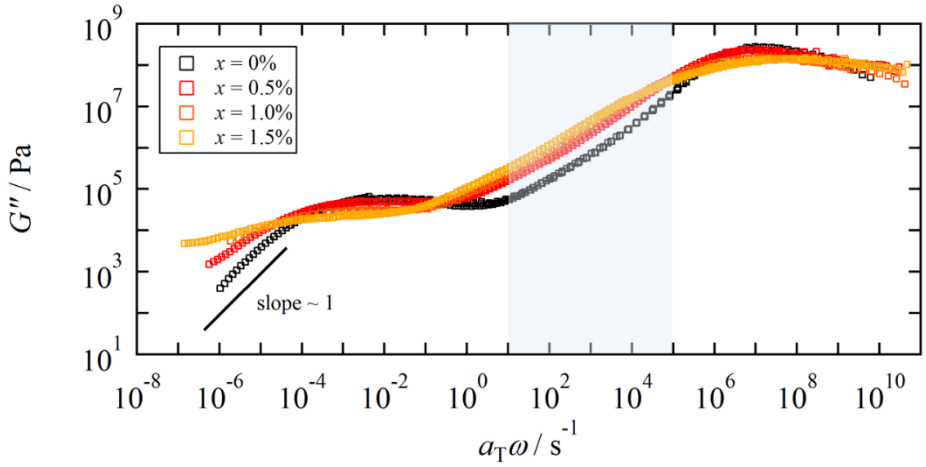

(C)

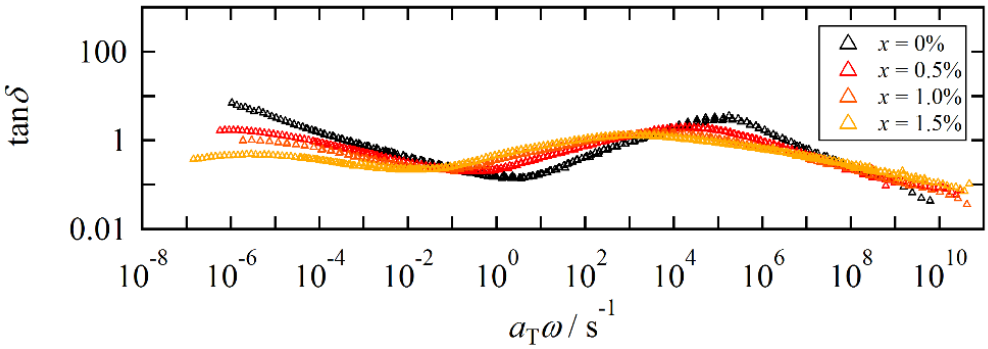

Figure 3-5. Composite curves of PEA-AcγCD(x) at $T_r = T_g + 50$°C. Circle, square and triangle represent **(A)** storage modulus, **(B)** loss modulus, and **(C)** loss tangent, respectively. Black, red, orange and yellow symbols represent results of x = 0, 0.5, 1.0, 1.5%, respectively.

The prepared polymer networks consist of linear polymer chains that have certain molecular weights because the network chains do not have chemical crosslinks. The change of the molecular weights of polymer chains is expected to change the number of the movable crosslinks and thus is very important to control the mechanical properties. However, it is difficult to determine the molecular weight precisely because of the existence of rotaxane-type crosslinks which interlocks polymer chains and prevents them from dissolving in solvents. Therefore, in order to confirm how the change of the molecular weight affects the linear viscoelastic behavior at least qualitatively, the initiator concentration x_{ini} was varied at a fixed x (=1.0 mol%) in the sample preparation step, and different molecular weight samples were prepared. Figure 3-6 shows x_{ini} dependence of composite curves for PEA-AcγCD(1.0). In the higher frequency region at $a_T\omega \geq 10$ s^{-1}, G', G'', and tanδ for all the x_{ini} samples overlap each other, while they differ in the terminal region at $a_T\omega < 10^{-3}$ s^{-1}. This means that the molecular weight of the constituent polymer chain does not affect the short time scale dynamics such as glass dynamics, segmental dynamics, and Rouse dynamics, but affects the terminal relaxation behavior. For x_{ini} = 1.0mol% (lowest molecular weight), G' and G'' show the frequency dependence of $\omega^{0.5}$ in the low ω region, indicating that the network structure is not sufficiently developed and exhibits critical gel-like behavior. For x_{ini} = 0.2mol% and 0.5mol%, the power of ω becomes smaller $\omega^{0.2}$ and the G', G'' and tanδ curves almost overlap each other. This means that above a certain molecular weight, permanent crosslinks, even though their number is small, are formed and the terminal relaxation goes beyond the experimental window. As a result, the viscoelastic spectra become the same and the observed power-law decay may reflect the partial relaxation due to the large-scale sliding motion of movable crosslinks.

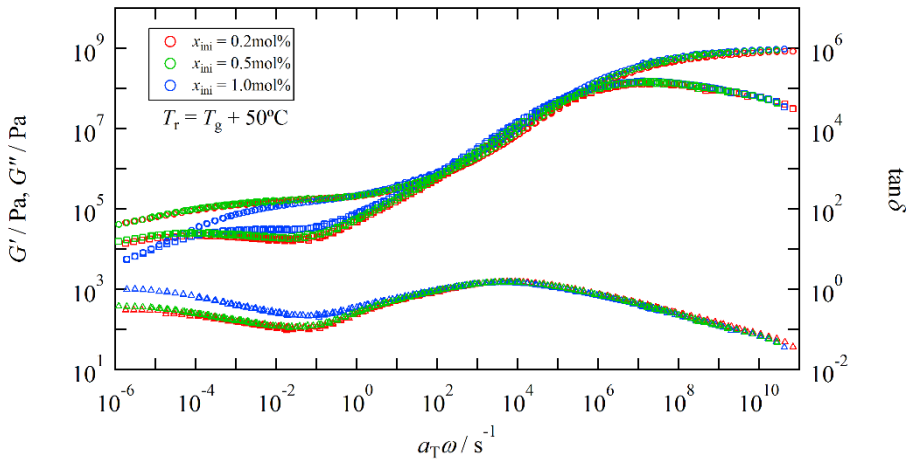

Figure 3-6. Initiator concentration dependence on composite curves of PEA-AcγCD(1.0). Red, Green, and blue symbols represent the result of x_{ini} = 0.2mol%, x_{ini} = 0.5mol%, and x_{ini} = 1.0mol%, respectively.

3-3-3. Broadband dielectric spectroscopy

Figure 3-7 shows the ω dependence of dielectric loss ε'' and the derivative of permittivity $\varepsilon'_{der} = -\frac{\pi}{2}\frac{\partial\varepsilon'}{\partial \ln\omega}$ for PEA-AcγCD(x) with x_{ini} = 1.0 mol% and x = 0, 0.5, 1.0, and 1.5 mol%, respectively at 303, 308, 313 and 318 K, which approximately correspond to T_g + 50 °C. The ε'' spectra exhibit segmental relaxation (α-relaxation) peaks at $\omega \sim 10^6$ s^{-1} and upturns on the low-frequency side due to ionic conductivity. The spectra of samples, including movable crosslinks, seem to exhibit broad ε'', which indicates an additional process between α-relaxation and conductivity. This is especially obvious in the case of PEA-AcγCD(1.5). In addition, because of no contribution of the ionic conductivity, the ε'_{der} spectra clearly exhibit these new relaxation peaks at $\omega = 10^2 \sim 10^3$ rad^{-1} in addition to the α-relaxation. Here, this new relaxation is named "slow mode" because the relaxation time given by the reciprocal of the frequency where ε'_{der} peaks is about 3 decades slower than that of the α-relaxation. It is noted that the peak frequency of the slow mode indicated by the arrow in Figure 3-7 is close to the position of the new relaxation mode observed as the G' and G'' shoulders in Figure 3-5(B), suggesting that they

have similar mechanisms.

To separate the contribution of each mode and extract the characteristic parameters, ε' and ε'' at each temperature were fitted by the following Havriliak-Negami (HN) functions;

$$\varepsilon^* = \varepsilon' - \mathrm{i}\varepsilon'' = \varepsilon_\infty + \frac{\Delta\varepsilon_\alpha}{\left[1+(\mathrm{i}\omega\tau_{\mathrm{HN},\alpha})^{\gamma\alpha}\right]^{\beta\alpha}} + \frac{\Delta\varepsilon_{\mathrm{slow}}}{\left[1+(\mathrm{i}\omega\tau_{\mathrm{HN,slow}})^{\gamma_{\mathrm{slow}}}\right]^{\beta_{\mathrm{slow}}}} + \frac{\sigma_0}{\mathrm{i}\omega\varepsilon_0} \qquad (3\text{-}1)$$

where ε^* is the complex permittivity, ε_∞ is the permittivity at high-frequency limit, σ_0 is the conductivity, and ε_0 is the vacuum permittivity. Here, the relaxation strength $\Delta\varepsilon_\alpha$ and $\Delta\varepsilon_{\mathrm{slow}}$, relaxation time $\tau_{\mathrm{HN},\alpha}$ and $\tau_{\mathrm{HN,slow}}$, broadness index γ_α and γ_{slow}, and asymmetry parameter β_α and β_{slow} are fitting parameters of α-relaxation and slow mode, respectively. The solid curves in Figure 3-7(A) and (B) show the fitting results by eq. 3-1. For the PEA-AcγCD(0) (PEA homopolymer), eq. 3-1 with a single relaxation mode (k = 1) could fit both the ε'' and $\varepsilon'_{\mathrm{der}}$ data well, which indicates PEA-AcγCD(0) has only the segmental relaxation and ionic conductivity components. The shapes of the segmental relaxation peak at several temperatures were represented by almost temperature-independent shape parameters: γ = 0.45 ~ 0.55 and β = 0.40 ~ 0.50. In contrast, for copolymers, the shapes of the α-relaxation were broader than that of PEA-AcγCD(0), and the slow mode peaks observed in $\varepsilon'_{\mathrm{der}}$ also became broad. Therefore, for the copolymer data, it was assumed that β for the slow mode is unity and independent of temperature in order to reduce the number of free fit parameters. This assumption worked well and provided a good fit for the spectra. In the discussion part, the maximum relaxation time τ_{max}, corresponding to the reciprocal of the peak frequency of $\varepsilon''(\omega)$ is used as the representative time scale for each mode. For this purpose, τ_{max} was calculated by the following equation;

$$\tau_{\mathrm{max}} = \tau_{\mathrm{HN}} \left(\sin\frac{\gamma\pi}{2(1+\beta)}\right)^{-1/\gamma} \left(\sin\frac{\gamma\beta\pi}{2(1+\beta)}\right)^{1/\gamma} \qquad (3\text{-}2)$$

For the PEA-AcβCD(x) samples, similar dielectric behavior was observed. All the other data were similarly fitted by eq. 3-1 and the relaxation strength $\Delta\varepsilon$ and the relaxation times τ_{max} were determined.

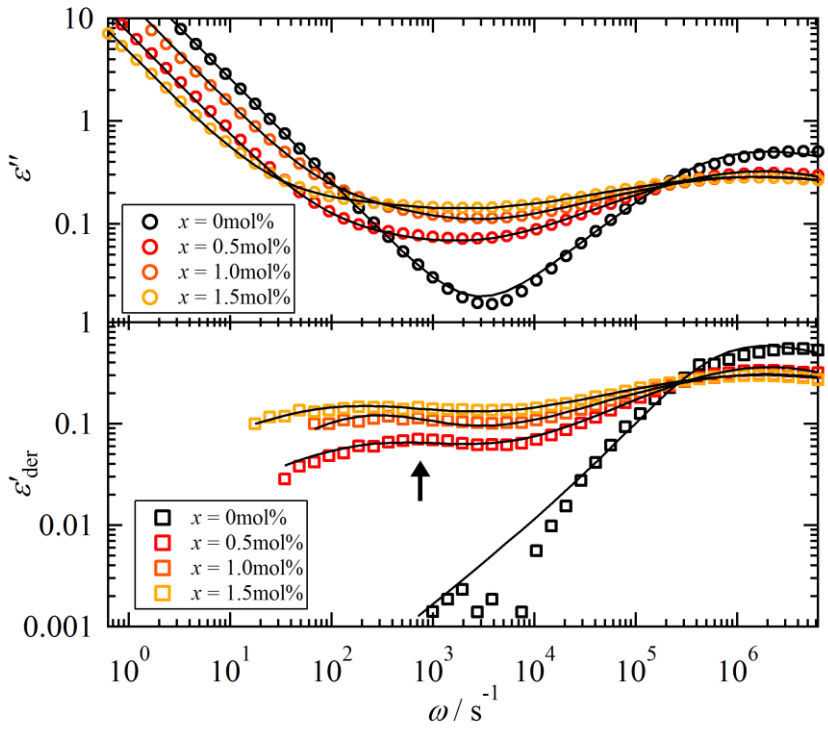

Figure 3-7. Frequency dependence of dielectric loss ε'' and derivative of permittivity ε'_{der} for PEA-AcγCD(x) of x_{ini} = 1.0mol% at T_g + 50°C. Black lines represent the fitting results derived from Havriliak-Negami functions. Black arrows represent the new relaxation peak derived from the movable crosslink.

Figure 3-8(A) shows the x dependence of $\Delta\varepsilon_{slow}$ for PEA-AcγCD(x) and PEA-AcβCD(x) with x_{ini} = 1.0 mol%. As for both systems, $\Delta\varepsilon_{slow}$ is proportional to x, indicating that the slow mode is related to the motion of the CD moieties. Since the temperature dependence of the $\Delta\varepsilon_{slow}$ for both systems are weak as shown in Figure 3-8(B), the proportionality between $\Delta\varepsilon_{slow}$ and x was found to hold at different temperatures examined in this study.

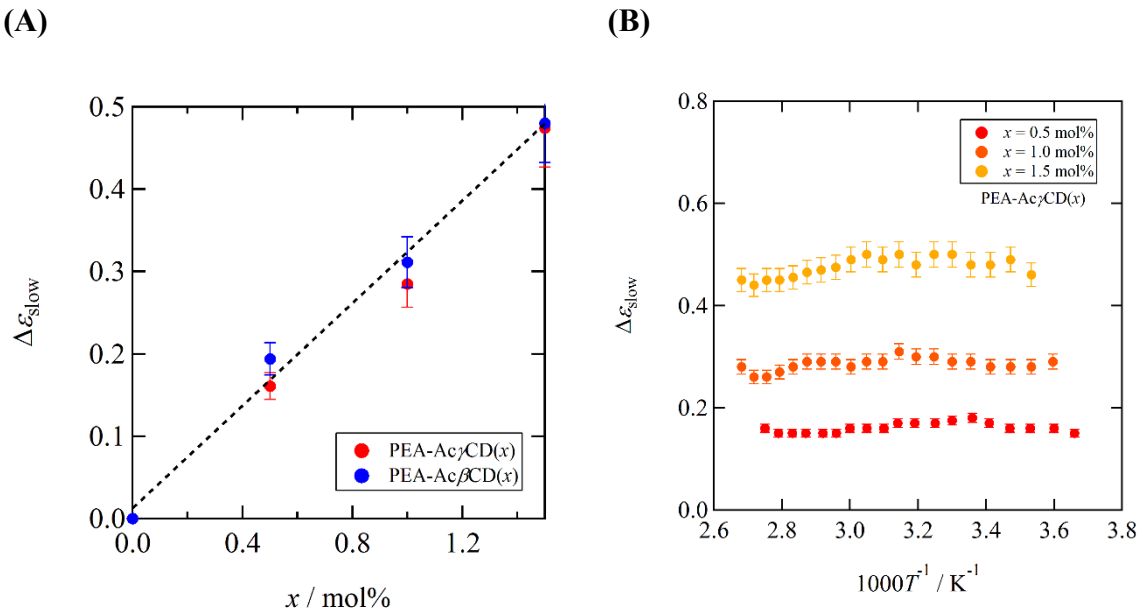

Figure 3-8. (A) Molar fraction dependence of $\Delta\varepsilon_{slow}$ for PEA-AcγCD(x) and PEA-AcβCD(x). **(B)** The temperature dependence of the $\Delta\varepsilon_{slow}$ for PEA-AcγCD(x).

Figure 3-9(A) and (B) show the temperature dependence of two characteristic time scales deduced from eq. 3-2: those of the α-relaxation τ_α and the dielectric slow mode τ_{slow} for PEA-AcγCD(x) and PEA-AcβCD(x) with x_{ini} = 1.0mol%. To reduce the T_g difference for each sample, the inverse of the temperature in abscissa is scaled by each T_g determined by DSC measurements. As for α-relaxation, all the data are independent of x and fall on the same curve. The black dashed lines represent the fitting results to the PEA-AcγCD(0) by the VFT equation as follows;

$$\tau_\alpha = \tau_0 \exp\left(\frac{A}{T-T_0}\right) \tag{3-3}$$

where τ_0, A, and T_0 are fitting parameters: $\tau_0 = 6.50\times10^{-14}$ s, A = 1320 K, and T_0 = 215 K for PEA-AcγCD(0). It is seen that all the data represent good accordance with the VFT equation. These results suggest that the introduction of the movable crosslinking has little effect on the

average segmental relaxation time except the shift of T_g. On the other hand, as for the temperature dependence of τ_{slow}, almost the universal T_g/T dependence regardless of x is also seen. This result indicates that the slow mode relaxation is related to the segmental dynamics, namely, the segmental relaxation (about 3 decades faster compared with τ_{slow} at T_g + 50°C) can be one of the rate-determining processes for the slow mode related to the CD motions.

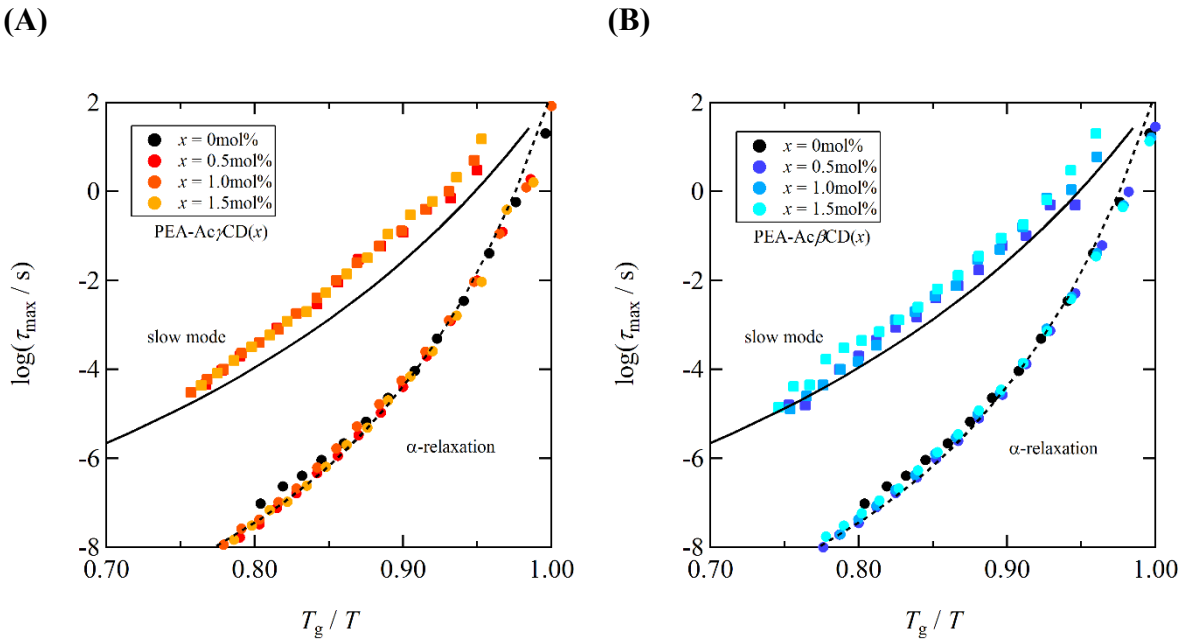

Figure. 3-9 Temperature dependences of τ_α and τ_{slow} derived from HN fittings at various temperatures for **(A)** PEA-AcγCD(x) and **(B)** PEA-AcβCD(x). The horizontal axes are scaled by T_g to ignore the concentration dependence of T_g. The dashed lines are the VFT fit results. The solid lines shown represents the T-dependence of the chain mode reproduced from ref 15.

The temperature dependence of τ_{slow} is, however, apparently different from that of τ_α. Figure 3-10 shows the ratios of τ_{slow}/τ_α plotted against T_g/T, clearly indicating that τ_{slow} and τ_α have different temperature dependences. τ_{slow}/τ_α are almost constant values at $T_g/T < 0.85$ regardless of x, and it decreases monotonically at $T_g/T > 0.85$. The clear reason for this peculiar temperature dependence of τ_{slow}/τ_α is unknown at this stage. Similar temperature dependence is

known to appear for the ratio of the normal mode relaxation time τ_n reflecting the whole polymer chain (end-to-end vector) dynamics to τ_α[12-14]. The slow mode process in BDS is due to the orientational relaxation of dipoles, *i.e.*, CD dipoles here. Apparently, the CD cannot reorient with a single segment. It may be related to the reorientation of a significant part of the chain, *i.e.*, some sub-chains. As a result, its temperature dependence can possibly follow to what is expected for the polymer chain motion rather than for segments. Ding *et al*. reported that chain relaxation times τ_n for several polymer species could be represented by an almost universal function while the corresponding τ_α values exhibited different T dependence[15]. The universal T-dependence of τ_n has been shown in Figure 3-9(A) and (B) by the solid black line (vertically shifted for the easy comparison with τ_{slow}). It is seen that the slow mode has more Arrhenius-like dependence given by the following equation than that expected for chain modes:

$$\tau_{\mathrm{slow}} = \tau_0 \exp\left(\frac{E_a}{RT}\right) \tag{3-4}$$

where τ_0 is the relaxation time at high-temperature limit, E_a is the activation energy, and R is the gas constant. Figure 3-10(A) and (B) show the fitting results of the relaxation times of the slow mode by eq. 3-4. For all the data, eq. 3-4 well describes experimental results as indicated by the solid lines except for a few points at the lowest temperatures. The obtained parameters are listed in Table 1. Note that τ_0 values are about 10^{-24} s^{-1} even for the slowest one (x = 1.5 mol%). This relaxation time is too fast for a molecular motion in dense systems. From this perspective, τ_{slow} is considered to deviate from the Arrhenius-type temperature dependence and should become weaker on the higher temperature side.

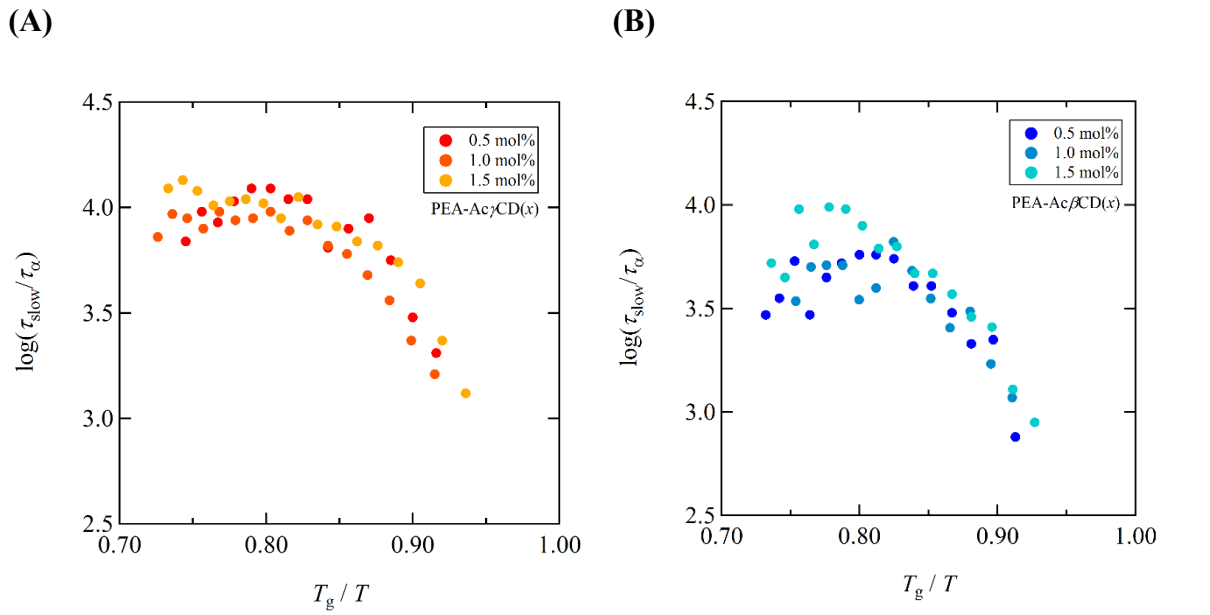

Figure 3-10. Temperature dependence of the ratio of τ_{slow} to τ_α for (A) PEA-AcγCD(x) and (B) PEA-AcβCD(x) with x_{ini} = 1.0mol%.

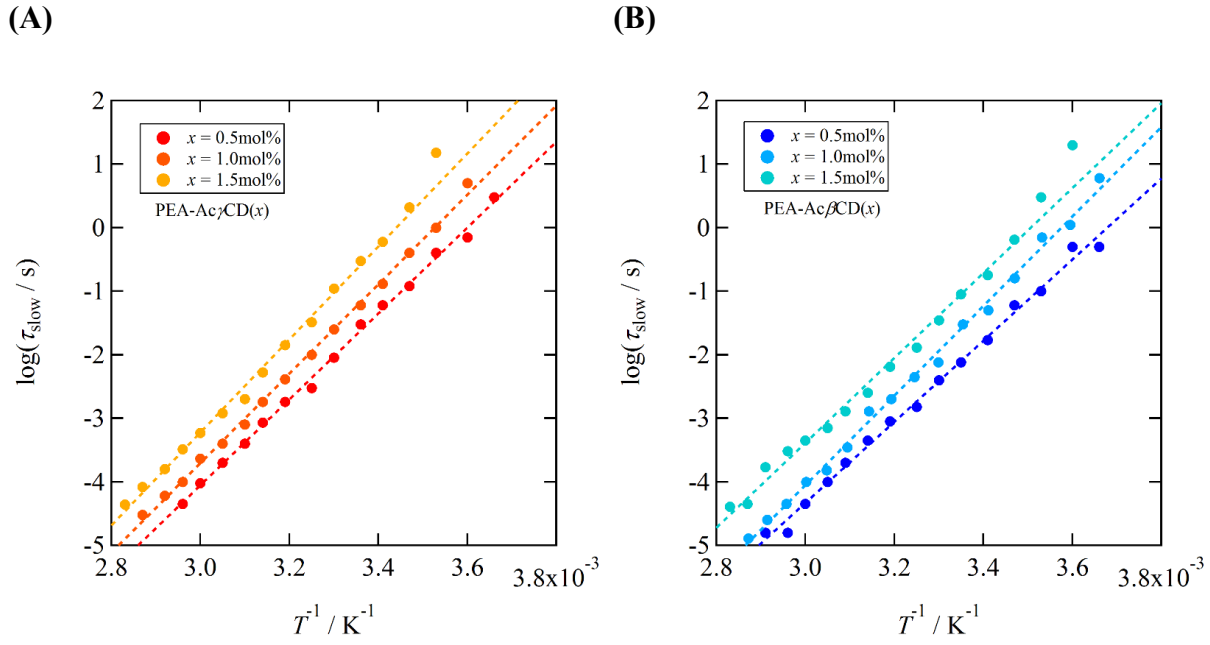

Figure 3-11. Arrhenius fittings of the temperature dependence of the slow mode for (A) PEA-AcγCD(x) and (B) PEA-AcβCD(x) with x_{ini} = 1.0mol%.

Table 1. Fitting parameters obtained from eq. 3-4

	x / mol%	log (τ_0 / s)	E_a / kJ mol^{-1}
PEA-AcγCD(x)	0.5	-24.3	129
	1.0	-24.8	135
	1.5	-25.2	140
PEA-AcβCD(x)	0.5	-23.5	122
	1.0	-25.2	135
	1.5	-23.4	128

3-4. Discussion

3-4-1. Broadening of glass and Rouse mode spectra

As mentioned in sections 3-3-2 and 3-3-3, the G'' peak around $a_T\omega = 10^{10} – 10^5$ s^{-1} and the ε'' peak became broader with increasing the x (see Figures 3-5 and 3-7). These are related to the widening of the segmental relaxation time distribution. One of the possible reasons for this broadening is "dynamic heterogeneity"[16] due to the difference in the relaxation times between the segments with and without CD moieties. The transition width of the DSC curves also became broader with increasing x as shown in Figure 3-3, which is consistent with the viscoelastic and dielectric results.

Regarding the Rouse mode spectra, in the glass to rubber zone, the formation of movable crosslinks can play an important role. At high CD concentration, there are three types of CD structure in the network: trapped rotaxane, untrapped rotaxane, and free CD as shown in Figure 3-12. In the trapped rotaxane structure, one rotaxane type CD crosslink is sandwiched by two other CD monomers and cannot go through these bulky parts. On the other hand, the sliding motion of the untrapped rotaxane structure is not inhibited by other CDs. Therefore, untrapped rotaxanes can dissociate from the axial polymer chain and become free CD structure.

The formation of both trapped and untrapped rotaxane structures can retard the Rouse

relaxation of a network strand: rearrangement of the sub-chain constrained by the rotaxane structure becomes slower than the free one[17]. This conformational rearrangement of the sub-chain can be accompanied by the short-length scale sliding motion of CD moieties along the main chain. The relevant length scale of the sliding movement of CD moieties should be at least longer than the Rouse segment and shorter than that of the length between entanglements. Considering the molecular weight of acetylated CDs ($m_{\beta CD}$ = 2057.6 g mol^{-1}, $m_{\gamma CD}$ = 2345.7 g mol^{-1}), these values are comparable or slightly higher than the molecular weight of Rouse segments for typical polymers[18]. Therefore, it is considered that free CDs may also contribute to the slow Rouse relaxation mode. In section 3-4-3, the relationship between the slow Rouse mode and dielectric slow mode will be explained and the possible mechanism of the slow mode will be discussed.

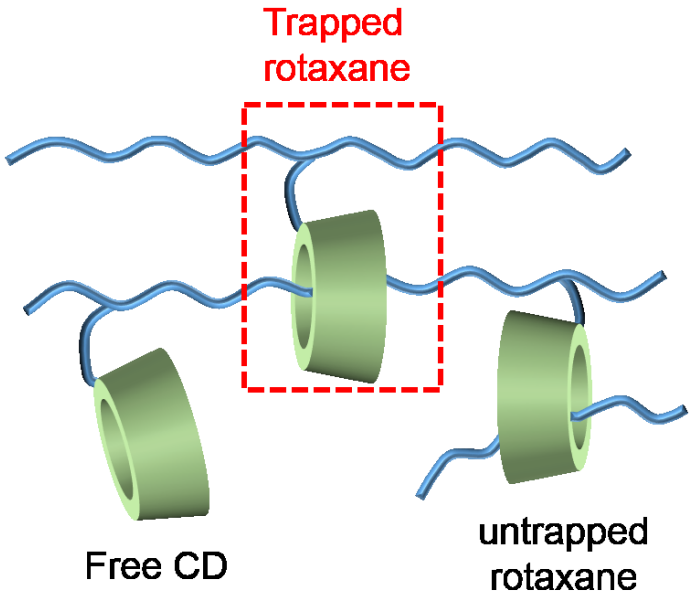

Figure 3-12. The schematic illustration of the trapped rotaxane, untrapped rotaxane, and free CD structures in MCN.

3-4-2. Terminal Behavior

Incorporating the rotaxane structure is also related to the appearance of long-lived or terminal components in the terminal region as shown in Figure 3-5 and 3-6. Focusing on the frequency range around $a_T\omega < 10^{-3}$ s^{-1}, the slopes of G' and G'' gradually became larger with increasing x. This change in the terminal spectra indicates the emergence of long-lived components. In the G' spectrum of the x = 1.5mol% sample shown in Figure 3-5(A), the second plateau region was clearly observed. As for such viscoelastic long-lived components, Kato *et al*. reported similar behavior (appearance of two-step plateaus) in slide ring gels[19]. They concluded that the long-lived components were due to non-relaxing crosslinks interlocked by the rotaxane structure and the mechanism of the relaxation taking place between the first plateau and the second plateau was ascribed to the large scale sliding motion of CDs on a polymer backbone in their system[6]. It is considered that a similar relaxation process occurs in this MCN system. The movable crosslink can slide along the main chain between two points where bulky CD group exists. In this process, the relevant length scale of this relaxation might be the average distance between two CD moieties in a single chain. This value is estimated to be about 70 ~ 200 monomer units for x = 0.5 to 1.5mol%. The trapped rotaxane works as both a movable and permanent crosslink responsible for the critical gel-like behavior and the appearance of the second plateau in rheological terminal region.

Especially for PEA-AcγCD(1.5), the effective chain density μ_{eff} can be estimated from the second plateau modulus G_N determined as the G' value at the lowest ω by using the affine network model[20]:

$$\mu_{\mathrm{eff}} = \frac{\nu_{\mathrm{eff}}}{2} = \frac{G_{\mathrm{N}}}{2RT} \tag{3-5}$$

where ν_{eff} is the effective crosslinker density, R is the gas constant, and T is the absolute

temperature. From this calculation, μ_{eff} was estimated to be 2.9 mol m^{-3}. On the other hand, the feed monomer concentration of the γCD monomer c_{CD} value in the case of x = 1.5mol% is calculated to be 140 mol m^{-3}, which is more than 10 times larger than ν_{eff}. This estimate suggests that only about 2% of the CD moieties in the system act as long-lived crosslinks, and the rest 98% of CDs do not form a non-relaxing rotaxane-like structure, which can hold stress in the long time region.

3-4-3. Dielectric slow mode relaxation

As shown in Figure 3-8, the relaxation strength of the slow mode $\Delta\varepsilon_{slow}$ increased proportionally with increasing x for both PEA-AcγCD(x) and PEA-AcβCD(x), which indicated that the slow mode reflected the CD motion including trapped and untrapped rotaxane. To confirm how each CD component contributes to the slow mode, copolymers of butyl acrylate and AcβCD (PBA-AcβCD(1.0)) are synthesized, and the dielectric measurements of them were performed. The butyl acrylate has longer alkyl side chains than ethyl acrylate, and thus the rotaxane structure is hardly formed even when the CD concentration is high[3]. Figure 3-13(A) shows the comparison of the dielectric data between PBA-AcβCD(1.0) and PEA-AcβCD(1.0). The relaxation strength of the slow mode for PBA-AcβCD(1.0) is obviously much smaller than that of PEA-AcβCD(1.0). This trend is remarkable for higher CD concentration, as shown in Figure 3-13(B). These results suggest that the motion of *rotaxane structure*, including both trapped and untrapped ones, is responsible for the dielectric slow mode. Regarding the low dielectric strength mode observed in PBA-AcβCD(1.0), one of the possible origins of this mode could be due to the completely trapped rotaxane, which cannot slide because its relaxation time is about 4-5 times slower than that of the slow mode of PEA-AcβCD(1.0). The completely trapped rotaxane structure could be formed during the polymerization process with a much lower possibility. Once this structure is formed, the CD moiety is fixed in a certain part of the main

chain due to the longer side chain size of butyl groups. In this case, only the motion of polymer chains can induce the rotational relaxation of the immovable trapped rotaxanes.

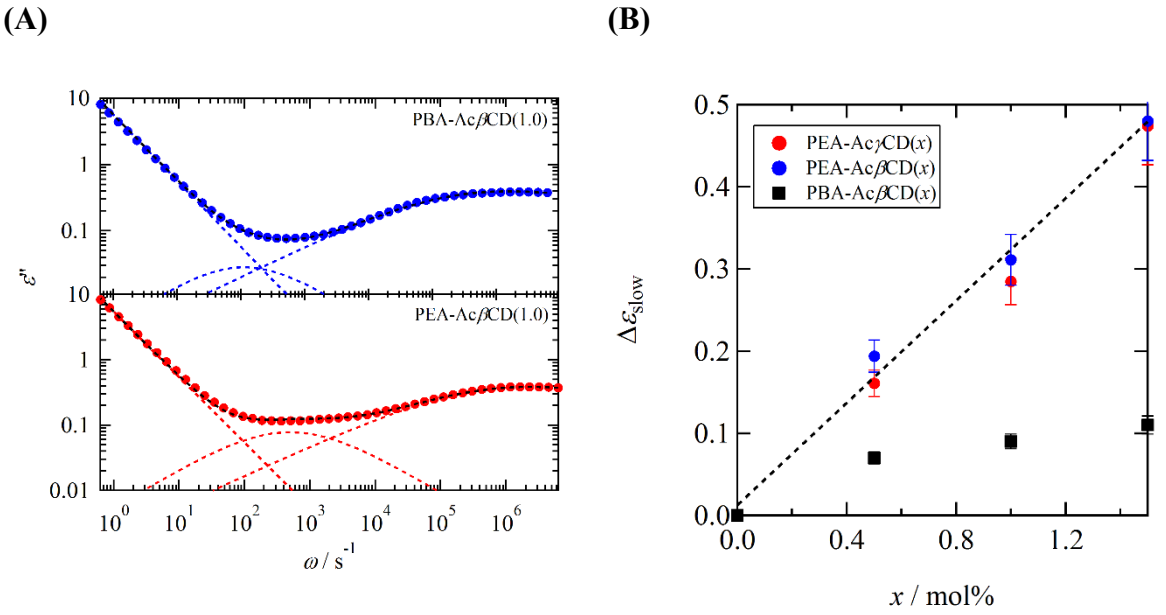

Figure 3-13. (A) Comparison of the dielectric loss data between PEA-AcβCD(1.0) and PBA-AcβCD(1.0) at $T = T_g + 50$°C. The dashed lines represent the fitting results with eq. 3-1. **(B)** The feed CD concentration x dependence of the relaxation strength of the slow mode for PEA-AcγCD(x), PEA-AcβCD(x) and PBA-AcβCD(x).

In order to evaluate how much the trapped and untrapped rotaxanes contribute to the slow mode in PEA-AcγCD(x) and PEA-AcβCD(x) systems, the dielectric relaxation data for the mixtures of PEA/AcγCD monomer (1.0 mol%) and PBA/AcβCD monomer (1.0 mol%) are also compared in Figure 3-14. In PEA/AcγCD, the slow mode is observed with a similar intensity to the copolymer case. Since trapped rotaxane structure does not exist in this mixture, the result of Figure 3-14 indicates that untrapped rotaxanes strongly contribute to the slow mode. Since the number of trapped rotaxanes is very small, as was discussed in section 3-4-2, the main component of the slow mode is ascribed to the untrapped rotaxane structure. Furthermore, the

dielectric data of PBA / AcβCD monomer (equivalent to 1.0 mol%) shows that no isolated slow mode peak exists. This data also supports that the slow mode is due to the rotaxane structure and not due to the free CD.

(A)

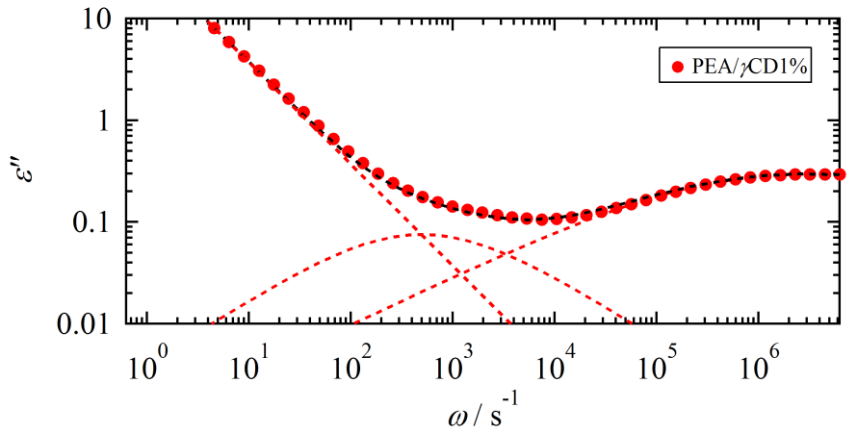

(B)

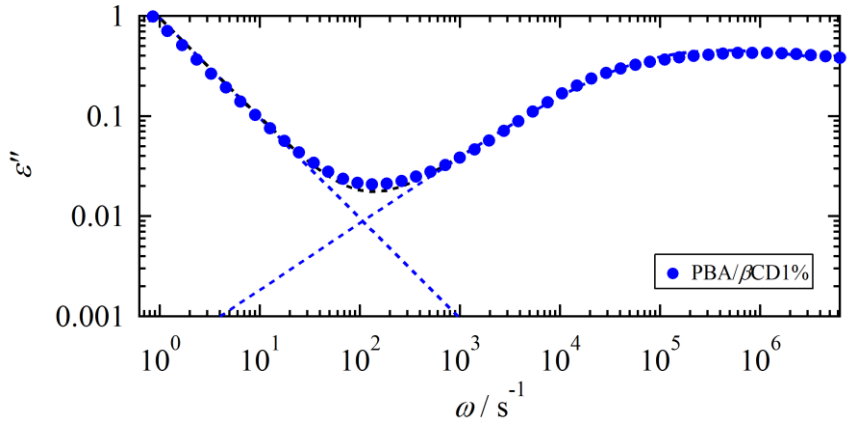

Figure 3-14. Frequency dependence of dielectric loss ε'' and derivative of permittivity ε'_{der} for **(A)** PEA/γCD monomer mixture with the molar concentration of the γCD monomer to be 1.0mol% at T = 313K and **(B)** PBA/βCD monomer mixture with the molar concentration of the βCD monomer to be 1.0mol% at T = 313K. Black lines represent the sum of fitting results derived from HN functions. Red or blue lines represent each component used in the fitting by HN functions.

The effective CD concentration contributing to the slow mode can be estimated from the dielectric intensity, $\Delta\varepsilon_{slow}$. To analyze the relaxation strengths the following Onsager equation is used:

$$\Delta\varepsilon = \frac{\varepsilon_s(\varepsilon_h+2)^2\mu^2 c_{eff}}{9(2\varepsilon_s+\varepsilon_h)\varepsilon_0 RT} \quad (3\text{-}6)$$

where ε_s and ε_h are the permittivity on the low- and high-frequency sides for the slow mode relaxation process, μ is the dipole moment of the CD moiety, c_{eff} is the effective molar concentration of CD contributing to the dielectric slow mode, and ε_0 is the vacuum permittivity. To determine the dipole moment of AcγCD precisely, the dielectric measurements of the benzene solutions of AcγCD monomer were performed with different concentrations. The details are summarized in section 3-6: Appendix. From these experiments, the dipole moment ($\mu_{\gamma CD}$) of AcγCD was determined to be $\mu_{\gamma CD}$ = 7.0 D. Using this value and eq. 3-6, the c_{eff} of PEA-AcγCD(1.5) is calculated to be 30.4 mol m^{-3}. This value is almost 22% of the feed molar concentration of AcγCD (c_{CD} ~ 140 mol m^{-3}). As discussed in Section 3-4-2, trapped rotaxane, which works as permanent crosslinks, was estimated to be at least 2% of the feed concentration. Therefore, the number of rotaxane structures which is related to the slow mode is about 10 times bigger than the permanent rotaxanes. Even though the c_{eff} determined by the dielectric relaxation strength can be affected by several factors such as an internal electric field or the correlation factor (Kirkwood factor) between dipoles, it is surely said that the untrapped rotaxane structure mainly contributes to the slow mode.

Based on the above discussion, the free CD component is about half of the feed concentration. Even though the free CD component exist in the MCN systems, the proportionality between $\Delta\varepsilon_{slow}$ and x holds as shown in Figure 3-8. This may be because the free CDs and untrapped rotaxanes are under equilibrium condition and the molar ratio of the

two components can always be constant.

In this study, free CD relaxation could not be separated in the dielectric spectra, even for the system of PBA/Ac*β*CD blend or PBA-Ac*β*CD(x) as shown in Figure 3-13(A) and 3-14(B), where free CD structure is the main part. Based on these results, the relaxation of free CD is possibly involved in the broad α-relaxation spectra or the dipole moment of a free CD structure is much smaller than that of the rotaxane CD for some reason (*e.g.* acetyl groups are embedded into the CD cavity and the dipole moments cancel out with each other) and became dielectrically invisible. The relaxation time of free CD is considered to be shorter than those of typical Rouse segments. It is unlikely that the slow mode is caused by the relaxation of free CD components because the free CD rich systems exhibited very weak or no slow mode as shown above. In addition, the temperature dependence of free CDs should have similar temperature dependence of segmental mode or normal mode because the CD components are chemically connected to polymer chains. However, τ_{slow} has different temperature dependence (apparently Arrhenius temperature dependence as shown in Figure 3-9). This result also supports the idea that the origin of the slow mode is not due to the motion of free CDs but that of rotaxane-type CDs.

The rotational motion of rotaxane-type CDs, which have a large dipole plays a key role in the dielectric slow mode. This rotational motion is considered to be allowed by the sliding motion of CD moieties along the polymer backbone accompanied by the chain conformational change. This mechanism is schematically shown in Figure 3-15. Because the viscoelastic Rouse mode appears in a similar time scale to the slow mode, the CD motion should be strongly correlated with the chain motion. If the sliding motion did not occur and only the chain motion induced the CD dipole rotation during this process, the temperature dependence of τ_{slow} would become similar to that of τ_{α} or the chain relaxation time. The fact that temperature dependencies of τ_{slow} and τ_{α} are apparently different as shown in Figures 3-9 and 3-11 also

supports the idea that the sliding motion also plays a crucial role for the dielectric slow mode. The difference between the viscoelastic Rouse mode and dielectric slow mode would be that the former reflects the motion of the network strand (which can transmit stress) accompanied with the sliding motion of CD units, while the latter directly picks up the CD rotation through both the sliding and chain motion.

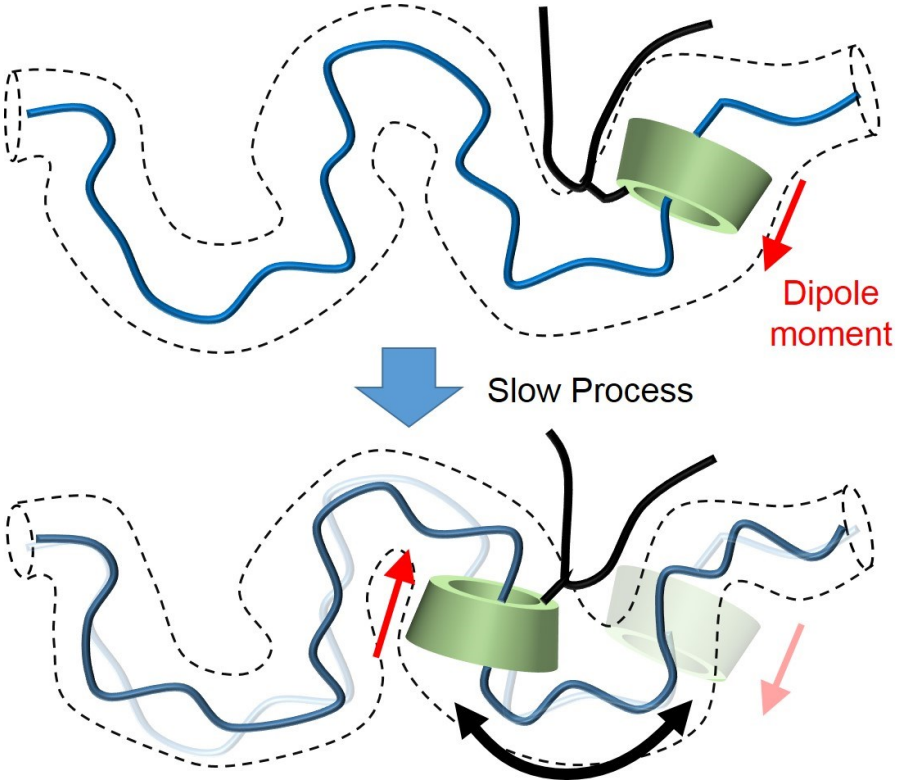

Figure 3-15. Schematic illustration for the mechanism of the dielectric slow mode where the dipole moment of CD moieties change through the sliding motion accompanied by the conformational change of the chain backbone.

To summarize the discussion above, for the slow mode relaxation, the following two processes are necessary: (1) the sliding motion of a CD moiety along a polymer chain backbone, and (2) the cooperative movement with the segments surrounding and/or being connected to the CD moiety. For (1), the CD needs to cross the activation barrier to moving along a polymer

chain axis. For (2), the CD has to wait until the surrounding segments, and the connected segment relax. Both processes have to occur for the completion of the slow mode. Urakawa *et al.* proposed a two-step relaxation model to describe the hierarchical relaxation process[14]. In this model, one primitive process occurs, and after that, the other process is allowed to occur. The relaxation time of such a two-step process is approximately given as the sum of the two relaxation times for each process. Here it is assumed that the slow mode is the two-step relaxation of (1) and (2) with the relaxation times (1) for the sliding motion τ_{slide} and (2) for the relaxation of the surrounding media $\tau_{\alpha 2}$. Moreover, τ_{slide} is given by the Arrhenius equation, and $\tau_{\alpha 2}$ is given by the VFT equation, which is proportional to the α-relaxation time $\tau_{\alpha 2}$ ($=K\tau_{\alpha}$), τ_{slow} can be written as;

$$\tau_{\mathrm{slow}} = \tau_{\mathrm{slide}} + \tau_{\alpha 2} = \tau_1 \exp\left(\frac{E_{\mathrm{a}1}}{RT}\right) + \tau_2 \exp\left(\frac{A_2}{T-T_2}\right) \qquad (3\text{-}7)$$

To determine the K value the VFT equation of the α-relaxation was shifted to superpose to the τ_{slow} values at low temperature as shown in Figure 3-16, since the slow mode at low T is governed by the matrix segmental motion. The $\tau_{\alpha 2}(T)$ shown in this figure might be regarded as the relaxation time of free CD for which no sliding motion occurs. The fitting results for τ_{slow} of PEA-AcγCD(x) with eq. 3-7 are shown in Figure 3-16 by the solid line. The fitting parameters are as follows: $\tau_1 = 5.80\times10^{-26}$ s, $E_{\mathrm{a}1} = 131$ kJ/mol, $A_2 = 1.32\times10^3$ K, $T_2 = 215$ K, $K = 1.26\times10^3$. The A_2 and T_2, values have been already given previously. Eq. 3-7 shows good agreement with the experimental results in the whole temperature range, which suggests that the slow mode is governed by the two relaxation processes: the sliding motion of rotaxane type CD along the main chain and segmental relaxation.

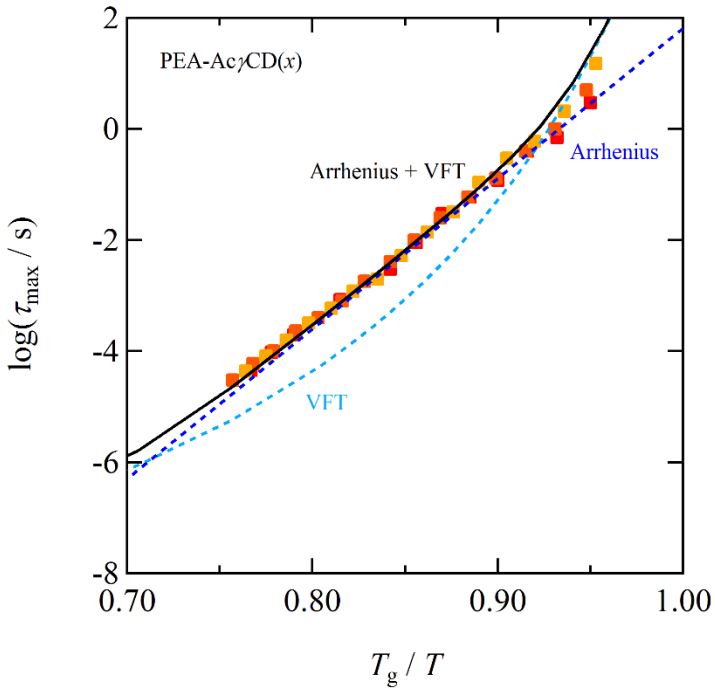

Figure 3-16. Schematic illustration representing temperature dependence of slow mode of PEA-AcγCD(x).

3-5. Conclusion

In this Chapter, the dynamics of the movable crosslinking network are investigated in detail, based on the rheological and dielectric data. The results are summarized as follows: (1) The DSC measurements showed that the glass transition temperature increases and the transition region broaden with increasing the feed CD concentration. (2) The dynamic viscoelastic measurements revealed the slow Rouse mode appeared in the low-frequency side of the transition zone. This relaxation was ascribed to the local fluctuation of the network structure due to the movable crosslink. (3) Low-frequency rheological data in the terminal region revealed that large-scale sliding motion of the movable crosslink occurred, and two-step plateaus appeared for the sample with high CD contents (x = 1.5mol%). Normal entanglements and permanent movable crosslink were considered to be responsible for the high frequency and low-frequency plateaus, respectively. (4) The broadband dielectric spectroscopy measurements

clarified the existence of the slow mode, which could be the relaxation process of the movable crosslink including both trapped and untrapped rotaxanes. (5) The temperature dependence of the slow mode relaxation time τ_{slow} could be approximately represented by the sum of the Arrhenius and VFT equations (two-step model). This temperature dependence suggested the segmental motion of a polymer chain and the sliding motion of a CD moiety play an important role in the dielectric slow mode.

3-6. Appendix: Determination of Dipole Moment for PAc*γ*CD

For the estimation of the dipole moment of Ac*γ*CD monomers, we conducted dielectric relaxation measurements on the benzene solutions of Ac*γ*CD. Figure 3-17 (A) and (B) show the frequency dependencies of the dielectric loss spectra and the molar concentration dependence of the dielectric intensity $\Delta\varepsilon$, respectively. It is seen that the relaxation intensity linearly increases with the CD concentration. By using the Onsager equation given by eq. 3-6, the dipole moment of AcγCD monomer $\mu_{Ac\gamma CD}$ was estimated to be 7.0 D. Shikata *et al*. studied the dielectric relaxation behavior of the aqueous solution of permethylated *γ*CD (Me*γ*CD). They reported the value of the dipole moment as $\mu_{Me\gamma CD}$ =13 D, which is larger than $\mu_{Ac\gamma CD}$ determined here. This difference might be ascribed to the more flexible acetyl groups in Ac*γ*CD, taking some stable conformations to cancel their dipole moments compared with the case of methoxy groups in Me*γ*CD.

(A)

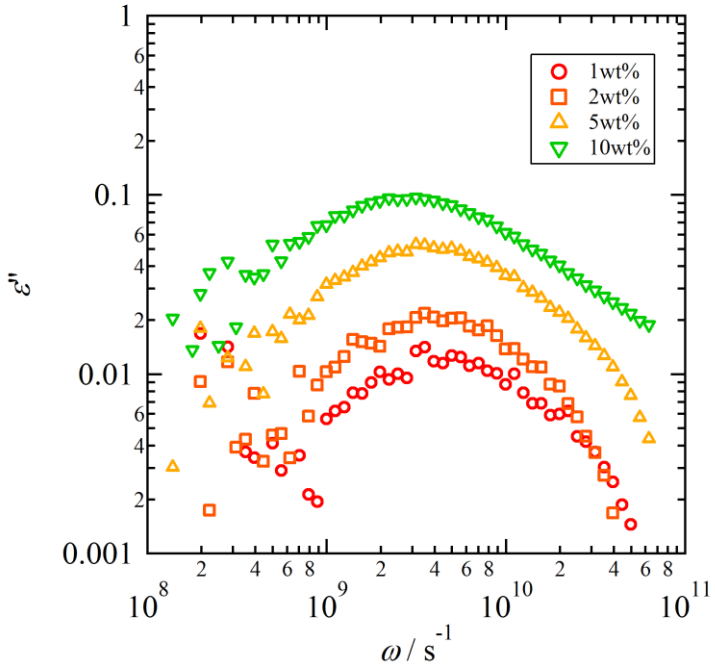

(B)

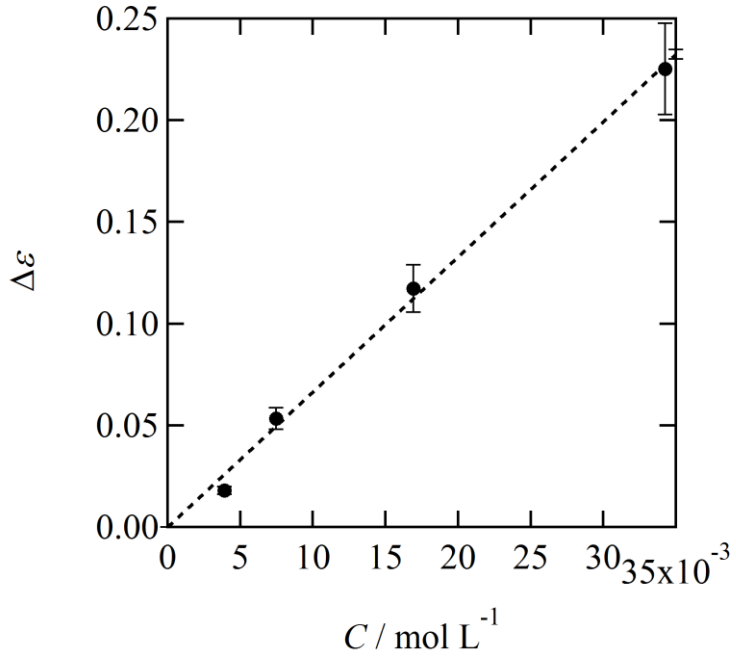

Figure 3-17. (A) Frequency dependence of dielectric loss for AcγCD/benzene solutions with various concentrations, and **(B)** the *C* dependence of Δε.

3-7. References

1. Kashiwagi, Y.; Katashima, T.; Nakahata, M.; Takashima, Y.; Harada, A.; Inoue, T., Linear viscoelastic studies on a transient network formed by host–guest interaction. *Journal of Polymer Science Part B: Polymer Physics* **2018,** *56* (15), 1109-1117.
2. Kashiwagi, Y.; Katashima, T.; Takashima, Y.; Harada, A.; Inoue, T., Effect of Host-Guest Interaction on Swelling Behavior and Equilibrium Swollen State of Host-Guest Gel. *Nihon Reoroji Gakkaishi* **2019,** *47* (3), 99-104.
3. Ikura, R.; Park, J.; Osaki, M.; Yamaguchi, H.; Harada, A.; Takashima, Y., Supramolecular Elastomers with Movable Cross-Linkers Showing High Fracture Energy Based on Stress Dispersion. *Macromolecules* **2019,** *52* (18), 6953-6962.
4. Okumura, Y.; Ito, K., The Polyrotaxane Gel: A Topological Gel by Figure-of-Eight Cross-links. *Advanced Materials* **2001,** *13* (7), 485-487.
5. Kondo, Y.; Urayama, K.; Kidowaki, M.; Mayumi, K.; Takigawa, T.; Ito, K., Applicability of a particularly simple model to nonlinear elasticity of slide-ring gels with movable cross-links as revealed by unequal biaxial deformation. *The Journal of Chemical Physics* **2014,** *141* (13), 134906.
6. Kato, K.; Yasuda, T.; Ito, K., Viscoelastic Properties of Slide-Ring Gels Reflecting Sliding Dynamics of Partial Chains and Entropy of Ring Components. *Macromolecules* **2012,** *46* (1), 310-316.
7. Shikata, T.; Takahashi, R.; Satokawa, Y., Hydration and Dynamic Behavior of Cyclodextrins in Aqueous Solution. *The Journal of Physical Chemistry B* **2007,** *111* (42), 12239-12247.
8. Gordon, M.; Taylor, J. S., Ideal copolymers and the second-order transitions of synthetic rubbers. i. non-crystalline copolymers. *Journal of Applied Chemistry* **1952,** *2* (9), 493-500.
9. Wood, L. A., Glass transition temperatures of copolymers. *Journal of Polymer Science* **1958,** *28* (117), 319-330.
10. Fox, T. G., Influence of Diluent and of Copolymer Composition on the Glass Temperature of a Poly-mer System. *Bull. Am. Phys. Soc.* **1956,** *1*, 123.
11. Winter, H. H., The Critical Gel. In *Structure and Dynamics of Polymer and Colloidal Systems*, Borsali, R.; Pecora, R., Eds. Springer Netherlands: Dordrecht, 2002; pp 439-470.
12. Schoenhals, A., Relation between main and normal mode relaxations for polyisoprene studied by dielectric spectroscopy. *Macromolecules* **1993,** *26* (6), 1309-1312.
13. Sokolov, A. P.; Hayashi, Y., Breakdown of time–temperature superposition: From experiment to the coupling model and beyond. *J Non-Cryst Solids* **2007,** *353* (41), 3838-3844.
14. Urakawa, O.; Yamane, M.; Tomie, S.; Inoue, T.; Shikata, T.; Adachi, K., Relationship between global and segmental dynamics of poly(butylene oxide) studied by broadband dielectric spectroscopy. *The Journal of Chemical Physics* **2018,** *148* (3), 034904.

15. Ding, Y.; Sokolov, A. P., Breakdown of Time−Temperature Superposition Principle and Universality of Chain Dynamics in Polymers. *Macromolecules* **2006,** *39* (9), 3322-3326.
16. Lodge, T. P.; McLeish, T. C. B., Self-Concentrations and Effective Glass Transition Temperatures in Polymer Blends. *Macromolecules* **2000,** *33* (14), 5278-5284.
17. Yasuda, Y.; Hidaka, Y.; Mayumi, K.; Yamada, T.; Fujimoto, K.; Okazaki, S.; Yokoyama, H.; Ito, K., Molecular Dynamics of Polyrotaxane in Solution Investigated by Quasi-Elastic Neutron Scattering and Molecular Dynamics Simulation: Sliding Motion of Rings on Polymer. *Journal of the American Chemical Society* **2019,** *141* (24), 9655-9663.
18. Inoue, T.; Osaki, K., Role of Polymer Chain Flexibility on the Viscoelasticity of Amorphous Polymers around the Glass Transition Zone. *Macromolecules* **1996,** *29* (5), 1595-1599.
19. Kato, K.; Mizusawa, T.; Yokoyama, H.; Ito, K., Effect of Topological Constraint and Confined Motions on the Viscoelasticity of Polyrotaxane Glass with Different Interactions between Rings. *The Journal of Physical Chemistry C* **2017,** *121* (3), 1861-1869.
20. Xu, B.; Wu, J.; McKenna, G. B., Mechanical and Swelling Behaviors of End-Linked PDMS Rubber and Randomly Cross-Linked Polyisoprene. *Macromolecules* **2013,** *46* (5), 2015-2022.

Chapter 4

Nonlinear Rheological Behavior of Movable Crosslinking Networks under Uniaxial Large Deformation

4-1. Introduction

Tough polymeric materials are desired not only in the scientific field but also in the engineering field. For more than decades, to improve the toughness of polymeric materials, many new structural designs have been proposed, *e.g.*, filler filled rubbers[1], ionomers[2-4], and double network gels[5-6], etc. As shown in Chapter 3, the MCN is one of the candidates for the tough polymeric materials. The crosslink is formed by the rotaxane-type acetylated cyclodextrin connected to the polymer backbone, which can slide along a polymer chain and also work as permanent crosslinks. Figure 4-1 shows the representative true stress-strain curves of a MCN. At all the measurement temperatures, the movable crosslinking network has high rupture strain and high rupture stress, suggesting that the movable crosslink had a crucial contribution to enhancing the toughness of polymeric materials.

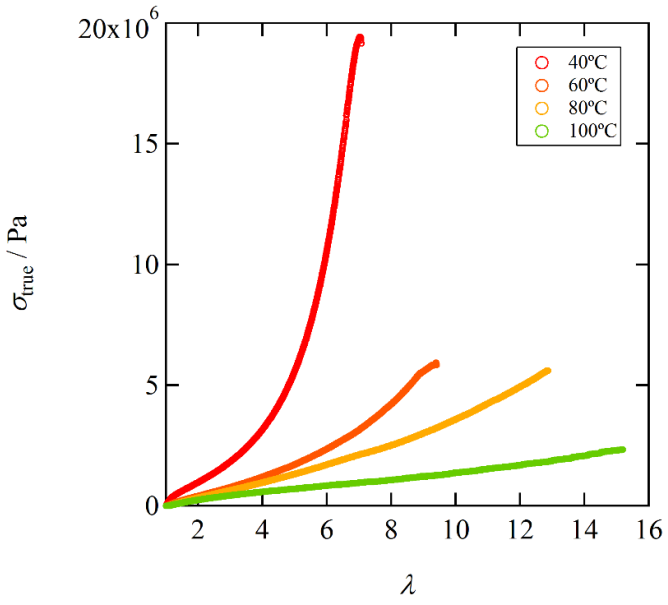

Figure 4-1. True stress-strain curves of PEA-AcγCD(2.0) at various temperatures. The crosshead speed is 1 mm s^{-1} constant.

One of the possible reasons for this excellent mechanical property is the change of the chain length between the crosslinks accompanied by the sliding motion of the movable crosslinks. In general, the maximum strain ratio of a network is determined by the chain length between crosslinks[7]. In the case of Gaussian networks composed of a uniform network strand length, the maximum stretch ratio of the network, λ_{max}, is determined by the maximum stretch ratio of the strand, and hence $\lambda_{max} \sim N^{0.5}$, where N is the number of the Kuhn segment per network strand.. For chemically crosslinked networks, the elastic modulus, G, is proportional to the number of effective network strands and hence $G \sim N^{-1}$. On the other hand, in the MCN, the crosslinks can slide along the polymer chain even under the deformation[8], which results in adjusting the effective chain length between crosslinks. Furthermore, the energy dissipation, accompanied by both the entropy and enthalpy changes by the sliding motion can, contribute to the high mechanical toughness[9-10]. These molecular mechanisms are expected to be dominant in the non-equilibrium state, and lead to the nonlinear viscoelastic response: stress-strain curve under large deformation. Unfortunately, the nonlinear properties of the movable crosslinks, which are important to accomplish the high mechanical toughness, have not been analyzed experimentally in detail. In this Chapter, nonlinear viscoelastic properties of the movable crosslinking network are investigated through cycle tests of the large uniaxial deformation. The experimental results are fully analyzed by using the BKZ-type constitutive equation[11]. The molecular bases of obtained new parameters through the BKZ analysis will be discussed how they are related to nonlinear behavior. The results of this chapter will contribute to the understanding of the molecular dynamics of the movable crosslinking network and designing the tough polymeric materials.

4-2. Experimental

4-2-1. Sample preparation

The method of the sample preparation was almost the same as that described in Chapter 3[8]. The peracetylated γ-cyclodextrin (AcγCD) was mixed with ethyl acrylate (99%, TCI) as a movale crosslinker by an ultrasonic stirrer for 1 hour to make a completely mixed solution. After that, 1-hydroxycyclohexyl phenyl ketone (99%, Sigma Aldrich) was mixed with this monomer solution by an ultrasonic stirrer for 5 minutes. The obtained solution was poured into the mold, and UV light was irradiated through a 1 mm thick glass plate for 30 minutes at 25°C to initiate bulk radical copolymerization. The molar ratio of crosslinker and initiator are constant at 2.0 mol% and 1.0 mol%, respectively. The obtained samples were dried at 60°C in a vacuum oven for 1 day before all the measurements to remove residual monomer components.

4-2-2. Linear and nonlinear stress relaxation

The linear shear stress relaxation measurements were carried out with the stain-controlled rheometer ARES-G2 (TA instruments) equipped with a parallel-plate fixture of 4 mm diameter. The temperature was varied from 40°C to 100°C and the strain amplitude was fixed to be 5.0% to ensure the linear viscoelastic response.

The nonlinear tensile stress relaxation measurements were carried out with the uniaxial extensional creep meter RE-33005-2L2 (YAMADEN). The relaxation stress was measured after the step strain of $\lambda = 2 - 8$. The rectangular specimens (length ~ 12 mm, width ~ 5.0 mm, thickness ~ 1.0 mm) were used for measurements. The temperature was varied from 40 to 100°C.

4-2-3. Loading and unloading cycle tests

The loading and unloading cycle tensile tests were carried out with the uniaxial extensional apparatus (YAMADEN). The rectangular specimens (length ~ 12 mm, width ~ 5.0 mm,

thickness ~ 1.0 mm) were used. Stretching and retracting rates were constant: 0.1, 0.5, 1, 5, or 10 mm s^{-1}, and the loading and unloading process was repeated 1or 2 times. The temperature was also varied from 60 to 100°C.

4-3. Results and Discussion

4-3-1. Linear viscoelastic behavior

In this section, the linear viscoelastic behavior of PEA-AcγCD(2.0) will be overviewed. Figure 4-2(A) shows the composite curves of storage modulus G', loss modulus G'', and loss tangent tanδ of PEA-AcγCD(2.0). As same with the behavior discussed in Chapter 3, introducing the movable crosslink affects the complex modulus in two frequency regions: (1) broadening of the glass and Rouse modes and (2) appearance of a long relaxation time component in the terminal region. Regarding (1), the shoulders of both G' and G'' in the transition region become broader, which indicates that the relaxation strength of the "slow mode" becomes larger with increasing movable crosslinker concentration. The enhancement of the slow mode was attributed to the sliding motion within a short-range at most a few segments in Chapter 3. Besides, the second plateau modulus was attributed to the permanently trapped rotaxane structure in which one CD molecule is sandwiched by two other bulky groups. The plateau modulus of G' in the terminal region is larger than that of PEA-AcγCD(1.5) (shown in Figure 3-5 of Chapter 3), which is consistent because the number of the permanent crosslinks formed by trapped rotaxane structure should increase when the feed concentration of the movable crosslinker increases.

Figure 4-2(B) shows the time t dependence of the relaxation modulus $G(t)$ of PEA-AcγCD(2.0) at various temperatures. $G(t)$ monotonically decreases with increasing t, and becomes almost constant in the longest time of the present study even at T = 100°C. This result is consistent with the terminal flow region shown in Figure 4-2(A). This broad relaxation mode between first to second plateau modulus is attributed to disentanglements of chains. The height

of the first plateau modulus is almost same as that of the poly(ethyl acrylate) homopolymer (~ 2.0×10^5 Pa). Therefore, in this relaxation process, the entangled network strands are partially disentangled but the permanent crosslinks composed of the trapped rotaxane and trapped entanglements responsible for the second plateau modulus are preserved in the longer time region.

(A)

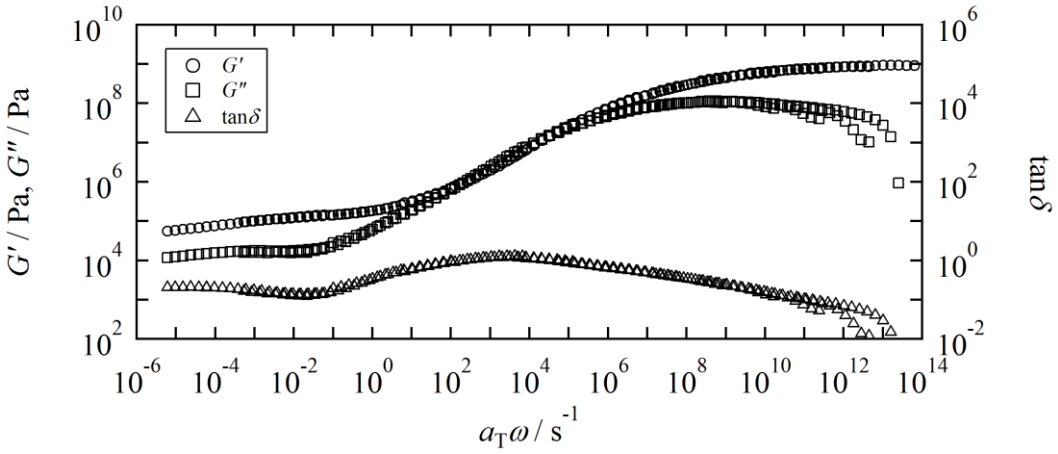

(B)

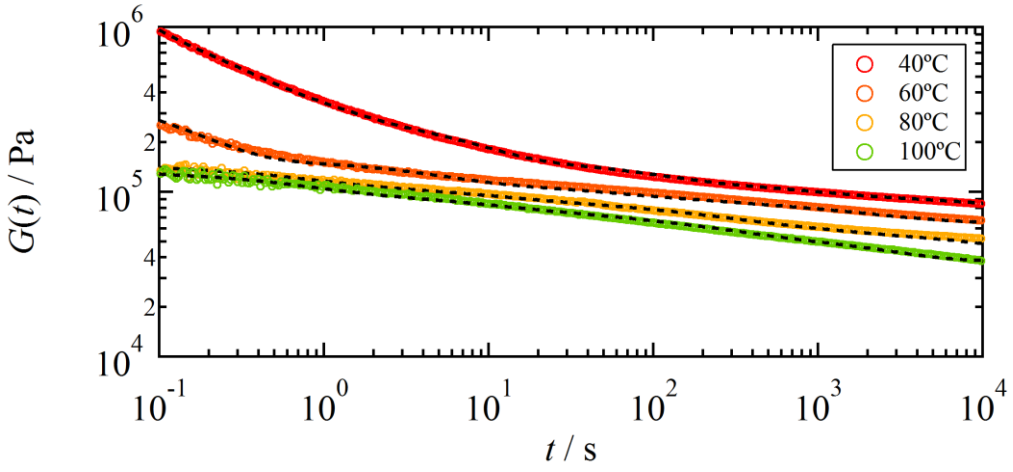

Figure 4-2. (A) Composite curves of G' (circle), G'' (square), and tanδ (triangle) for PEA-AcγCD(2.0). The reference temperature T_r is set to be 60°C. **(B)** Time dependence of relaxation modulus $G(t)$. Black dotted lines represent the fitting results by eq. 4-6.

4-3-2. Cycle tests under uniaxial deformation

Figure 4-3 shows the true stress-strain curve of the first loading-unloading test with a crosshead speed of 1 mm s^{-1} at T = 60°C. When focusing on the loading process, the stress sharply increases at the low strain region ($\lambda \leq 2$), and then the increase of the stress becomes weaker at the intermediate strain region ($2 \leq \lambda \leq 4$), and finally, the stress sharply increases again in the high strain condition ($4 \leq \lambda$). Besides, unlike chemically crosslinked rubbers, the stress in the unloading process becomes much smaller than that in the loading process and shows a pronounced hysteresis the residual strain. This hysteresis should be attributed to the energy dissipation under deformation, including the viscoelastic effect and the nonlinear strain dependence of the stress due to the plastic deformation. To understand the above features in the tensile test, a phenomenological approach using the BKZ type constitutive equation is examined in the next section.

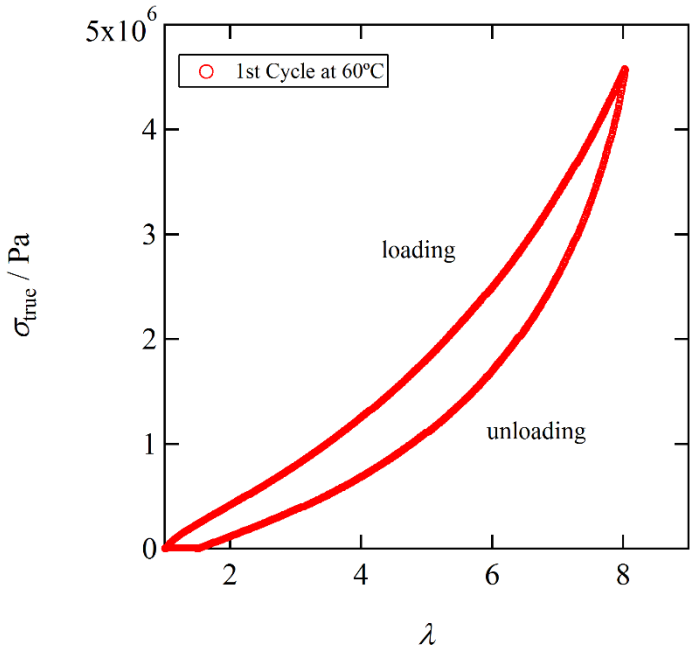

Figure 4-3. True stress-strain curves of the first loading-unloading process for PEA-AcγCD(2.0) at T = 60°C.

4-3-3. Theoretical approach based on the BKZ Model

For phenomenological analysis of the nonlinear rheological behavior, especially about the cycle tests of PEA-Ac*γ*CD(2.0), the BKZ model is employed[11-13]. This model assumes that the constitutive equation for viscoelastic bodies are utilized by expressing the free energy change due to the deformation history from a certain past time, t', to a current time, t. By integrating the strain energy function with respect to t', the stress at a current time, $\sigma(t)$, is formulated. To introduce the effect of viscoelasticity, the strain energy function U is assumed to change with time and given by the following equation.

$$U = U[t - t'; I_1(t, t'), I_2(t, t')] \tag{4-1}$$

where I_1 and I_2 are the first and the second invariant in the Finger deformation tensor, respectively. Assuming the time-strain separability, free energy is rewritten as follows:

$$U = \mu(t - t')H(I_1, I_2) \tag{4-2}$$

where $\mu(t - t')$ is the memory function, which represents the time-dependent decay of the deformation energy resulting in the viscoelastic effect, and $H(I_1, I_2)$ is the strain-dependent function, which represents the stored energy during the deformation. In eq. 4-2, the memory function is assumed to be independent of the applied strain. By differentiating eq. 4-2 with respect to strain, the stress at time t, $\sigma(t)$, is given by the following equation:

$$\boldsymbol{\sigma}(t) = \int_{-\infty}^{t} \mu(t - t')[h_1(I_1, I_2)\boldsymbol{C}_t^{-1}(t') + h_2(I_1, I_2)\boldsymbol{C}_t(t')]\mathrm{d}t' \tag{4-3}$$

$$h_1(I_1, I_2) = 2\frac{\partial H(I_1, I_2)}{\partial I_1} \tag{4-4}$$

$$h_2(I_1, I_2) = 2\frac{\partial H(I_1,I_2)}{\partial I_2} \tag{4-5}$$

where $h_1(I_1, I_2)$ and $h_2(I_1, I_2)$ are the damping functions relating to the strength of nonlinear strain dependence. $\boldsymbol{C}_t^{-1}$ and $\boldsymbol{C}_t$ are the relative Finger strain tensor and the relative Cauchy strain tensor, respectively.

The memory function $\mu(t)$ is obtained from the relaxation modulus $G(t)$ through the relation of $\mu(t) = \mathrm{d}G(t)/\mathrm{d}t$. To do this conversation $G(t)$ is fitted by the generalized Maxwell models:

$$G(t) = G_N + \sum_i G_i \exp\left(-\frac{t}{\tau_i}\right) \tag{4-6}$$

where G_i and τ_i are the relaxation intensity and time of the i-th mode, respectively. G_N is the equilibrium plateau modulus estimated in the long-time limit. As shown in Figure 4-2(B), it is seen that eq. 4-6 well describes the experimental results. On the other hand, as for the damping functions, there have been many phenomenological attempts proposed.

Firstly, the Lodge model[14], the simplest version of eqs. 4-3~4-5, is applied, which corresponds to the case of $h_1 = 1$ and $h_2 = 0$. This model assumes only the affine deformation of network stands and considers neither the coupling of strains along different axes nor any nonlinear effects such as strain hardening and strain softening, etc. The true stress under the uniaxial stretching is given by,

$$\sigma(t) = \int_{-\infty}^{t} \sum_i \frac{G_i}{\tau_i} \exp\left(-\frac{t-t'}{\tau_i}\right) \times \left[\frac{\lambda^2(t)}{\lambda^2(t')} - \frac{\lambda(t')}{\lambda(t)}\right] \mathrm{d}t' + G_N\left(\lambda^2(t) - \frac{1}{\lambda(t)}\right) \tag{4-7}$$

Figure 4-4(A) compares the $\sigma(t)$ data of PEA-AcγCD(2.0) at T = 60°C with the prediction of eq. 4-7, which is shown by a dotted line. In the small deformation region ($\lambda = 3$), the calculated curve by eq. 4-7 almost overlaps with the experimental data. On the other hand, in the larger deformation region, the theoretical value becomes higher than the experiment, and the deviation becomes prominent with the increase of λ. In general, the lower true stress than the theoretical prediction in the intermediate strain regime is attributed to the cross-coupling effect between the strain components with different principle axes. Many early studies have pointed out the presence of the explicit cross-coupling effect (necessity of the introduction of I_2 term) to express the stress of chemically crosslinked rubbers and polymer gels[15-17]. In the Moony Rivlin equation often used to fit the stress-strain curve of rubbers[18], I_2 term is known in be involved in the so-called C_2 term. Early studies have attributed the cross-coupling effect to the contribution of interaction between network strands such as entanglement interaction[16], excluded volume effect[17] or nematic interaction[19-20], etc. Urayama *et al*. performed the biaxial stretching for polyacrylamide gels and observed the explicit cross effect in the strain tensor components. In the phenomenological constitutive model, this cross effect can be described by the introduction of the second invariant of the Finger tensor, I_2, into the strain energy density function. On the other hand, when a polymer chain is highly stretched, the strain hardening is often observed, which is attributed to the finite extensibility of a real chain. Conventionally, this strain hardening is modeled by introducing the finite strain value at which the stress diverges. In this study, the Gent-type H function is adopted[21]:

$$H = -\frac{I_m-3}{2}\ln\left(1-\frac{I_1-3}{I_m-3}\right) \tag{4-8}$$

where I_m is the maximum I_1 value at which the stress becomes infinite. As discussed in Chapter 3, the trapped rotaxanes work as permanent crosslinks even though they slide a certain distance

along the threaded chain backbone. Therefore, the slidable distance of the permanent crosslinks should largely contribute to the strain hardening effect.

Considering the cross coupling between the principal axes and also the nonlinear finite extensibility, the constitutive model can be rewritten as follows:

$$\sigma(t) = \int_{-\infty}^{t} \left(\sum_i \frac{G_i}{\tau_i} \exp\left(-\frac{t-t'}{\tau_i} \right) \times \left[r\left(\frac{\lambda^2(t)}{\lambda^2(t')} - \frac{\lambda(t')}{\lambda(t)} \right) + (1-r)\left(\frac{\lambda(t)}{\lambda(t')} - \frac{\lambda^2(t')}{\lambda^2(t)} \right) \right] \right) dt' + G_{\mathrm{N}} \left[r\left(\lambda^2(t) - \frac{1}{\lambda(t)} \right) + (1-r)\left(\lambda(t) - \frac{1}{\lambda^2(t)} \right) \right] \left(1 - \frac{\lambda^2(t) + \frac{2}{\lambda(t)} - 3}{I_{\mathrm{m}} - 3} \right)^{-1} \tag{4-9}$$

where r is the fitting parameter that determines the contribution ratio of the I_2 term. Figure 4-4(B) shows the fitting results with eq. 4-9. In the loading process, the fitting curve shows a better agreement than that with eq. 4-7. This indicates that the sharp increase of the true stress in the large deformation region is attributable to the nonlinear finite extensibility of polymer strands. On the other hand, in the unloading process, the hysteresis of the experimental data is much larger than the calculated curve, and a large discrepancy between them is seen especially in the large deformation region. These results suggest that the hysteresis is mostly dependent on other factors, except for the time dependence of the memory function incorporated in eq. 4-9. To explain this discrepancy, I will discuss the nonlinearity effect between stress and strain in the next section.

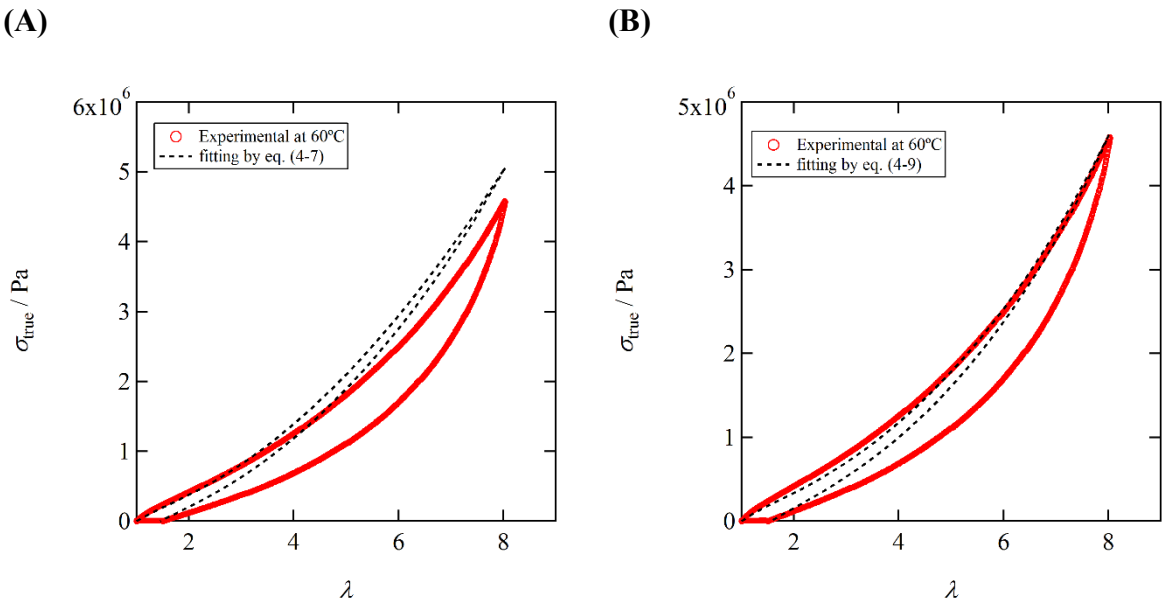

Figure 4-4. Fitting results of true stress at T = 60°C by **(A)** eq. 4-7 and **(B)** eq. 4-9 (I_m = 300, r = 0.60).

4-3-4. Nonlinear stress relaxation

The nonlinear stress relaxation measurements under large uniaxial deformation were conducted to examine the time dependence for nonlinearity. Figure 4-5 shows the time dependence of the true stress for PEA-AcγCD(2.0) under large tensile deformation. The maximum stretch ratio was changed from 2.0 to 8.0. The stress gradually decayed after the imposition of the maximum strain. It is seen that the slope of the stress decay became stronger with increasing the maximum stretch ratio, and thus, these curves are not overlapped even by a simple vertical shift. Doi-Edward (DE) model predicts that in well-entangled polymer systems, the stress relaxation after a large step strain occurs firstly through the chain contraction accompanied with the decrease of the number of entanglements, and then through the reptational motion. According to the DE model, the nonlinearity of the stress relaxation is described by a single damping function that depends only on the strain (time-strain separability). For the data shown in Fig. 4-5, the damping function is evaluated and applied to the BKZ equation to analyze the loading-unloading stress-strain data shown in Fig. 4-4.

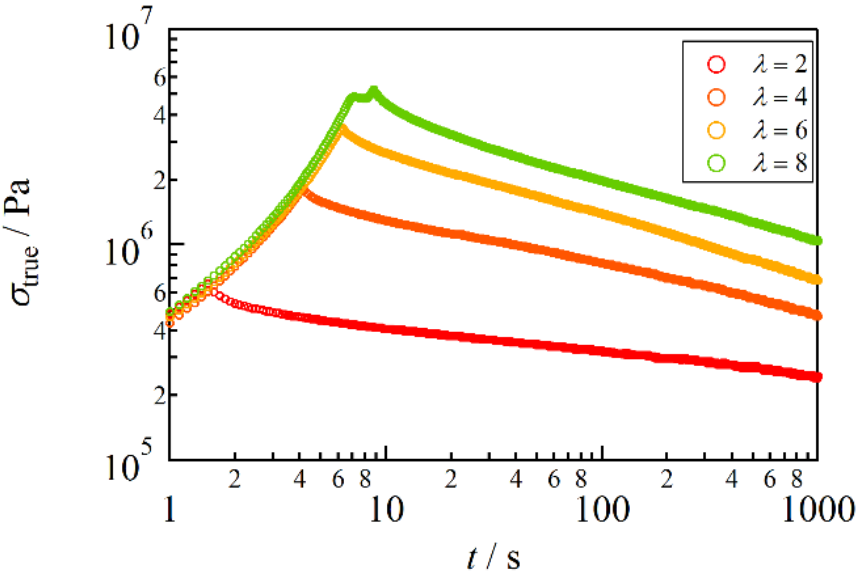

Figure 4-5. Time dependence of the true strain under nonlinear stress relaxation measurements with different maximum stretch ratio at $T = 60°C$.

Firstly, to evaluate the damping function for the relaxation components, the contribution of permanent crosslinks at the longest time was subtracted from the stress data, and then the stress of each maximum stretch ratio was vertically shifted and superposed on the linear data: the shear modulus $G(t)$. To take into the account the difference of the deformation mode, the true stress was converted to $G(t)$ by the following equation[22]:

$$G(t) = \frac{\sigma(t)-\sigma_N}{h[\exp(2\varepsilon)-\exp(-\varepsilon)]} = \frac{\sigma(t)-\sigma_N}{h[\lambda^2-\lambda^{-1}]} \quad (4\text{-}10)$$

where h is the damping function (the vertical shift factor), ε is the Hencky strains defined by $\varepsilon = \ln\lambda$, and σ_N is the limiting plateau stress in the longest time region at each temperature. Figures 4-6(A), (B), and (C) show the time dependence of converted $G(t)$ obtained with the different maximum stretch ratios at $T = 60°C$, 80°C, and 100°C, respectively. All of the data are well

superposed to the linear $G(t)$ data in the long time region. From these superpositions, the damping functions at each temperature are obtained and shown in Figure 4-6(D). The λ dependence of the dumping function becomes stronger with increasing the measurement temperature, which indicates the nonlinearity of the MCN becomes stronger with increasing temperature. This might be related to the change in the number of the untrapped rotaxane crosslinks.

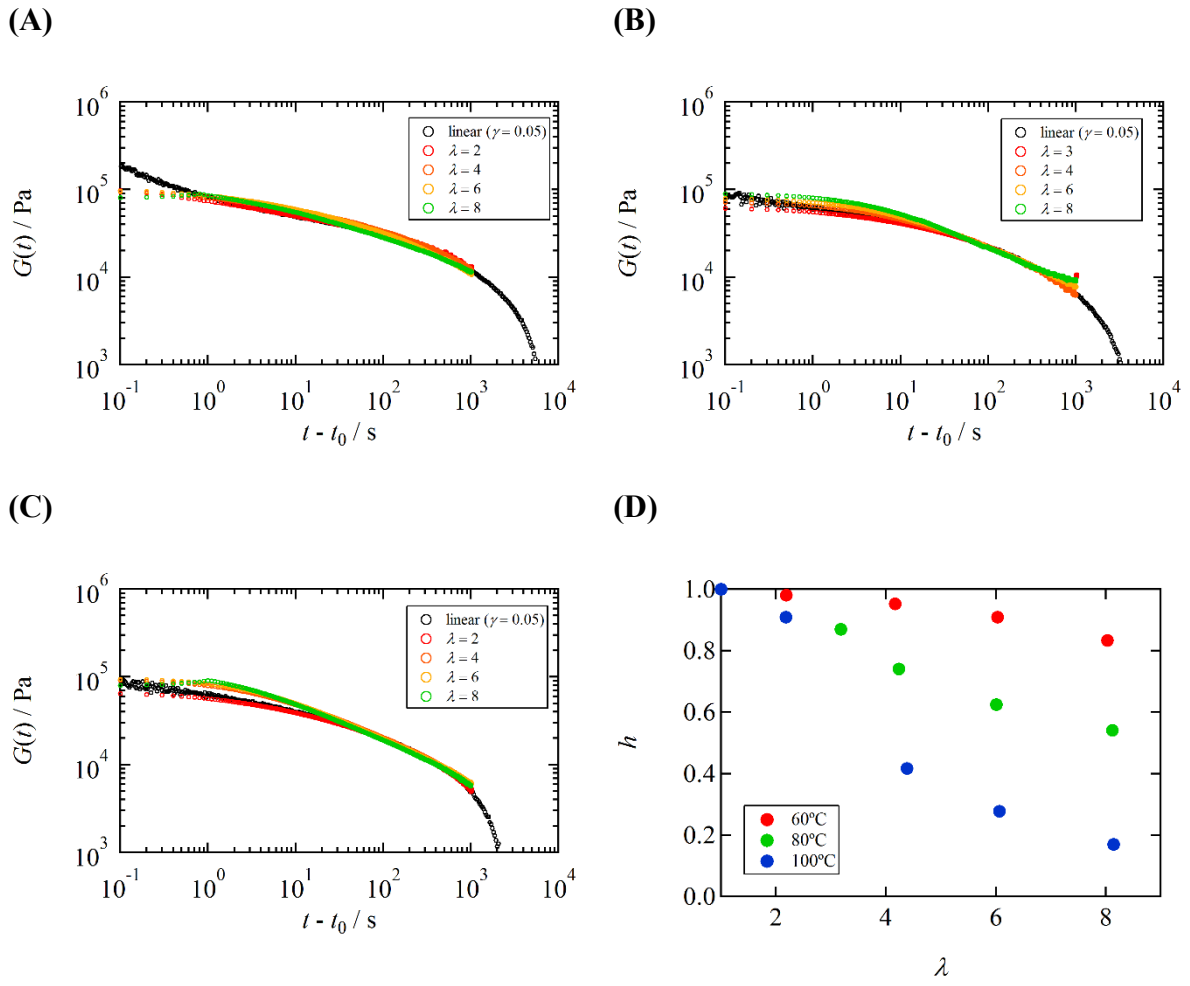

Figure 4-6. Time dependence of the converted $G(t)$ by eq. 4-10 with different stretching ratio at **(A)** $T = 60°C$, **(B)** $T = 80°C$, and **(C)** $T = 100°C$. **(D)** The damping function h vs. the maximum stretching ratio defined in eq. 4-10.

4-3-5. Introducing the irreversible effect

As shown in the previous section, it is revealed that the viscoelastic relaxation time is hardly affected by the deformation amplitude and also that the time-strain separability holds. In this section, to fit the functional form of the obtained damping function, the following PSM type damping function is employed which is one of the most widely used for polymer melts[23]:

$$h(I_1, I_2) = \frac{\alpha}{(\alpha-3)+\beta I_1+(1-\beta)I_2} = \frac{\alpha}{(\alpha-3)+I_1} \quad (\beta = 1) \tag{4-11}$$

where α and β are fitting parameters. Here, β is set to be 1 for simplicity, which indicates that the I_2 term has no contribution to the damping functions. Using eq. 4-9 and 4-11, the true stress under uniaxial deformation can be described as follows:

$$\sigma(t) = \frac{\alpha_1}{(\alpha_1-3)+I_1}\int_{-\infty}^{t}\left(\sum_i \frac{G_i}{\tau_i}\exp\left(-\frac{t-t'}{\tau_i}\right)\times\left[r\left(\frac{\lambda^2(t)}{\lambda^2(t')}-\frac{\lambda(t')}{\lambda(t)}\right)+(1-r)\left(\frac{\lambda(t)}{\lambda(t')}-\frac{\lambda^2(t')}{\lambda^2(t)}\right)\right]\right)\mathrm{d}t'$$
$$+\frac{\alpha_2}{(\alpha_2-3)+I_1}G_{\mathrm{N}}\left[r\left(\lambda^2(t)-\frac{1}{\lambda(t)}\right)+(1-r)\left(\lambda(t)-\frac{1}{\lambda^2(t)}\right)\right]\left(1-\frac{\lambda^2(t)+\frac{2}{\lambda(t)}-3}{I_{\mathrm{m}}-3}\right)^{-1} \tag{4-12}$$

where α_1 and α_2 are fitting parameters that determine the damping functions of the relaxation and permanent components, respectively. Furthermore, the damping functions are assumed not to recover and to keep a constant value during the unloading process. This means that the modulus damped by the large strain does not recover implying the irreversibility of the structural change. The α_1 value in eq. 4-12 was determined from the experimental damping functions shown in Figure 4-6(D) by fitting the data with eq. 4-11. Figure 4-7(A) shows the fitted results of the damping function, indicating that all of the functions are well reproduced by eq. 4-11. Furthermore, utilizing these α_1 values, the true stress-strain curve shown in Figure

4-3 was fitted by eq. 4-12. The results are shown in Figure 4-7(B). It is seen that eq. 4-12 well reproduce the experimental results, including the large hysteresis loss.

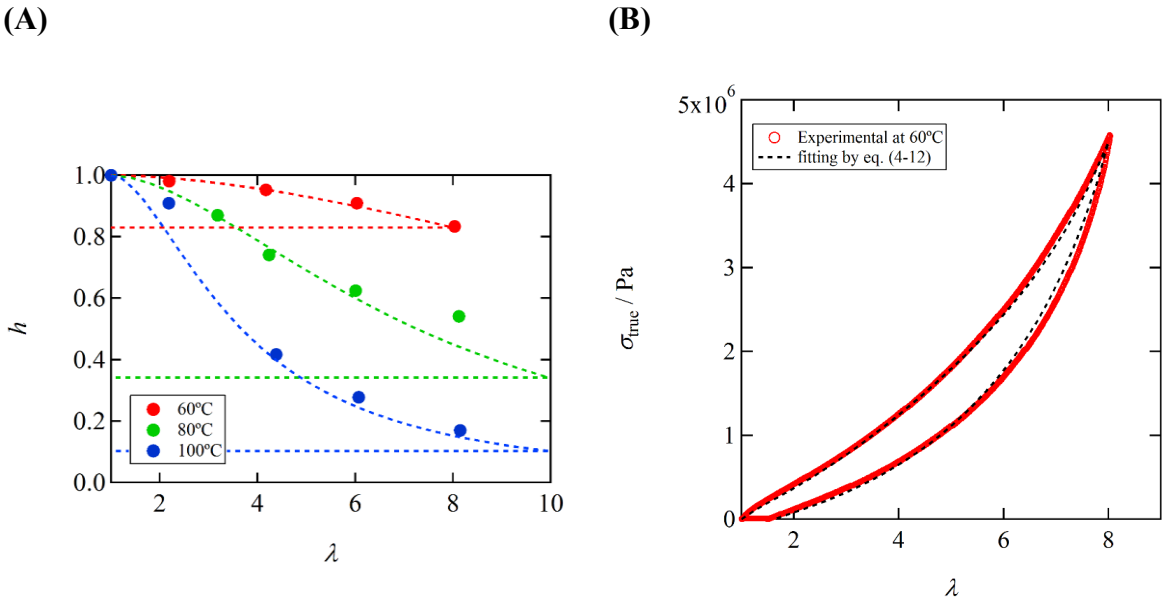

Figure 4-7. (A) Fitting results of damping functions at each temperature by eq. 4-11. **(B)** The black dotted line represent the fitting result of loading-unloading process for PEA-AcγCD(2.0) at T = 60°C by eq. 4-12 with I_m = 108, r = 0.81, α_1 = 300, α_2 = 38.

4-3-6. Temperature and deformation rate dependence

Figure 4-8(A) shows the results of the first loading-unloading process at different temperatures with a crosshead speed of 1 mm s^{-1}. The fitting results by eq. 4-12 are also shown by black dotted lines. All of the experimental data are well reproduced by eq. 4-12 with the α_1 values obtained from the fittings in Figure 4-7(A), which validates the eq. 4-12 as a universal constitutive equation describing the relationship between strain and stress under the uniaxial deformation.

Figure 4-8(B) shows the temperature dependence of I_m used in fitting in Figure 4-8(A). I_m is the strain invariant, at which the stress becomes infinite in the Gent model, monotonically increased with increasing temperature, which indicates the finite extensibility is strongly

dependent on the temperature. This behavior is different from chemically crosslinked networks, and thus is attributable to the sliding motion of the movable crosslinks. At low temperatures, the crosslinks cannot slide along the polymer chain because of the inactive thermal motion, and behaves like chemical crosslinks. In such a case, the finite extensibility of network chains would be observed in a smaller strain. On the other hand, at high temperatures, the mobility of the crosslinks increases with increasing temperatures. Therefore, a whole chain can move through the deformation of the specimen, and the finite extensibility of network chains becomes less likely to be observed. These results suggest that the strain-induced sliding motion would play a key role in the finite extensibility of network chains.

Figure 4-8(C) shows the temperature dependence of the parameter r representing the contribution of I_1 term in eq. 4-12. With increasing the temperature, r decreases. This result suggests that the contribution of the strain cross term between different axes are increased with the temperature. This can also be explained by the sliding motion of the movable crosslinks. For conventional chemically crosslinked rubbers, the crosslinks are fixed at a certain point of a polymer chain by covalent bonds, and in this case, a macroscopic strain causes molecular level deformation affinely. On the other hand, for the MCN, the crosslinks can slide under the macroscopic deformation resulting in the non-affine deformation at the molecular level. In such a case, the contribution of the cross term, namely I_2 term, is considered to become larger. In general, the contribution of I_2 term is reported to be 20% ($r \sim 0.8$) for conventional rubber systems. The experimental value at 60°C estimated from the fitting is consistent with this value, which indicated the consistency of the above discussion. The increase of the temperature induces the sliding motion of the movable crosslinks under deformation, and therefore the contribution of I_2 term became larger due to the increase in the non-affinity.

(A)

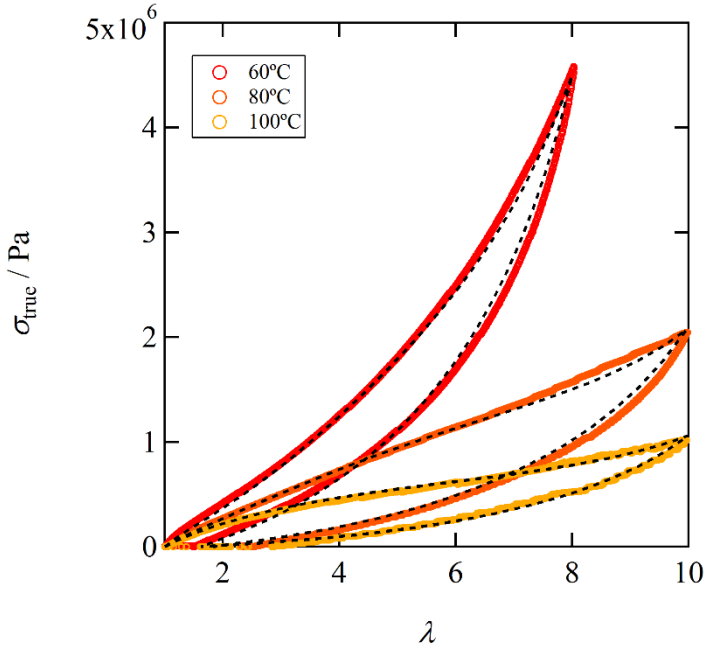

(B) **(C)**

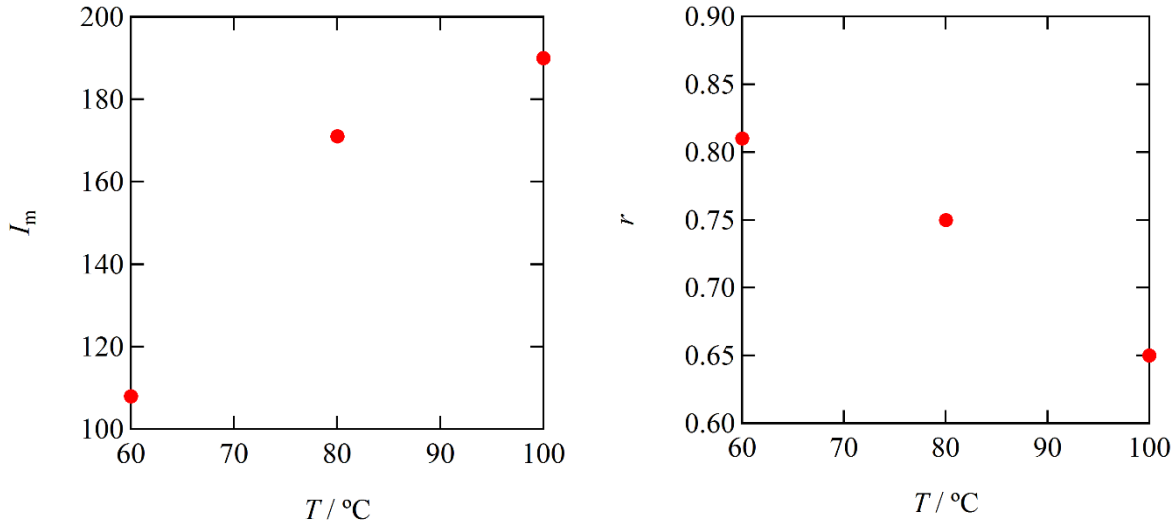

Figure 4-8. (A) Comparison of fitting results of 1st loading-unloading process at T = 60°C, 80°C and 100°C. Fitting parameters are I_m = 171, r = 0.75, α_1 = 50, α_2 = 19 at T = 80°C and at I_m = 190, r = 0.65, α_1 = 11, α_2 = 16 at T = 100°C, respectively. The temperature dependence of **(B)** I_m and **(C)** r are also shown.

Figure 4-9(A) shows the results of the first loading-unloading cycle at $T = 60°C$ with different crosshead speeds. The fitting results by eq. 4-12 are also shown by black dotted lines. All of the experimental results are well reproduced by eq. 4-12, indicating that the constitutive equation proposed in this study is the universal form irrespective of not only temperatures but also deformation rates. Besides, the values of α_1 and r are almost independent of the crosshead speed, and experimental results are reproduced by changing only I_m and α_2 in eq. 4-12. This result suggests that the relaxation component in the constitutive equation is almost independent of the deformation rate; however, the nonlinearity and the finite extensibility of the permanent network component are dependent on the deformation rate. Figure 4-9(B) shows the crosshead speed dependence of the I_m used in the fittings in Figure 4-9(A). Im monotonically decreases with increasing the crosshead speed, which is consistent with the results of the temperature dependence of I_m. When the deformation rate is low, the CD molecule can slide along a polymer chain and behaves as a movable crosslink. On the other hand, when the deformation rate becomes high, the sliding motion cannot follow the whole deformation, and crosslinks behave like chemical crosslinks. Therefore, finite extensibility is observed at the lower strains for the case of high deformation rates.

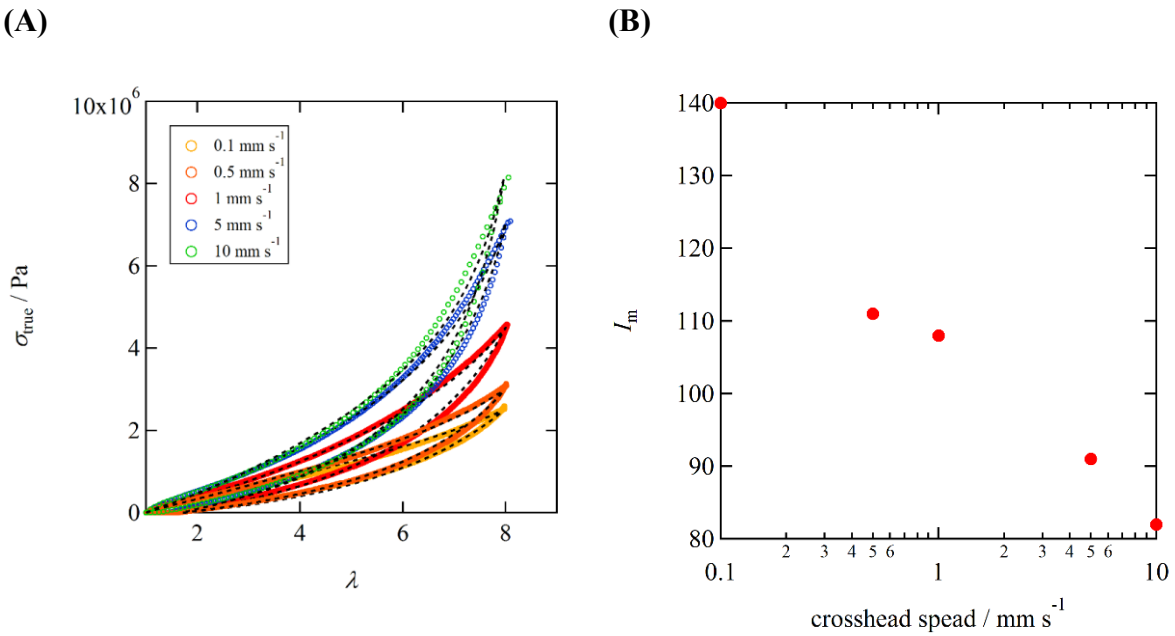

Figure 4-9. (A) Results of cycle tests with different crosshead speeds. Fitting results by eq. 4-12 are also shown with black dotted lines. Fitting parameters are 0.1 mm s^{-1}: $I_m = 140$, $r = 0.80$, $\alpha_1 = 300$, $\alpha_2 = 26$, 0.5 mm s^{-1}: $I_m = 111$, $r = 0.80$, $\alpha_1 = 300$, $\alpha_2 = 19$, 1 mm s^{-1}: $I_m = 108$, $r = 0.81$, $\alpha_1 = 300$, $\alpha_2 = 38$, and 5 mm s^{-1}: $I_m = 91$, $r = 0.81$, $\alpha_1 = 290$, $\alpha_2 = 49$. **(B)** Semi-logarithmic Plot of crosshead speed dependence of I_m used in the fitting in Figure 4-9(A).

To summarize the above-mentioned results for the first loading-unloading cycle test, the finite extensibility of the network chains can be affected by the deformation rate and temperature. Figure 4-10 shows the schematic illustration of the relationship between the sliding motion of the movable crosslinks and the finite extensibility of the network chains. There is a correlation between the deformation rate and the measurement temperature, which is similar to the time-temperature superposition in dynamic viscoelastic measurement. From the molecular perspective of the sliding motion of the movable crosslink, fast deformation rate corresponds to low-temperature deformation, and slow deformation corresponds to high temperature one. This interrelation suggests that the finite extensibility is affected by the mobility of the movable crosslinks in the network. In the material design of movable

crosslinking networks, the control of not only the kind of CD molecule and its concentration but also the chain mobility, namely the glass transition temperature of polymers, is important to control their nonlinear mechanical properties.

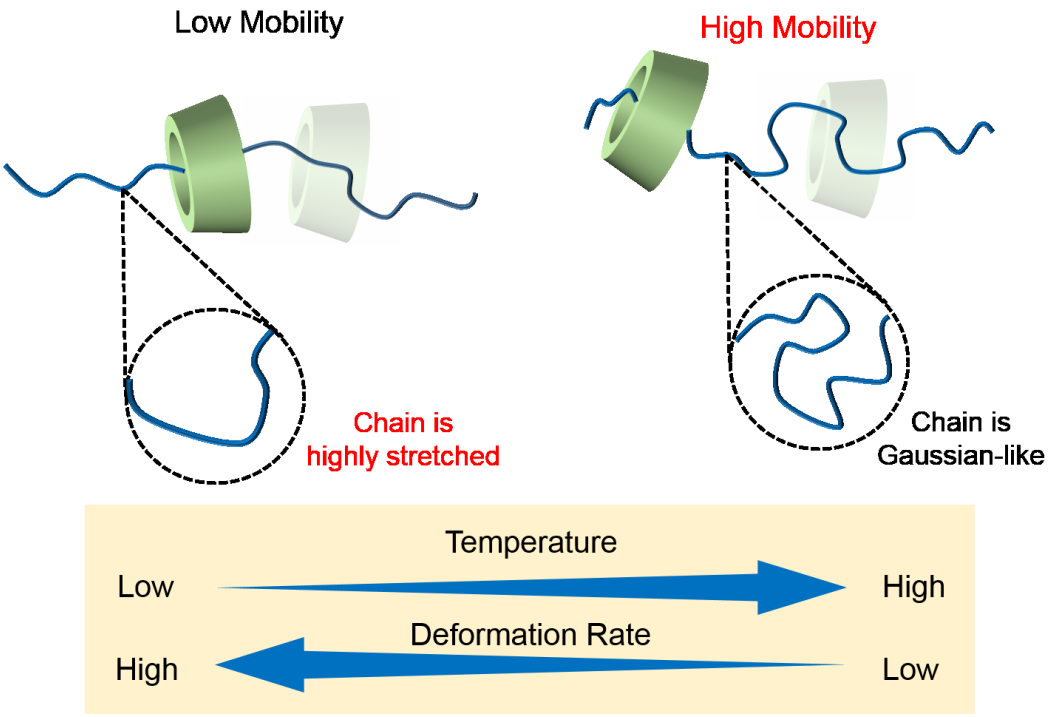

Figure 4-10. Relationship between the sliding motion and finite extensibility of network chains.

4-3-7. Evaluation of irreversible effects

To evaluate the nonlinearity of the hysteresis components, recovery cycle tests were conducted. Figure 4-11(A) shows the time dependence of the applied strain in recovery tests. After the first loading-unloading test was performed, the sample was allowed to stand for a certain interval time t_{int} at $\lambda = 1$, and then the second loading-unloading test was performed with the same tensile condition in the first cycle. The measurement temperature was always kept at $T = 60°C$ during these tests. Figure 4-11(B) and (C) show the results of the recovery tests at $T = 60°C$ with different t_{int}. In both the measurements, compared with the first cycle, the stress in the second

cycle is always smaller than that of the first cycle in all λ regimes. Besides, even in the result with the longer recovery time (t_{int} = 60 min), a similar stress behavior was observed with that of t_{int} = 30 min. Blue dotted lines in Figures 4-11 (B) and (C) represent the vertically shifted stress of the second process with the factor of 1.13 (times) for both t_{int}. It is seen that the stress in the second process can be superposed to those in the first process. This suggests that the recovery ratio of the nonlinearity in the MCN does not change and becomes constant when t_{int} is longer than 30 minutes. Furthermore, the stress in the first process could be well reproduced with one vertical shift factor in all λ regions, which suggests that the material fracture occurs homogeneously in both parts corresponding to the permanent and relaxation components. These recovery tests revealed that the mobility of the movable crosslink itself can recover in a large extent even after a large deformation.

(A)

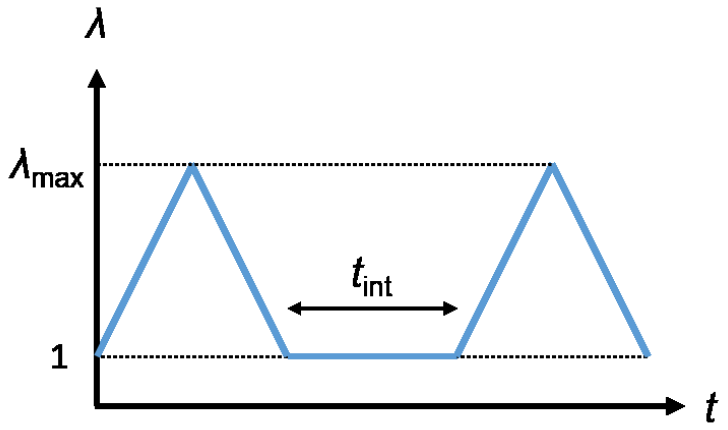

(B) **(C)**

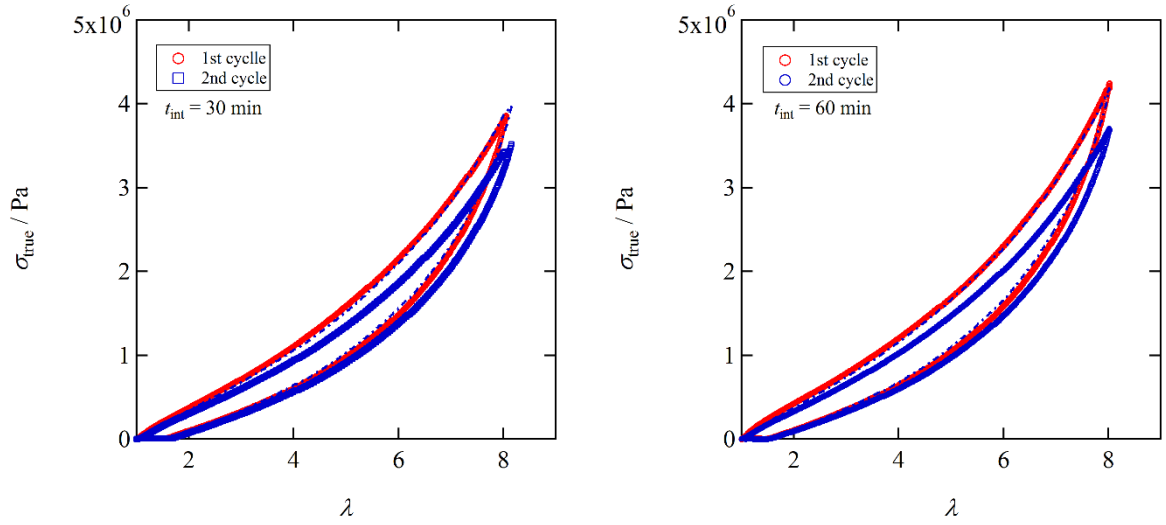

Figure 4-11. (A) Time dependence of the strain in recovery tests. True stress-strain curves of 1st and 2nd loading-unloading process at **(B)** T = 60°C and **(C)** T = 80°C are also shown. Blue dotted lines represent the results of the shifted 2nd cycles with a vertical shift factor = 1.13.

4-4. Conclusion

In this Chapter, the nonlinear rheological behavior of the movable crosslinking network was examined under the large uniaxial deformation. The obtained results are summarized as follows: (1) a new constitutive equation for the movable crosslinking network was proposed by modifying the BKZ-type constitutive equation. In this constitutive equation, the cross terms to other principal axes, finite extensibility of network chains, and the two damping functions for the relaxation and permanent components were necessary to be included; (2) linear and nonlinear viscoelastic relaxation measurements revealed that the time-strain separability was valid, and the damping function could be experimentally determined for the relaxation components deduced by subtracting the contribution of the permanent crosslinks; (3) the experimental results of the first loading-unloading cycle test could be well described by the obtained BKZ-type constitutive equation proposed with the damping functions represented by the PSM-type model; (4) the results of cycle tests with different temperatures and deformation rates could be also reproduced by the same constitutive equation by adjusting the cross term ratio r and finite extensibility I_m. From the fitting results, it is concluded that the finite extensibility is dominated by the mobility of the movable crosslink; (5) the recovery tests revealed that the movable crosslinking network was homogeneously destroyed, and a part of the network could not be recovered. On the other hand, the nonlinearity did not affect the mobility of the movable crosslinks. In this chapter, the phenomenological approach using the BKG type constitutive equation was effective in analyzing the nonlinear mechanical behavior of the movable crosslinking network system. I believe this approach can contribute to the development of a new class of supramolecular networks in the future.

4-5. References

1. Kumar, S. K.; Benicewicz, B. C.; Vaia, R. A.; Winey, K. I., 50th Anniversary Perspective: Are Polymer Nanocomposites Practical for Applications? *Macromolecules* **2017,** *50* (3), 714-731.
2. Chen, Q.; Bao, N.; Wang, J.-H. H.; Tunic, T.; Liang, S.; Colby, R. H., Linear Viscoelasticity and Dielectric Spectroscopy of Ionomer/Plasticizer Mixtures: A Transition from Ionomer to Polyelectrolyte. *Macromolecules* **2015,** *48* (22), 8240-8252.
3. Shabbir, A.; Huang, Q.; Chen, Q.; Colby, R. H.; Alvarez, N. J.; Hassager, O., Brittle fracture in associative polymers: the case of ionomer melts. *Soft Matter* **2016,** *12* (36), 7606-7612.
4. Huang, C.; Wang, C.; Chen, Q.; Colby, R. H.; Weiss, R. A., Reversible Gelation Model Predictions of the Linear Viscoelasticity of Oligomeric Sulfonated Polystyrene Ionomer Blends. *Macromolecules* **2016,** *49* (10), 3936-3947.
5. Gong, J. P.; Katsuyama, Y.; Kurokawa, T.; Osada, Y., Double-Network Hydrogels with Extremely High Mechanical Strength. *Advanced Materials* **2003,** *15* (14), 1155-1158.
6. Gong, J. P., Why are double network hydrogels so tough? *Soft Matter* **2010,** *6* (12), 2583-2590.
7. Rubinstein, M.; Colby, R. H., *Polymer Physics*. OUP Oxford: 2003.
8. Ikura, R.; Park, J.; Osaki, M.; Yamaguchi, H.; Harada, A.; Takashima, Y., Supramolecular Elastomers with Movable Cross-Linkers Showing High Fracture Energy Based on Stress Dispersion. *Macromolecules* **2019,** *52* (18), 6953-6962.
9. Okumura, Y.; Ito, K., The Polyrotaxane Gel: A Topological Gel by Figure-of-Eight Cross-links. *Advanced Materials* **2001,** *13* (7), 485-487.
10. Kato, K.; Yasuda, T.; Ito, K., Viscoelastic Properties of Slide-Ring Gels Reflecting Sliding Dynamics of Partial Chains and Entropy of Ring Components. *Macromolecules* **2012,** *46* (1), 310-316.
11. Bernstein, B.; Kearsley, E. A.; Zapas, L. J., A Study of Stress Relaxation with Finite Strain. *Rubber Chem. Technol.* **1965,** *38* (1), 76-89.
12. Tanner, R. I., From A to (BK)Z in Constitutive Relations. *Journal of Rheology* **1988,** *32* (7), 673-702.
13. Larson, R. G., *Constitutive Equations for Polymer Melts and Solutions*. Butterworth-Heinemann: 1988.
14. Lodge, A. S., A network theory of flow birefringence and stress in concentrated polymer solutions. *Transactions of the Faraday Society* **1956,** *52* (0), 120-130.
15. Urayama, K.; Ogasawara, S.; Takigawa, T., Pure shear deformation of physical and chemical gels of poly(vinyl alcohol). *Polymer* **2006,** *47* (19), 6868-6873.
16. Kawabata, S.; Kawai, H., Strain energy density functions of rubber vulcanizates from biaxial extension

Molecular Properties. In *Adv. Polym. Aci.*, 1977; Vol. 24, pp 89-124.
17. Gao, J.; Weiner, J. H., Chain force concept in systems of interacting chains. *Macromolecules* **1991,** *24* (18), 5179-5191.
18. Mooney, M., A theory of large elastic deformation. *Journal of Applied Physics* **1940,** *11* (9), 582-592.
19. Bladon, P.; Warner, M., Elasticity of nematic networks and nematic effects in conventional rubbers. *Macromolecules* **1993,** *26* (5), 1078-1085.
20. Deloche, B.; Samulski, E. T., Short-range nematic-like orientational order in strained elastomers: a deuterium magnetic resonance study. *Macromolecules* **1981,** *14* (3), 575-581.
21. Gent, A. N., A new constitutive relation for rubber. *Rubber Chem. Technol.* **1996,** *69* (1), 59-61.
22. Takahashi, M.; Urakawa, O.; Golshan Ebrahimi, N.; Isaki, T.; Masuda, T., Functional Form of a Damping Function for the BKZ Equation Derived from Experimental Data in Entangled Polymer Systems. *Nihon Reoroji Gakkaishi(Journal of the Society of Rheology, Japan)* **1996,** *24* (1), 37-42.
23. Papanastasiou, A. C.; Scriven, L. E.; Macosko, C. W., An Integral Constitutive Equation for Mixed Flows: Viscoelastic Characterization. *Journal of Rheology* **1983,** *27* (4), 387-410.

Chapter 5.

Summary and Conclusion

The aim of this thesis is to elucidate details of the molecular dynamics in the supramolecular networks formed by cyclodextrins and its derivatives, which are expected to work as temporary and topological crosslinks. Concerning on the aim, the top results and conclusion are summarized as follows.

In Chapter 2, the rheological properties of the supramolecular network formed by the host-guest interaction between β-cyclodextrin and adamantane were investigated based on linear viscoelastic and swelling measurements. The host-guest interaction worked as the temporary crosslinks and retarded the Rouse motion of the network strands. These features were confirmed based on the experiments utilizing the host competitor solutions and were well described by the sticky reptation model. On the other hand, the β-cyclodextrins which did not form the temporary crosslinks are revealed to create the rotaxane structure. This topological crosslink was revealed to behave as a physical and long-life junction point. This unique structure, including temporary and topological crosslinks, can make the host-guest gel a unique entity.

In Chapter 3, the molecular dynamics of the movable crosslinking networks were investigated based on the linear viscoelastic and broadband dielectric measurements. The movable crosslinks in which a polymer chain was threaded through the cavity of acetylated γ-cyclodextrin could affect the dynamics in two-time scales. Firstly, a part of the movable crosslinks was sandwiched by other bulky groups, which resulted in the permanent crosslinks in the lowest frequency region. Secondly, the slow mode relaxation accompanied by the sliding motion of the movable crosslinks were observed especially by broadband dielectric measurements in the higher frequency range. The temperature dependence of the relaxation

time of the slow mode revealed that both the segmental relaxation of network strands and the sliding motion of the movable crosslinks played a key role in the slow mode.

In Chapter 4, the nonlinear rheological behaviors of the movable crosslinking networks were investigated mainly based on the large uniaxial stretching cycle test. The movable crosslinking networks showed the large hysteresis, which was attributed to the topologically unique structure. A new time- and strain-dependent constitutive equation was proposed based on the BKZ-type equation. This new equation included the effect of cross-terms to other principal axes, finite extensibility of the network strands between crosslinks, and damping functions for the relaxation and permanent components. This new equation could well describe the experimental results independent of the temperature and deformation rate by adjusting the cross-term ratio and finite extensibility. Obtained parameters revealed that the mobility of the movable crosslinks dominated the degree of the finite extensibility. These results prove that the sliding motion of the movable crosslink has a large contribution to the material toughness.

In summary, the author revealed the dynamics of the supramolecular networks formed by temporary and topological crosslinks with the aid of “molecular rheology”, a science field to clarify the relationship between the macroscopic rheological phenomena and molecular dynamics. The swelling experiments indicated that cyclodextrins phenomenologically work not only as temporary crosslinks but also as topological permanent crosslinks. Focusing on this topologically unique structure, the linear and nonlinear rheological properties of the movable crosslinking networks demonstrated that the movable crosslinks work as both slidable and permanent crosslinks. Besides, the author has pointed out the importance of ordinary entanglements, which also work as sliding crosslinks. The nonlinear tensile experiments have revealed that the sliding motion under large deformation is strongly related to the material toughness. Through this work, the molecular mechanisms of temporary and topologically crosslinked networks are clarified concerning the toughness of polymeric materials. The author

hoped that the results of this research would lead to the advanced molecular design of tough polymers.

List of Publications

Original Papers

1. Linear viscoelastic studies on a transient network formed by host-guest interaction
   Y. Kashiwagi, T. Katashima, M. Nakahata, Y. Takashima, A. Harada, and T. Inoue
   Journal of Polymer Science Part B: Polymer Physics, **2018**, 56, 1109-1117

2. Effect of Host-Guest Interaction on Swelling Behavior and Equilibrium Swollen State of Host-Guest Gel
   Y. Kashiwagi, T. Katashima, Y. Takashima, A. Harada, and T. Inoue
   Nihon Reoroji Gakkaishi, **2019**, 47(3), 99-104

3. Dynamics of Topological Network formed by Movable Crosslinks: Effect of Sliding Motion on Dielectric and Viscoelastic Relaxation Behavior
   Y. Kashiwagi, O. Urakawa, S. Zhao, Y. Takashima, A. Harada, and T. Inoue
   submitted to Macromolecules

4. Nonlinear rheological behavior of supramolecular networks formed by movable crosslinks
   Y. Kashiwagi, O. Urakawa, Y. Takashima, A. Harada, and T. Inoue
   in preparation

Other related papers

1. A Self-Build Apparatus for Oscillatory Flow Birefringence Measurements in a Co-Cylindrical Geometry
   R. Tanaka, S. Li, Y. Kashiwagi, and T. Inoue
   Nihon Reoroji Gakkaishi, **2018**, 46(5), 221-226

2. Viscoelastic Relaxation of Cellulose Nanocrystals in Fluids: Contributions of Microscopic Internal Motions to Flexibility
   R. Tanaka, Y. Kashiwagi, Y. Okada, and T. Inoue
   Biomacromolecules, **2020**, 21, 408-417

3. Design and mechanical properties of supramolecular polymeric materials based on host-guest interactions: the relation between relaxation time and fracture energy
   S. Konishi, Y. Kashiwagi, G. Watanabe, M. Osaki, T. Katashima, O. Urakawa, H. Yamaguchi, T. Inoue, A. Harada, and Y. Takashima
   Polymer Chemistry, **2020**, 11(42), 6811-6820